A Study on Analysis Methods for Electromagnetic Waveguide Discontinuities

KIYOSHI ISE

1

A Study on Analysis Methods for Electromagnetic Waveguide Discontinuities

KIYOSHI ISE

Department of Electronic Engineering
Hokkaido University

CONTENTS

Chapter 1. Preface 1

Chapter 2. Three-dimensional finite-element method with traditional tetrahedral elements 6

2.1 Introduction 6

2.2 Variational formulation 8

2.3 Finite-element formulation 9

2.4 Substructure formulation 11

2.5 Analytical formulation 14

2.6 Numerical results 18

2.7 Conclusions 26

Chapter 3. Three-dimensional finite-element method with edge elements 27

3.1 Introduction 27

3.2 Variational formulation 28

3.3 Finite-element formulation 30

3.4 Analytical formulation 34

3.5 Numerical results 36

3.6 Conclusions 43

Chapter 4. A combination method of finite and boundary elements 44

4.1 Introduction 44

4.2 Basic equations 46

4.3 Boundary-element formulation 48
4.4 Finite-element formulation 49
4.5 Analytical formulation 50
4.6 Combination of finite and boundary elements 51
4.7 Numerical results 53
4.8 Conclusions 65

Chapter 5. Equivalent circuit for dielectric posts 68
5.1 Introduction 68
5.2 Basic equations 69
5.3 Outline of analysis method 70
5.4 Numerical results 74
5.5 Conclusions 90

Chapter 6. Conclusions 92

Acknowledgment 93
List of author's publication 94
References 95

CHAPTER 1

Preface

Owing to the extensive demand of information and communication, it has been desired that microwave and millimeter-wave circuits have high performance and high functionality and are of very small size, so that the techniques to analyze the high frequency circuits accurately have been required.

In these circumstances, the analysis of waveguide discontinuity is the most important in the microwave and millimeter-wave circuit designs and hence numerous analysis methods have been developed [1]–[27]. Of these, the finite-element method [28]–[39] and the boundary-element method [40]–[45] are used widely as useful techniques since they can easily be applied to arbitrarily shaped discontinuities.

The finite-element method and the boundary-element method play an important part in computational physics which is rapidly developed and comes to bear comparison with experimental physics and theoretical physics, and the researches into their application to electromagnetic waveguide problems are energetically made. By the way, the waveguide problems of finding propagation characteristics of waveguides and the resonant problems of finding resonant frequencies of resonators are of the eigenvalue type. In general, the finite-element analysis of three-dimensional electromagnetic problems

is based on the functional with three components of the electric or magnetic field. However, when the eigenvalue problems are solved by using this functional, spurious solutions appear. So suppression and elimination of these spurious solutions in the eigenvalue problems have been vigorously studied [46]−[62]. On the other hand, when the discontinuity problems are solved by using this functional, the question of whether or not spurious fields appear has hardly been discussed. Then, when the finite-element method is applied to the three-dimensional discontinuity problems, we need much computer memory to divide the analysis region into much elements and to obtain good numerical convergence. So we must introduce a new method to save computer memory or to use the computer memory economically. By the way, both the finite-element method and the boundary-element method are effective for the electromagnetic waveguide problems which can be treated as two-dimensional ones. For some problems, however, a combination of the finite and boundary element methods seems to be more effective than those two methods.

In the circumstances this paper shows that spurious solutions appear in the three-dimensional discontinuity problems when the functional with three components of magnetic field is directly used. And then, to suppress and eliminate spurious solutions, we try two approaches, that is, the penalty function method [63], [64] and the method using edge elements [65]. Moreover, we introduce a substructure method [63]−[65] to save computer memory and to have a good numerical convergence. This paper also shows that the finite-

element method using traditional tetrahedral elements cannot adequately treat the three-dimensional electromagnetic waveguide problems with metal wedges, and that the finite-element method using edge elements succeeds in the analysis of the problems with metal wedges [65]. Then, a combination method of the finite and boundary elements is formulated for the electromagnetic discontinuity problems which can be treated as two-dimensional ones [66]–[71]. This method is effectively applied to the waveguides loaded with ferrite as well as dielectric. Moreover, the way to represent a dielectric resonance in a rectangular waveguide by the equivalent circuit is investigated in detail [69], [70]. An outline of the paper is given as follows.

Chapter 2 shows that when the three-dimensional electromagnetic problems are solved by the finite-element method based on the functional with three components of magnetic field, spurious solutions appear if the traditional tetrahedral elements are used, and that the penalty function method is effective for suppression of these spurious solutions, but a new kind of spurious solutions dependent on the penalty coefficient is generated [63], [64]. The relationship between this kind of spurious solutions and the penalty coefficients is investigated in detail. Moreover, the substructure method is introduced in the finite-element method to save the computer memory and to have good numerical convergence. To confirm the validity and usefulness of the present approach, numerical examples are shown for a rectangular dielectric scattering obstacle in a waveguide, and are compared with the earlier theoretical results [3], [5].

In Chapter 3 the method using edge elements [65] is introduced

to suppress spurious solutions. It is confirmed that spurious solutions do not appear when the finite-element method using edge elements is applied to the three-dimensional electromagnetic discontinuity problems. This chapter also shows that the finite-element method using traditional tetrahedral elements cannot adequately treat the three-dimensional electromagnetic waveguide problems with metal wedges, and that the finite-element method using edge elements [65] succeeds in the analysis of the problems with metal wedges. To show the validity of this method, right-angle corner bend [37], [45], a concentric step discontinuity [2], and an E-plane ridge waveguide discontinuity [6] are investigated, and the computed results are compared with the earlier theoretical and experimental results.

Chapter 4 presents a formulation of new numerical methods for the problems of waveguide junctions which can be treated as two-dimensional problems. The junctions are loaded with arbitrarily shaped dielectric or ferrite. This approach is a combination of the finite and boundary element methods (CFBEM) [66]–[71] where the finite-element method and the boundary-element method are applied to the regions with and without dielectric or ferrite, respectively. Discontinuity problems with a large homogeneous region or with variations of the location of an inhomogeneous region can be effectively treated by this method. To show the validity and usefulness of the method, a lossy dielectric post in a rectangular waveguide [23] and a ferrite-slab-loaded waveguide nonreciprocal phase shifter [24] are investigated in detail, and the computed results are compared

with the earlier theoretical and experimental results.

In Chapter 5 dielectric post resonances are investigated using a combination of the finite and boundary element methods (CFBEM). Some of the lossless dielectric post resonances in a rectangular waveguide can be physically realized by a lattice circuit [69], [70], and the interaction between two posts can be evaluated by this circuit [69]. Moreover, the variations of the post location are related to the variations of the branch reactances of the lattice circuit, and it is found that there are two types of dielectric post resonances [70].

The results obtained are described in Chapter 6.

CHAPTER 2

Three-Dimensional Finite-Element Method with Traditional Tetrahedral Elements

2.1 Introduction

In recent years, problems in which the geometry forces a three-dimensional analysis of electromagnetic fields have been energetically studied by many researchers [1]–[6], [30]–[34], [46], [47], [57]–[62], [72]–[74]. For example, problems of finding resonant frequencies of a resonator [57]–[62], of finding scattering characteristics of a waveguide discontinuity [30]–[34], and of finding propagation characteristics of a waveguide with a periodic structure in the direction of propagation [46] have been analyzed by the three-dimensional finite-element method. The three-dimensional finite-difference method [72] and the three-dimensional boundary-element method [73], [74] have been applied to the resonator problems, and the three-dimensional finite-difference method [4], [5], the moment method [1], and the mode-matching procedure [3] have been applied to the discontinuity problems.

The resonant problems and the periodic waveguide problems are of the eigenvalue type. In general, the finite-element analysis of three-dimensional electromagnetic problems is based on the functional in terms of three components of electric or magnetic field [75],

[76]. However, when the eigenvalue problems are solved by using this functional, spurious solutions appear. So suppression and elimination of these spurious solutions in the eigenvalue problems have been vigorously studied [46]−[62].

On the other hand, when the discontinuity problems are solved by using this functional, the question of whether or not spurious solutions appear has been hardly discussed.

This paper shows that spurious fields like the spurious solutions generated in the finite-element analysis of three-dimensional eigenvalue problems can appear in the three-dimensional discontinuity problems when the functional in terms of three components of magnetic field is directly used. And then, to suppress and eliminate the spurious field, the penalty function method [46]−[53], [59] is applied to the finite-element analysis of three-dimensional discontinuity problems. Moreover, we show that a new kind of spurious field generated in the penalty function method is related to the penalty coefficient, so that true fields can be distinguished from spurious fields.

In the conventional three-dimensional analysis of discontinuities in a rectangular waveguide using the finite-element method [30]−[34] or the finite-difference method [4], [5], to combine the uniform waveguide with the discontinuity region only one propagating mode far away from the scattering obstacle has been used. In this paper, we take account of evanescent modes as well as propagating modes, so that the boundary planes which combine the uniform waveguide with the finite-element analysis region do not need to be far away from the scattering obstacle.

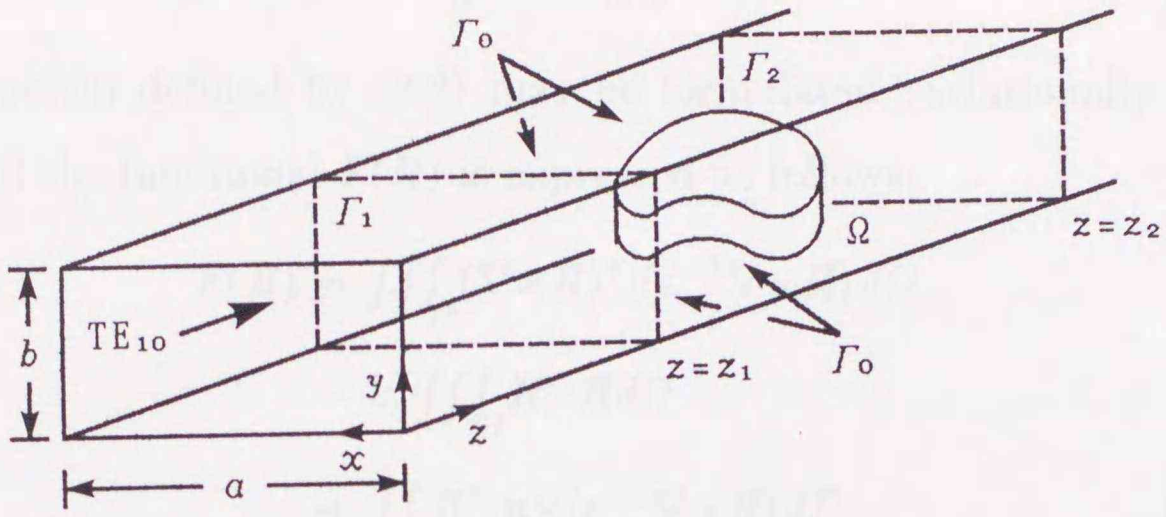

Fig. 2.1. Dielectric-loaded waveguide.

2.2 Variational Formulation

The dielectric-loaded waveguide as shown in Fig. 2.1 is considered. Here the boundary plane Γ_i connects the discontinuity region Ω to the rectangular waveguide $i(1=1,2)$, and the region Ω surrounded by Γ_1, Γ_2, and Γ_0 encloses the waveguide discontinuities completely. Γ_0 is assumed to be the perfectly-conducting wall. Maxwell's equations are given by

$$\nabla \times \boldsymbol{E} = -j\omega\mu_0 \boldsymbol{H} \tag{2.1a}$$

$$\nabla \times \boldsymbol{H} = j\omega\varepsilon_0 \varepsilon \boldsymbol{E} \tag{2.1b}$$

where $\boldsymbol{E}$ and $\boldsymbol{H}$ are the electric and magnetic field vectors, ω is the angular frequency, ε_0 and μ_0 are the permittivity and the permeability in vacuum, and ε is the relative permittivity.

Substituting (2.1b) into (2.1a), we obtain

$$\nabla \times (\varepsilon^{-1} \nabla \times \boldsymbol{H}) - k_0^2 \boldsymbol{H} = 0 \tag{2.2}$$

where

$$k_0^2 = \omega^2 \varepsilon_0 \mu_0. \tag{2.3}$$

The problem defined by (2.2) may be formulated variationally [75], [76], and the functional $F(\boldsymbol{H})$ is expressed as follows:

$$\begin{aligned} F(\boldsymbol{H}) = & \iiint_{\Omega} (\nabla \times \boldsymbol{H})^* \cdot (\varepsilon^{-1} \nabla \times \boldsymbol{H}) \, d\Omega \\ & - k_0^2 \iiint_{\Omega} \boldsymbol{H}^* \cdot \boldsymbol{H} d\Omega \\ & + \iint_{\Gamma} \boldsymbol{H}^* \cdot \boldsymbol{n} \times (\varepsilon^{-1} \nabla \times \boldsymbol{H}) \, d\Gamma \end{aligned} \tag{2.4}$$

where $\iiint_{\Omega} d\Omega$ is the volume integral in the region Ω, $\iint_{\Gamma} d\Gamma$ is the surface integral over the boundary $\Gamma (= \Gamma_1 + \Gamma_2 + \Gamma_0)$, $\boldsymbol{n}$ is the outward unit normal vector on the boundary Γ, and $*$ indicates complex conjugate.

When the eigenvalue problems are solved using this functional, spurious solutions not satisfying the condition $\nabla \cdot \boldsymbol{H} = 0$ appear. The penalty function method [46]–[53], [59] is the one that makes the condition $\nabla \cdot \boldsymbol{H} = 0$ be satisfied in a least squares-manner. In this method, the functional (2.4) is modified as

$$\widetilde{F}(\boldsymbol{H}) = F(\boldsymbol{H}) + s \iiint_{\Omega} (\nabla \cdot \boldsymbol{H})^* (\nabla \cdot \boldsymbol{H}) \, d\Omega \tag{2.5}$$

where s is an arbitrary positive number and is called the penalty coefficient.

2.3 Finite-Element Formulation

First, the region Ω is divided into brick elements [28]. Then, one brick element is divided into five tetrahedral elements [28]. The magnetic field H_r $(r = x,y,z)$ in each element is approximated by second-order polynomials, and then H_r is expanded in terms of the

values of H_r at ten nodes in the element as follows:

$$H_r = \{N\}^T \{H_r\}_e, \qquad r = x,y,z \tag{2.6}$$

where $\{H_r\}_e$ is the nodal magnetic field vector in each element, $\{N\}$ is the shape function vector [28], and T indicates a transpose.

When the finite-element method is applied to (2.5), the following matrix equation is obtained [46], [63], [64]:

$$\begin{aligned} &[S]\{H\} + s[U]\{H\} - k_0^2[T]\{H\} \\ &\quad - \sum_{e'} \iint_{e'} j\omega\varepsilon_0 [N](\boldsymbol{i}_z \times \boldsymbol{E})|_{\Gamma_1} d\Gamma \\ &\quad + \sum_{e'} \iint_{e'} j\omega\varepsilon_0 [N](\boldsymbol{i}_z \times \boldsymbol{E})|_{\Gamma_2} d\Gamma = \{0\} \end{aligned} \tag{2.7}$$

where $\{H\}$ is the nodal magnetic field vector in the whole region Ω, $[S]$ and $[T]$ are the matrices related to the first and second terms on right-hand side of (2.4), respectively, and $[U]$ is the matrix related to the penalty term of (2.5), and $\boldsymbol{i}_z$ is the unit vector along the z axis. $\sum_{e'}$ is the summation only over the elements related to the boundary Γ_1 and Γ_2, and $\iint_{e'} d\Gamma$ is the surface integral on each element on the boundaries Γ_1 and Γ_2. The matrix $[N]$ is given by

$$[N] = \begin{bmatrix} \{N\} & \{0\} & \{0\} \\ \{0\} & \{N\} & \{0\} \\ \{0\} & \{0\} & \{N\} \end{bmatrix} \tag{2.8}$$

where $\{0\}$ is a null vector.

Let $\{H\}_1$ and $\{H\}_2$ be the nodal magnetic field vectors related to the nodes on the boundaries Γ_1 and Γ_2, respectively. Also, let $\{H\}_0$ be the nodal magnetic field vector obtained by removing $\{H\}_1$

and $\{H\}_2$ from $\{H\}$. Then, equation (2.7) is rewritten as

$$\begin{bmatrix} [R]_{11} & [R]_{10} & [R]_{12} \\ [R]_{01} & [R]_{00} & [R]_{02} \\ [R]_{21} & [R]_{20} & [R]_{22} \end{bmatrix} \begin{bmatrix} \{H\}_1 \\ \{H\}_0 \\ \{H\}_2 \end{bmatrix}$$

$$= \begin{bmatrix} \sum_{e'} \iint_{e'} j\omega\varepsilon_0 [N](\boldsymbol{i}_z \times \boldsymbol{E})|_{\Gamma_1} d\Gamma \\ \{0\} \\ -\sum_{e'} \iint_{e'} j\omega\varepsilon_0 [N](\boldsymbol{i}_z \times \boldsymbol{E})|_{\Gamma_2} d\Gamma \end{bmatrix} \tag{2.9}$$

where $[R]_{11}, \cdots, [R]_{22}$ are the submatrices of the following matrix $[R]$:

$$[R] = [S] + s[U] - k_0^2[T]. \tag{2.10}$$

2.4 Substructure Formulation

The region Ω is divided into subregions $\Omega^{(j)}$ $(j = 1,2, \ldots, n)$ as shown in Fig. 2.2. Applying the finite-element method to the subregion $\Omega^{(1)}$, the following equation is obtained:

$$\begin{bmatrix} [R]_{11}^{(1)} & [R]_{10}^{(1)} & [R]_{12}^{(1)} \\ [R]_{01}^{(1)} & [R]_{00}^{(1)} & [R]_{02}^{(1)} \\ [R]_{21}^{(1)} & [R]_{20}^{(1)} & [R]_{22}^{(1)} \end{bmatrix} \begin{bmatrix} \{H\}_1^{(1)} \\ \{H\}_0^{(1)} \\ \{H\}_2^{(1)} \end{bmatrix}$$

$$= \begin{bmatrix} \sum_{e'} \iint_{e'} j\omega\varepsilon_0 [N](\boldsymbol{i}_z \times \boldsymbol{E})|_{\Gamma_1^{(1)}} \, d\Gamma \\ \{0\} \\ -\sum_{e'} \iint_{e'} j\omega\varepsilon_0 [N](\boldsymbol{i}_z \times \boldsymbol{E})|_{\Gamma_2^{(1)}} \, d\Gamma \end{bmatrix} \tag{2.11}$$

where the superscript (1) indicates that the quantities are related to

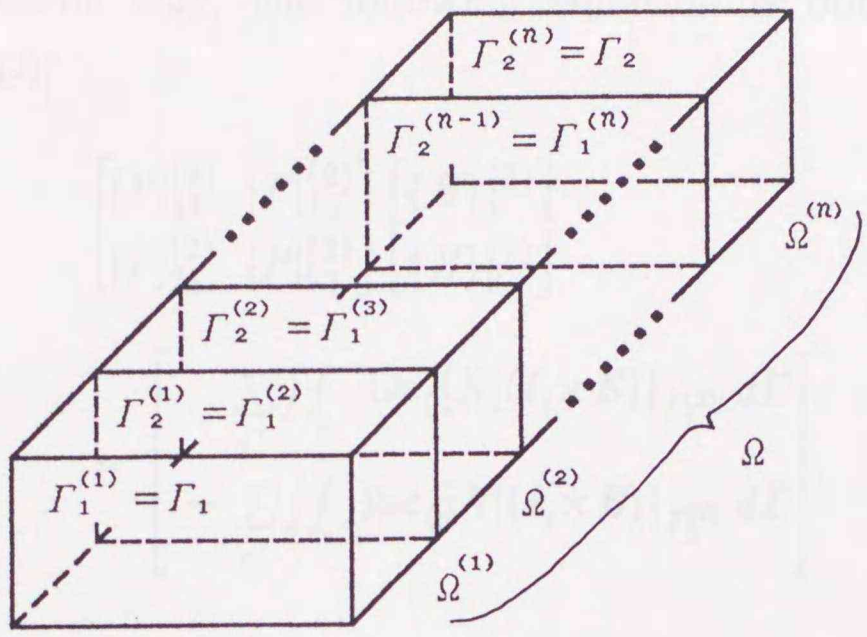

Fig. 2.2. Region Ω divided into subregions $\Omega^{(1)}$ to $\Omega^{(n)}$.

the subregion $\Omega^{(1)}$.

Eliminating $\{H\}_0^{(1)}$ from (2.11), we obtain the following equation:

$$\begin{bmatrix} [P]_{11}^{(1)} & [P]_{12}^{(1)} \\ [P]_{21}^{(1)} & [P]_{22}^{(1)} \end{bmatrix} \begin{bmatrix} \{H\}_1^{(1)} \\ \{H\}_2^{(1)} \end{bmatrix}$$

$$= \begin{bmatrix} \sum_{e'} \iint_{e'} j\omega\varepsilon_0 [N](\boldsymbol{i}_z \times E)|_{\Gamma_1^{(1)}} \, d\Gamma \\ -\sum_{e'} \iint_{e'} j\omega\varepsilon_0 [N](\boldsymbol{i}_z \times E)|_{\Gamma_2^{(1)}} \, d\Gamma \end{bmatrix} \tag{2.12}$$

where

$$[P]_{11}^{(1)} = [R]_{11}^{(1)} - [R]_{10}^{(1)} [R]_{00}^{(1)-1} [R]_{01}^{(1)} \tag{2.13a}$$

$$[P]_{12}^{(1)} = [R]_{12}^{(1)} - [R]_{10}^{(1)} [R]_{00}^{(1)-1} [R]_{02}^{(1)} \tag{2.13b}$$

$$[P]_{21}^{(1)} = [R]_{21}^{(1)} - [R]_{20}^{(1)} [R]_{00}^{(1)-1} [R]_{01}^{(1)} \tag{2.13c}$$

$$[P]_{22}^{(1)} = [R]_{22}^{(1)} - [R]_{20}^{(1)} [R]_{00}^{(1)-1} [R]_{02}. \tag{2.13d}$$

In the same way, the following equation is obtained for the subregion $\Omega^{(2)}$:

$$\begin{bmatrix} [P]_{11}^{(2)} & [P]_{12}^{(2)} \\ [P]_{21}^{(2)} & [P]_{22}^{(2)} \end{bmatrix} \begin{bmatrix} \{H\}_1^{(2)} \\ \{H\}_2^{(2)} \end{bmatrix}$$

$$= \begin{bmatrix} \sum_{e'} \iint_{e'} j\omega\varepsilon_0 [N](\boldsymbol{i}_z \times \boldsymbol{E})|_{\Gamma_1^{(2)}} \, d\Gamma \\ -\sum_{e'} \iint_{e'} j\omega\varepsilon_0 [N](\boldsymbol{i}_z \times \boldsymbol{E})|_{\Gamma_2^{(2)}} \, d\Gamma \end{bmatrix}. \tag{2.14}$$

The continuity condition of the magnetic field $\boldsymbol{H}$ at the interface $\Gamma_2^{(1)}(=\Gamma_1^{(2)})$ between subregions $\Omega^{(1)}$ and $\Omega^{(2)}$ is

$$\{H\}_2^{(1)} = \{H\}_1^{(2)}. \tag{2.15}$$

Using (2.15), we may combine (2.12) with (2.14) and obtain the following equation:

$$\begin{bmatrix} [P]_{11}^{(1)} & [P]_{12}^{(1)} & [0] \\ [P]_{21}^{(1)} & [P]_{22}^{(1)} + [P]_{11}^{(2)} & [P]_{12}^{(2)} \\ [0] & [P]_{21}^{(2)} & [P]_{22}^{(2)} \end{bmatrix} \begin{bmatrix} \{H\}_1^{(1)} \\ \{H\}_2^{(1)} \\ \{H\}_2^{(2)} \end{bmatrix}$$

$$= \begin{bmatrix} \sum_{e'} \iint_{e'} j\omega\varepsilon_0 [N](\boldsymbol{i}_z \times E)|_{\Gamma_1^{(1)}} \, d\Gamma \\ \{0\} \\ -\sum_{e'} \iint_{e'} j\omega\varepsilon_0 [N](\boldsymbol{i}_z \times E)|_{\Gamma_2^{(2)}} \, d\Gamma \end{bmatrix} \tag{2.16}$$

where [0] is a null matrix.

Eliminating $\{H\}_2^{(1)}$ ($= \{H\}_1^{(2)}$) from (2.16), we get the following equation:

$$\begin{bmatrix} [Q]_{11}^{(12)} & [Q]_{12}^{(12)} \\ [Q]_{21}^{(12)} & [Q]_{22}^{(12)} \end{bmatrix} \begin{bmatrix} \{H\}_1^{(1)} \\ \{H\}_2^{(2)} \end{bmatrix}$$

$$= \begin{bmatrix} \sum_{e'} \iint_{e'} j\omega\varepsilon_0 [N](\boldsymbol{i}_z \times \boldsymbol{E})|_{\Gamma_1^{(1)}} \, d\Gamma \\ -\sum_{e'} \iint_{e'} j\omega\varepsilon_0 [N](\boldsymbol{i}_z \times \boldsymbol{E})|_{\Gamma_2^{(2)}} \, d\Gamma \end{bmatrix} \tag{2.17}$$

where

$$[Q]_{11}^{(12)} = [P]_{11}^{(1)} - [P]_{12}^{(1)}([P]_{22}^{(1)} + [P]_{11}^{(2)})^{-1}[P]_{21}^{(1)} \tag{2.18a}$$

$$[Q]_{12}^{(12)} = \quad - [P]_{12}^{(1)}([P]_{22}^{(1)} + [P]_{11}^{(2)})^{-1}[P]_{12}^{(2)} \tag{2.18b}$$

$$[Q]_{21}^{(12)} = \quad - [P]_{21}^{(2)}([P]_{22}^{(1)} + [P]_{11}^{(2)})^{-1}[P]_{21}^{(1)} \tag{2.18c}$$

$$[Q]_{22}^{(12)} = [P]_{22}^{(2)} - [P]_{21}^{(2)}([P]_{22}^{(1)} + [P]_{11}^{(2)})^{-1}[P]_{12}^{(2)}. \tag{2.18d}$$

Here the superscript (12) indicates that the quantities relate to the subregions $\Omega^{(1)}$ to $\Omega^{(2)}$.

Iterating the same work from $\Omega^{(1)}$ to $\Omega^{(n)}$ shown in Fig. 2.2, we obtain the following equation:

$$\begin{bmatrix} [Q]_{11}^{(1n)} & [Q]_{12}^{(1n)} \\ [Q]_{21}^{(1n)} & [Q]_{22}^{(1n)} \end{bmatrix} \begin{bmatrix} \{H\}_1 \\ \{H\}_2 \end{bmatrix}$$

$$= \begin{bmatrix} \sum_{e'} \iint_{e'} j\omega\varepsilon_0 [N](\boldsymbol{i}_z \times \boldsymbol{E})|_{\Gamma_1} d\Gamma \\ -\sum_{e'} \iint_{e'} j\omega\varepsilon_0 [N](\boldsymbol{i}_z \times \boldsymbol{E})|_{\Gamma_2} d\Gamma \end{bmatrix} \tag{2.19}$$

where the superscript $(1n)$ indicates that the quantities relate to the subregions $\Omega^{(1)}$ to $\Omega^{(n)}$.

2.5 Analytical Formulation

At the cross-sectional plane Γ_i (i=1,2) in Fig. 2.1, the transverse electric $\boldsymbol{E}_t$ and magnetic $\boldsymbol{H}_t$ fields are represented in the following form:

$$E_t(x,y,z_i) = \sum_m \sum_n (a_{mn} e^{-j\beta_{mn} z_i} + b_{mn} e^{j\beta_{mn} z_i}) e_{1mn}(x,y)$$

$$+ \sum_m \sum_n \frac{j\beta_{mn}}{j\omega\varepsilon_0} (c_{mn} e^{-j\beta_{mn} z_i} - d_{mn} e^{j\beta_{mn} z_i}) e_{2mn}(x,y) \qquad (2.20)$$

$$H_t(x,y,z_i) = \sum_m \sum_n \frac{j\beta_{mn}}{j\omega\mu_0} (a_{mn} e^{-j\beta_{mn} z_i} - b_{mn} e^{j\beta_{mn} z_i}) h_{1mn}(x,y)$$

$$+ \sum_m \sum_n (c_{mn} e^{-j\beta_{mn} z_i} + d_{mn} e^{j\beta_{mn} z_i}) h_{2mn}(x,y) \qquad (2.21)$$

where a_{mn}, b_{mn}, c_{mn}, and d_{mn} are the mode amplitudes, and the propagation constant β_{mn} is given by

$$\beta_{mn} = \sqrt{k_0^2 - (\frac{m\pi}{a})^2 - (\frac{n\pi}{b})^2}. \qquad (2.22)$$

The mode functions e_{lmn} and h_{lmn} (l=1,2) are given by

$$e_{1mn}(x,y) = N_{mn} \left[-i_x \frac{n}{b} f_{mn}(x,y) + i_y \frac{m}{a} g_{mn}(x,y) \right] \qquad (2.23)$$

$$e_{2mn}(x,y) = N_{mn} \left[i_x \frac{m}{a} f_{mn}(x,y) + i_y \frac{n}{b} g_{mn}(x,y) \right] \qquad (2.24)$$

$$h_{lmn}(x,y) = i_z \times e_{lmn}(x,y), \qquad l=1,2 \qquad (2.25)$$

$$f_{mn}(x,y) = \cos\frac{m\pi}{a} x \sin\frac{n\pi}{b} y \qquad (2.26)$$

$$g_{mn}(x,y) = \sin\frac{m\pi}{a} x \cos\frac{n\pi}{b} y \qquad (2.27)$$

and these functions satisfy the normalized orthogonality relation

$$\iint_{\Gamma_i} e_{lmn} \cdot e^*_{l'm'n'} \, d\Gamma = \iint_{\Gamma_i} h_{lmn} \cdot h^*_{l'm'n'} \, d\Gamma$$

$$= \iint_{\Gamma_i} (\boldsymbol{e}_{lmn} \times \boldsymbol{h}^*_{l'm'n'}) \cdot \boldsymbol{i}_z \, d\Gamma$$

$$= \delta_{ll'} \delta_{mm'} \delta_{nn'}. \tag{2.28}$$

Here the subscripts $l = 1$ and $l = 2$ correspond to TE and TM waves, respectively, $\boldsymbol{i}_x$ and $\boldsymbol{i}_y$ are the unit vectors along the x and y axes, respectively, and the normalized constant N_{mn} is given by

$$N_{mn}^{-2} = \frac{1}{\nu_m \nu_n} \left[n^2 \frac{a}{b} + m^2 \frac{b}{a} \right], \qquad \nu_m, \nu_n = \begin{cases} 1 & m=0, n=0 \\ 2 & m \neq 0, n \neq 0. \end{cases} \tag{2.29}$$

Assuming that the dominant TE_{10} mode is incident from the left of Γ_1 as shown in Fig. 2.1, we may relate $\boldsymbol{E}_t$ to $\boldsymbol{H}_t$ as follows:

$$\begin{aligned} \boldsymbol{E}_t(x,y,z_i) &= \delta_{i1} 2 a_{10} e^{-j\beta_{10} z_i} \boldsymbol{e}_{110}(x,y) \\ &+ \sum_m \sum_n (-1)^i \frac{1}{j\beta_{mn}} \iint_{\Gamma_i} \boldsymbol{h}^*_{1mn}(x',y') \\ &\cdot j\omega\mu_0 \boldsymbol{H}_t(x',y') \, dx' \, dy' \, \boldsymbol{e}_{1mn}(x,y) \\ &+ \sum_m \sum_n (-1)^i \frac{j\beta_{mn}}{-k_0^2} \iint_{\Gamma_i} \boldsymbol{h}^*_{2mn}(x',y') \\ &\cdot j\omega\mu_0 \boldsymbol{H}_t(x',y') \, dx' \, dy' \, \boldsymbol{e}_{2mn}(x,y). \end{aligned} \tag{2.30}$$

Equation (2.30) can be discretized as follows:

$$\begin{bmatrix} \{E_x\}_i \\ \{E_y\}_i \end{bmatrix} = \begin{bmatrix} \{0\} \\ \delta_{i1}\{g\}_i \end{bmatrix} + (-1)^i \begin{bmatrix} [Z_{xx}]_i & [Z_{xy}]_i \\ [Z_{yx}]_i & [Z_{yy}]_i \end{bmatrix} \begin{bmatrix} j\omega\mu_0\{H_x\}_i \\ j\omega\mu_0\{H_y\}_i \end{bmatrix} \tag{2.31}$$

where

$$\{g\}_i = 2 a_{10} e^{-j\beta_{10} z_i} N_{10} \frac{1}{a} \{g_{10}\}_i. \tag{2.32}$$

Here the components of the $\{g_{10}\}_i$ vector are the values of $g_{10}(x,y)$

on the boundary Γ_i and $[Z_{xx}], \ldots, [Z_{yy}]$ are the matrices obtained by discretization of (2.30).

Letting $[A]_{11}, [A]_{12}, \ldots, [A]_{66}$ be the submatrices of $[Q]_{11}^{(1n)}, \ldots, [Q]_{22}^{(1n)}$, and combining (2.19) with (2.31), the final matrix equation is obtained as follows:

$$\begin{bmatrix} [\overline{A}]_{11} & [\overline{A}]_{12} & [A]_{13} & [A]_{14} & [A]_{15} & [A]_{16} \\ [\overline{A}]_{21} & [\overline{A}]_{22} & [A]_{23} & [A]_{24} & [A]_{25} & [A]_{26} \\ [A]_{31} & [A]_{32} & [A]_{33} & [A]_{34} & [A]_{35} & [A]_{36} \\ [A]_{41} & [A]_{42} & [A]_{43} & [\overline{A}]_{44} & [\overline{A}]_{45} & [A]_{46} \\ [A]_{51} & [A]_{52} & [A]_{53} & [\overline{A}]_{54} & [\overline{A}]_{55} & [A]_{56} \\ [A]_{61} & [A]_{62} & [A]_{63} & [A]_{64} & [A]_{65} & [A]_{66} \end{bmatrix} \begin{bmatrix} j\omega\mu_0\{H_x\}_1 \\ j\omega\mu_0\{H_y\}_1 \\ j\omega\mu_0\{H_z\}_1 \\ j\omega\mu_0\{H_x\}_2 \\ j\omega\mu_0\{H_y\}_2 \\ j\omega\mu_0\{H_z\}_2 \end{bmatrix} = \begin{bmatrix} [B]_1\{g\}_1 \\ \{0\} \\ \{0\} \\ \{0\} \\ \{0\} \\ \{0\} \end{bmatrix} \tag{2.33}$$

where

$$[\overline{A}]_{11} = [A]_{11} + [B]_1[Z_{yx}]_1 \tag{2.34a}$$

$$[\overline{A}]_{12} = [A]_{12} + [B]_1[Z_{yy}]_1 \tag{2.34b}$$

$$[\overline{A}]_{21} = [A]_{21} - [B]_1[Z_{xx}]_1 \tag{2.34c}$$

$$[\overline{A}]_{22} = [A]_{22} - [B]_1[Z_{xy}]_1 \tag{2.34d}$$

$$[\overline{A}]_{44} = [A]_{44} + [B]_2[Z_{yx}]_2 \tag{2.34e}$$

$$[\overline{A}]_{45} = [A]_{45} + [B]_2[Z_{yy}]_2 \tag{2.34f}$$

$$[\overline{A}]_{54} = [A]_{54} - [B]_2[Z_{xx}]_2 \tag{2.34g}$$

$$[\overline{A}]_{55} = [A]_{55} - [B]_2[Z_{xy}]_2 \tag{2.34h}$$

$$[B]_i = \sum_{e'} \iint_{e'} k_0^2 \{N\}\{N\}^T|_{\Gamma_i} d\Gamma. \tag{2.35}$$

The same procedure can be applied to (2.9) without a substructure process. The values of $\boldsymbol{H}_t(x,y)$ on $\Gamma_i(i=1,2)$ computed from (2.33) allow the determination of the reflection coefficient S_{11} and the transmission coefficient S_{21} of the TE_{10} mode as follows:

$$S_{11} = \frac{\iint_{\Gamma_1} \boldsymbol{h}^*_{110}(x,y)\cdot j\omega\mu_0 \boldsymbol{H}_t(x,y)\,d\Gamma - j\beta_{10}a_{10}e^{-j\beta_{10}z_1}}{-j\beta_{10}a_{10}e^{j\beta_{10}z_1}} \tag{2.36}$$

$$S_{21} = \frac{\iint_{\Gamma_2} h^*_{110}(x,y)\cdot j\omega\mu_0 \boldsymbol{H}_t(x,y)\,d\Gamma}{j\beta_{10}a_{10}e^{-j\beta_{10}z_2}}. \tag{2.37}$$

2.6 Numerical Results

The problem to be considered is shown in Fig. 2.3. A rectangular dielectric scattering obstacle is placed in a waveguide. The relative permittivity of the dielectric, ε, is 6.0, and d is the distance between the dielectric edge and cross-sectional plane $\Gamma_i(i=1,2)$. When the substructure method is not used, computer memory restricts the finite-element division to 160 (=4×2×4×5) tetrahedral elements as shown in Fig. 2.4.

Figs. 2.5(a), (b), and (c) show the magnitude of reflection coefficient $|S_{11}|$ versus the normalized frequency $k_0 b$ for the penalty coefficients s=0, 1, and 1.44, respectively, where d=0.8b. Figs. 2.6(a), (b), and (c) show the values of u and v related to $|\nabla\cdot\boldsymbol{H}|$ and $|\nabla\times\boldsymbol{H}|$, i.e., $u=|(j\omega\mu_0\{H\})^\dagger[U](j\omega\mu_0\{H\})|$, and $v=|(j\omega\mu_0\{H\})^\dagger[S](j\omega\mu_0\{H\})|$, versus $k_0 b$ for s=0, 1, and 1.44, respectively. It is found from Figs. 2.5(a) and 6(a) that many spurious solutions appear for s=0 at the frequencies where both u and v become rapidly enormous. Figs.

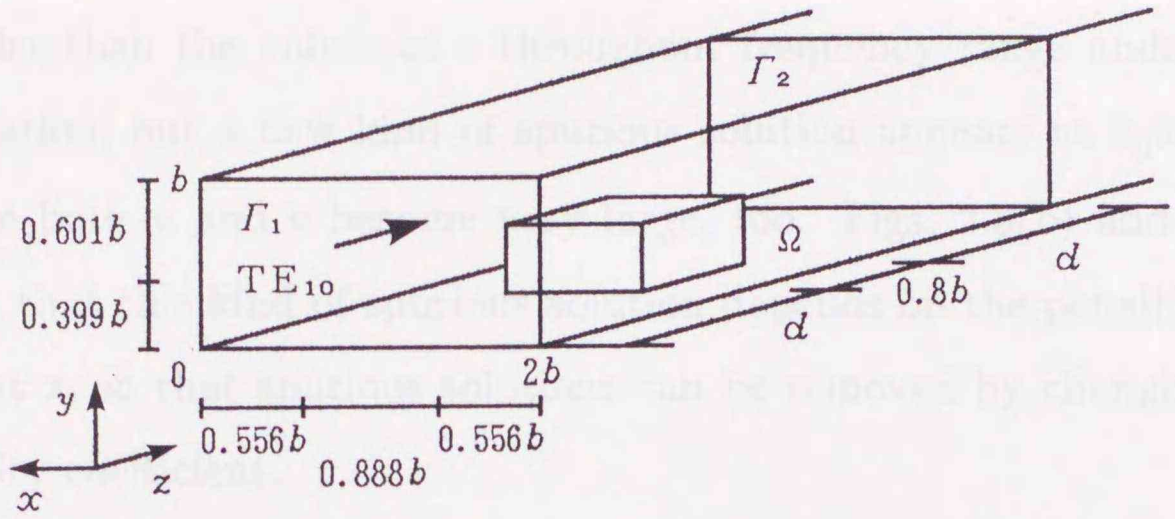

Fig. 2.3. Rectangular dielectric scattering obstacle in a waveguide.

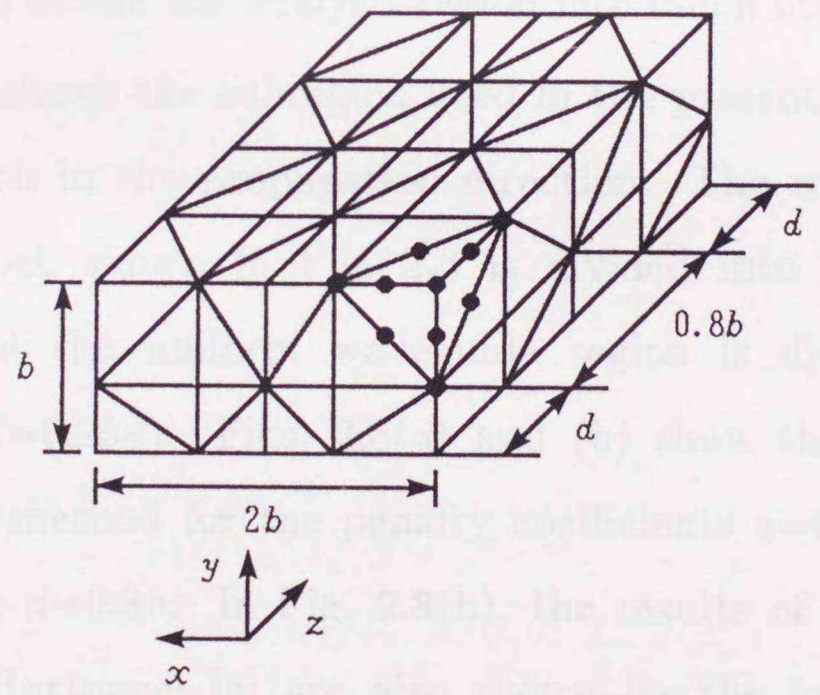

Fig. 2.4. Element division of the region Ω.

2.5(b) and 6(b) show that when s=1, the values of u are much smaller than the values of v throughout frequency range under consideration, but a new kind of spurious solution appears at k_0b=1.97, where both u and v become very large, too. Figs. 2.5(b) and 2.5(c) show that this kind of spurious solution depends on the penalty coefficient s, so that spurious solutions can be removed by changing the penalty coefficient.

In Fig. 2.5(b), the results of the mode matching method [3] and of the finite-difference method (d=4b) [5] are also shown by the broken and solid lines, respectively. Fig. 2.5(b) shows that our results disagree with these results at higher frequencies. This is because the division of the region Ω shown in Fig. 2.4 is not enough to obtain good numerical convergence. So the substructure method should be introduced to divide the analysis region into much more elements.

Fig. 2.7 shows the subregion used in the present analysis, where l is the length in the propagation direction. The region containing dielectric block shown in Fig. 2.3 is divided into four subregions (l=0.2b), and the uniform waveguide region is divided into four subregions (l=0.25d). Figs. 2.8(a) and (b) show the results of the substructure method for the penalty coefficients s=0 and 1, respectively, where d=0.8b. In Fig. 2.8(b), the results of Katzier [3] and Christ and Hartnagel [5] are also shown by the broken and solid lines, respectively. Fig. 2.8(a) shows that if s=0, spurious solution can appear even when the substructure method is introduced in the finite-element method. Fig. 2.8(b) shows that for the penalty coefficient s=1, the spurious solutions cannot appear in the frequency

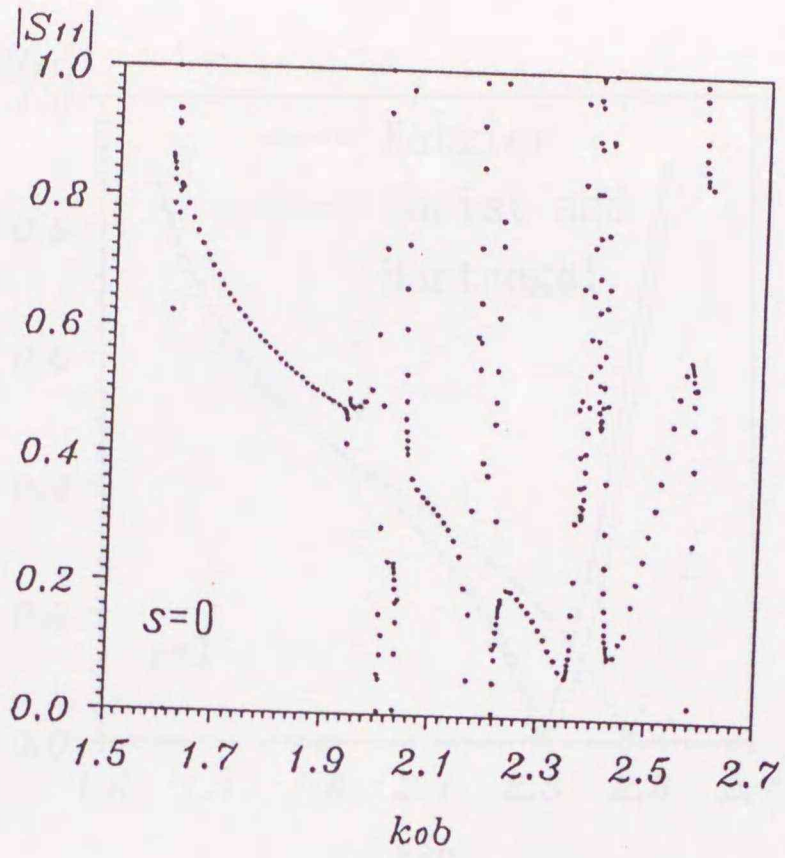

(a)

Fig. 2.5. Dependence of s on $|S_{11}|$'s obtained by using the element division of Fig. 2.4. (a) s=0. (b) s=1. (c) s=1.44.

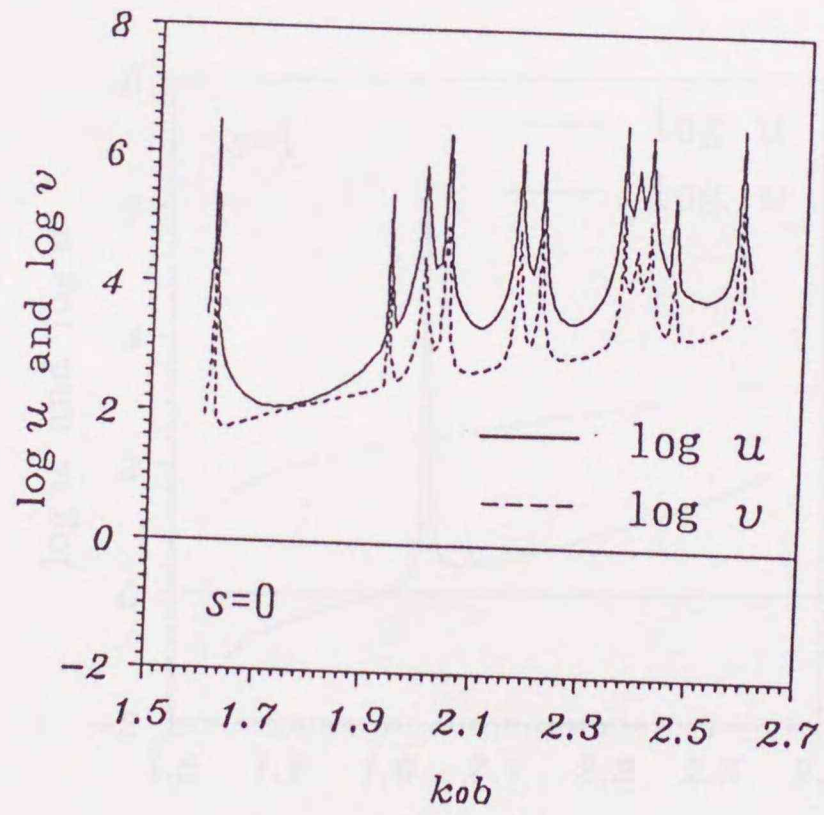

(a)

Fig. 2.6. Dependence of s on u and v obtained by using the element division of Fig. 2.4. (a) s=0. (b) s=1. (c) s=1.44.

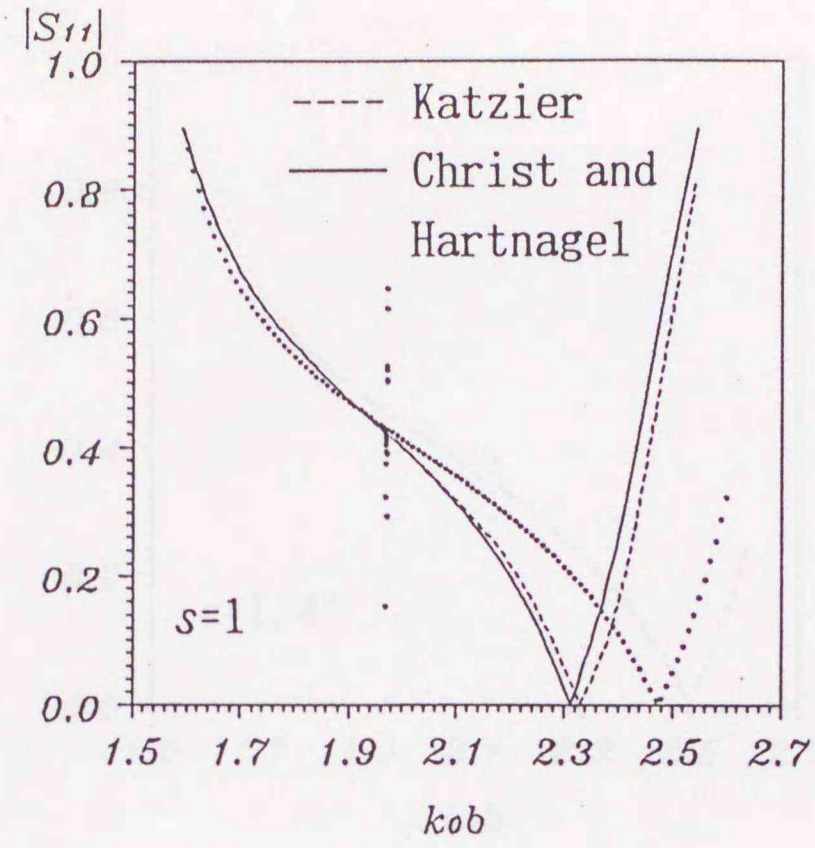

(b)

Fig. 2.5. Dependence of s on $|S_{11}|$'s obtained by using the element division of Fig. 2.4. (a) s=0. (b) s=1. (c) s=1.44.

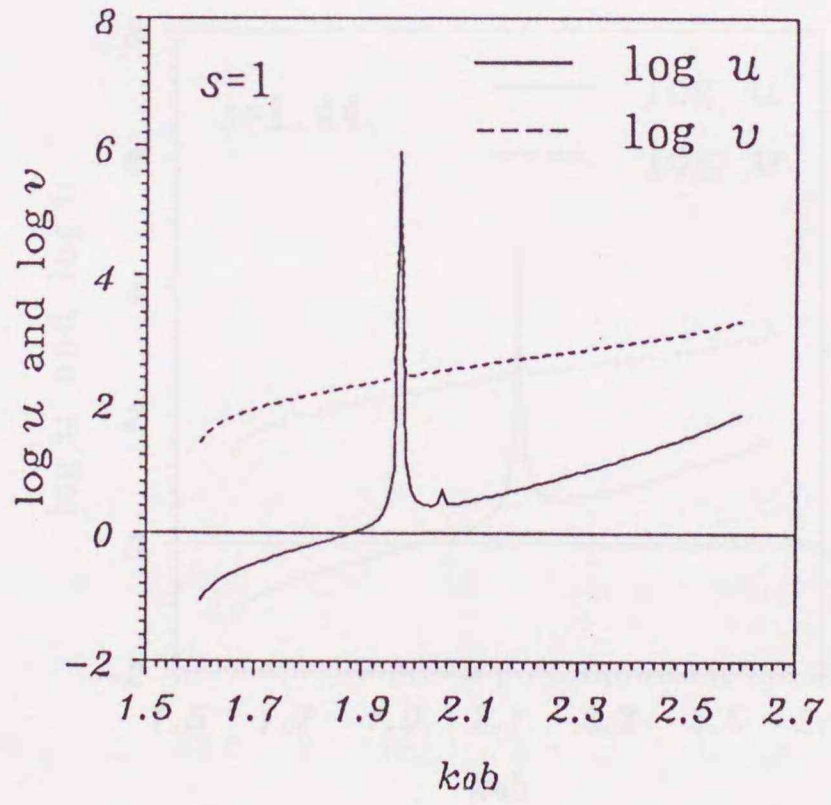

(b)

Fig. 2.6. Dependence of s on u and v obtained by using the element division of Fig. 2.4. (a) s=0. (b) s=1. (c) s=1.4

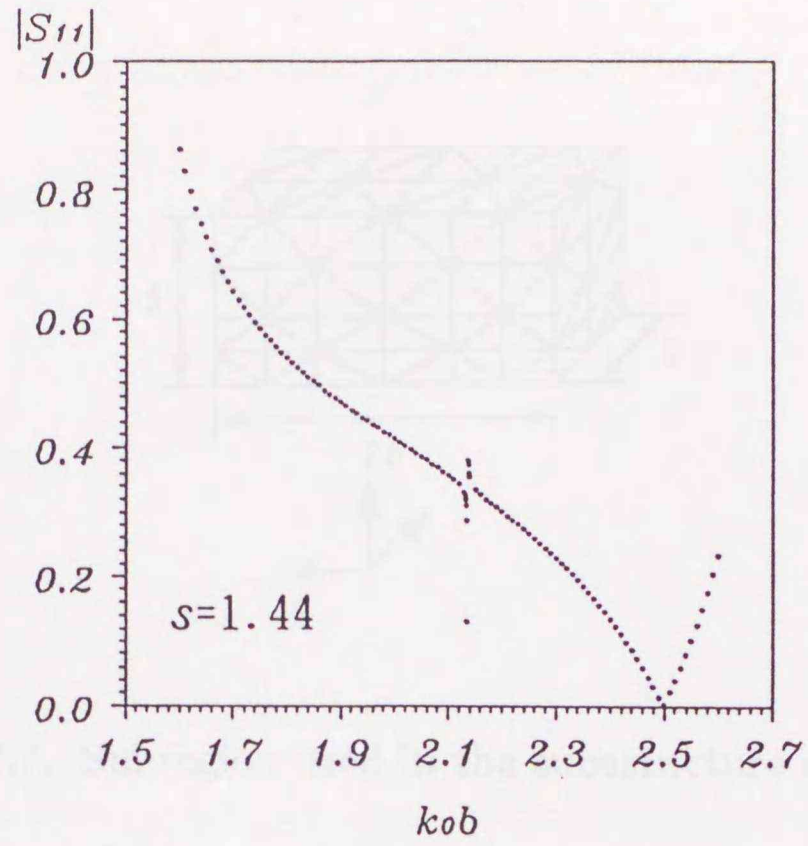

(c)

Fig. 2.5. Dependence of s on $|S_{11}|$'s obtained by using the element division of Fig. 2.4. (a) s=0. (b) s=1. (c) s=1.44.

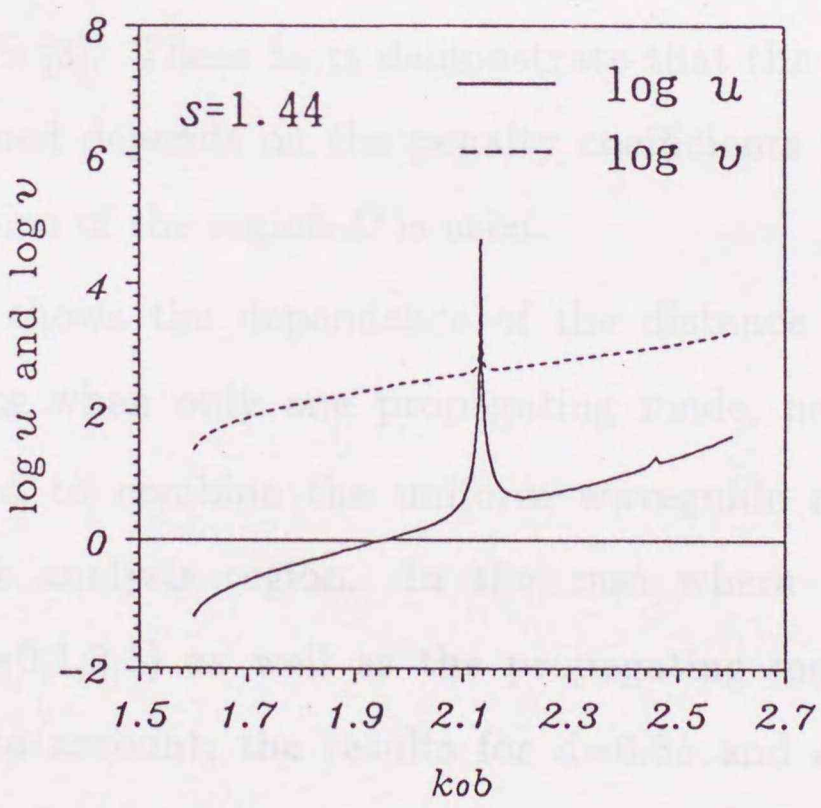

(c)

Fig. 2.6. Dependence of s on u and v obtained by using the element division of Fig. 2.4. (a) s=0. (b) s=1. (c) s=1.44.

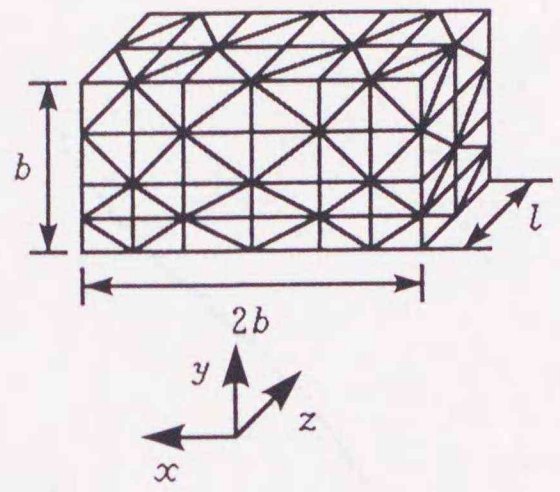

Fig. 2.7. Subregion used in the substructure method.

range under consideration.

Figs. 2.5 and 2.8 show that the results obtained are shifted to higher frequencies as the penalty coefficients become larger, and the true fields obtained by the substructure method for s=0 agree well with Katzier's [3]. These facts demonstrate that the precision of the results obtained depends on the penalty coefficients [53] if the same element division of the region Ω is used.

Fig. 2.9 shows the dependence of the distance d on reflection characteristics when only one propagating mode, namely the TE_{10} mode, is used to combine the uniform waveguide region with the finite-element analysis region. In the case where the evanescent modes (m,n=0,1,2,3) as well as the propagating mode (m=1,n=0) are taken into account, the results for d=0.8b and d=0.1b are also shown in this figure by the dot and square signs, respectively. Fig. 2.9 shows that we should consider the evanescent modes as well as a propagating mode if d is shorter than the height of the waveguide.

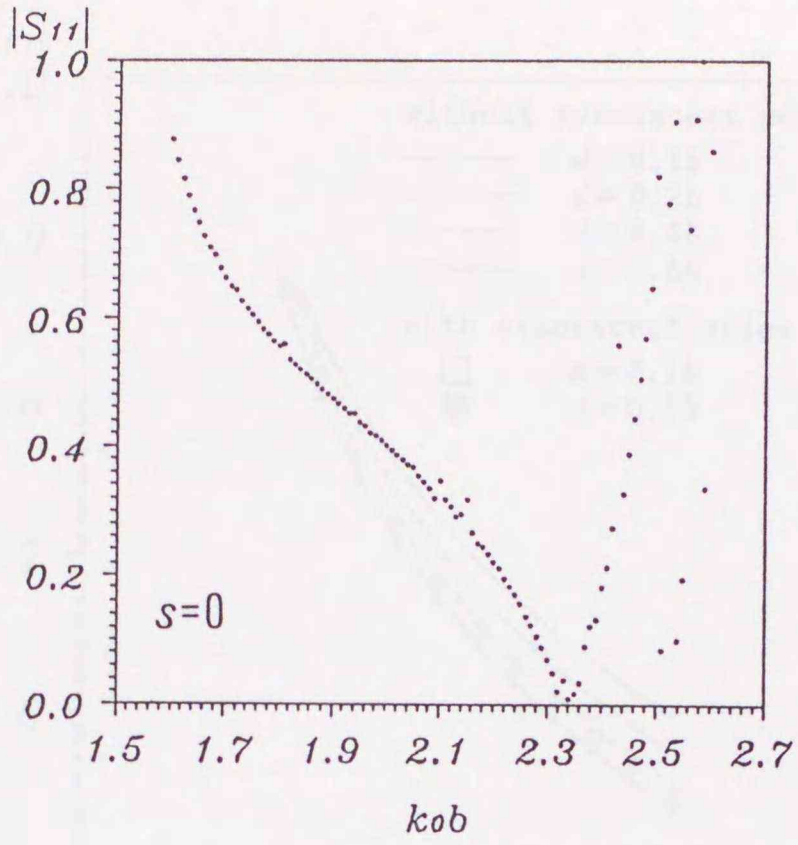

(a)

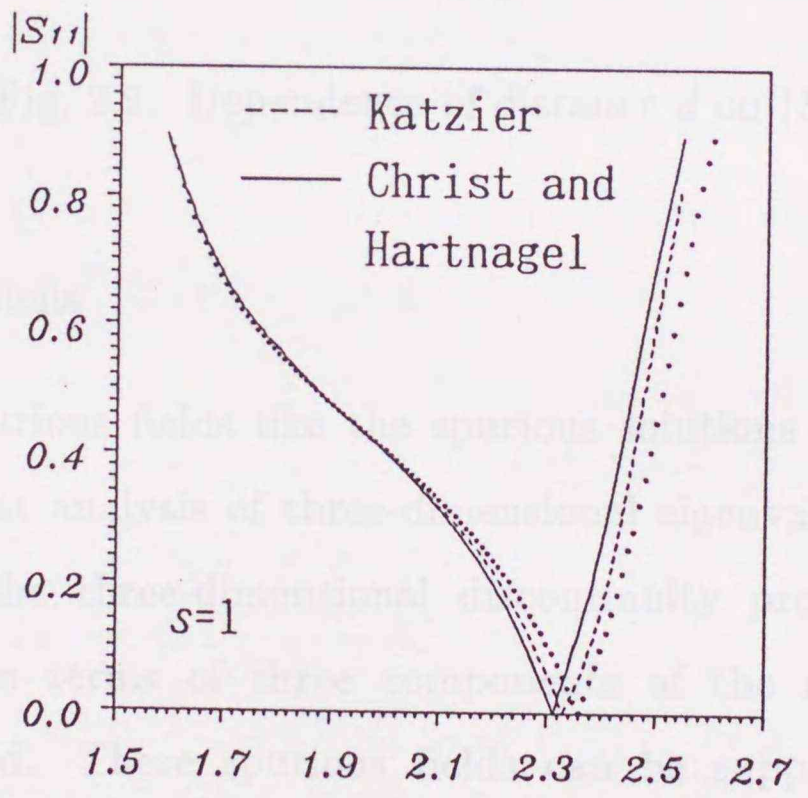

(b)

Fig. 2.8. Dependence of s on $|S_{11}|$'s obtained by using the element division of Fig. 2.7. (a) s=0. (b) s=1.

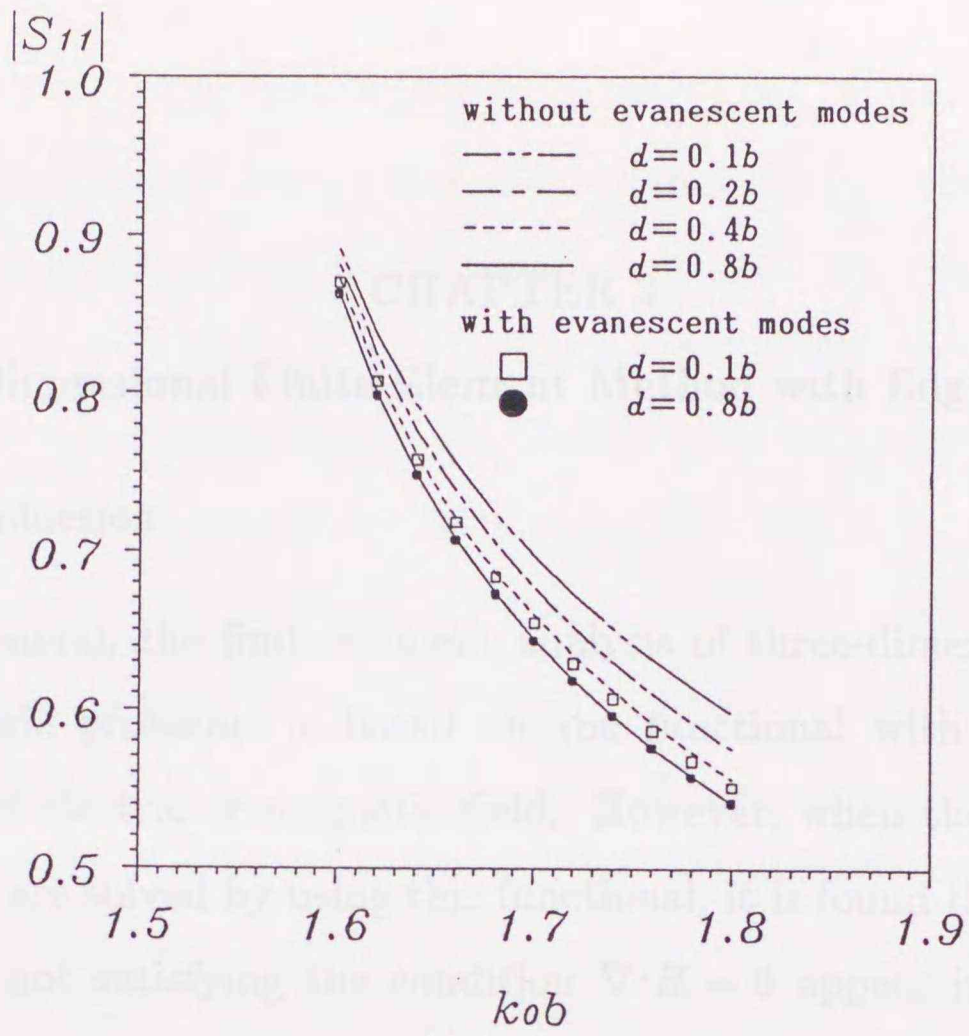

Fig. 2.9. Dependence of distance d on $|S_{11}|$'s.

2.7 Conclusions

The spurious fields like the spurious solutions generated in the finite-element analysis of three-dimensional eigenvalue problems can appear in the three-dimensional discontinuity problems when the functional in terms of three components of the magnetic field is directly used. These spurious fields can be suppressed and eliminated by using the penalty function method. The spurious fields generated in the penalty function method are confirmed to be related to the penalty coefficient.

CHAPTER 3

Three-Dimensional Finite-Element Method with Edge Elements

3.1 Introduction

In general, the finite-element analysis of three-dimensional electromagnetic problems is based on the functional with three components of electric or magnetic field. However, when the eigenvalue problems are solved by using this functional, it is found that spurious solutions not satisfying the condition $\nabla \cdot \boldsymbol{H} = 0$ appear if traditional tetrahedral elements are used [46]–[62].

Recently it has been reported that spurious solutions appear in the three-dimensional electromagnetic discontinuity problems and that the penalty function method is effective for suppression of these spurious solutions, but a new kind of spurious solution dependent on the penalty coefficient is generated [63], [64]. The penalty function method is the one that makes the condition $\nabla \cdot \boldsymbol{H} = 0$ be satisfied in a least-squares manner [46]–[53], [59].

In this paper the method using edge element is introduced to suppress spurious solutions. This method is the one that makes the condition $\nabla \cdot \boldsymbol{H} = 0$ be satisfied in each element. It is confirmed that spurious solutions do not appear when the finite-element method using edge element is applied to the three-dimensional electromagnetic discontinuity problems.

By the way, the finite-element method using three components cannot adequately treat the three-dimensional electromagnetic waveguide problems with metal wedges, because the transverse part of the magnetic or electric field is infinite at a sharp metal edge [77], [78] and the piecewise polynomials traditionally associated with finite elements cannot represent accurately an infinite field.

Webb succeeds in predicting dispersion in the two-dimensional waveguide problems with sharp metal edges by the finite-element method using singular trial functions which model the singular behavior of the field close to sharp edges [78]. However, it may be hard to develop this method and apply it to the three-dimensional problems.

This paper shows that it is difficult to prescribe boundary conditions on fine points of metal wedges when the finite-element method using traditional tetrahedral element is applied to the three-dimensional electromagnetic waveguide problems with metal wedges. On the other hand, variables for edge element are not at vertices but at edges, so that it is unnecessary to prescribe boundary conditions at fine points of metal wedges. We show that edge elements, therefore, may be available for the analysis of arbitrarily shaped waveguides.

3.2 Variational Formulation

The waveguide junction as shown in Fig. 3.1 is considered. The junction may be connected with some rectangular waveguides or may be loaded with arbitrarily shaped dielectric. Here the boundary

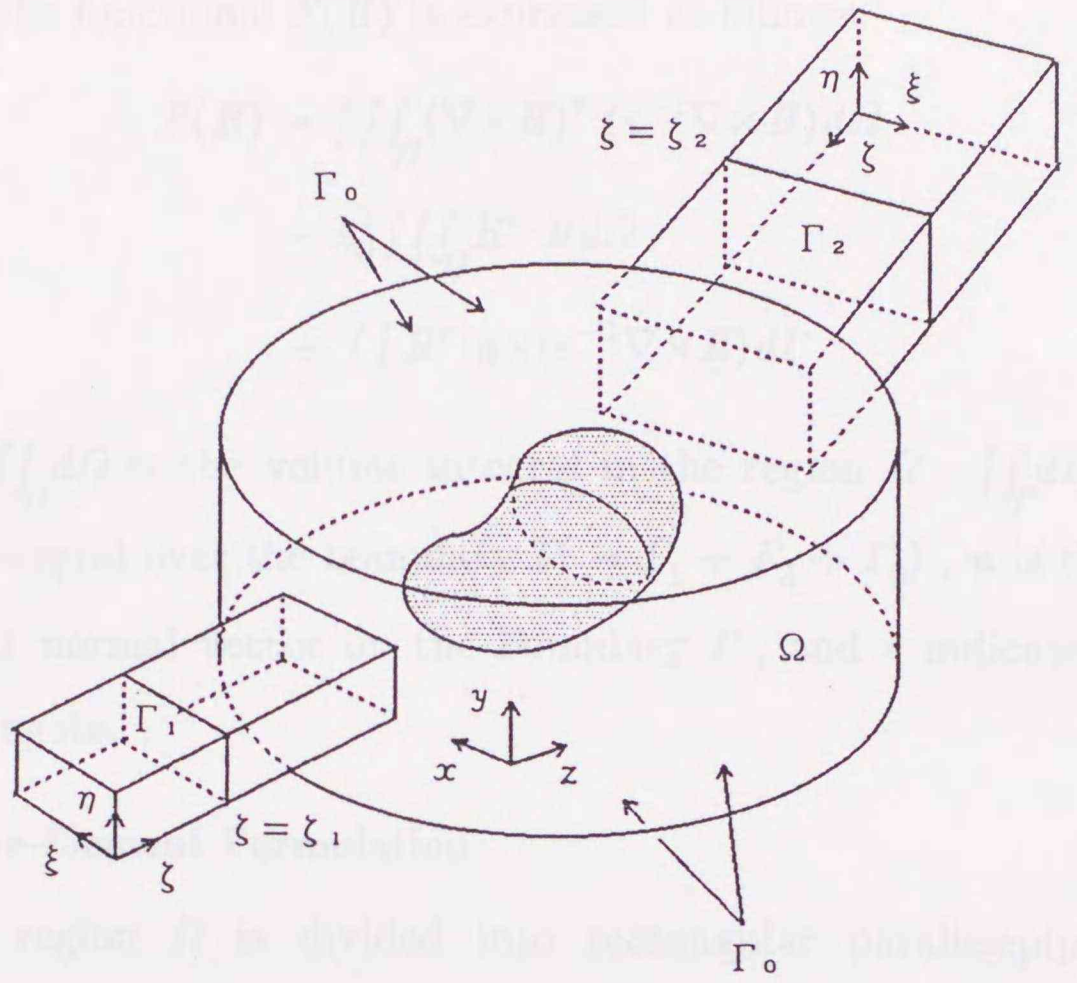

Fig. 3.1. Waveguide discontinuities.

plane Γ_i connects the discontinuity region Ω to the rectangular waveguide $i(i=1, 2)$, and the region Ω surrounded by Γ_1, Γ_2, and Γ_0 encloses the waveguide discontinuities completely. Γ_0 is assumed to be the perfectly-conducting wall.

From Maxwell's equation, the following vectorial wave equation is derived with respect to the magnetic field $\boldsymbol{H}$:

$$\nabla\times(\varepsilon^{-1}\nabla\times\boldsymbol{H}) - k_0^2\boldsymbol{H} = 0 \tag{3.1}$$

where

$$k_0^2 = \omega^2\varepsilon_0\mu_0. \tag{3.2}$$

The problem defined by (3.1) may be formulated variationally [75],

[76] and the functional $F(\boldsymbol{H})$ is expressed as follows:

$$\begin{aligned} F(\boldsymbol{H}) = & \iiint_{\Omega} (\nabla \times \boldsymbol{H})^* \cdot (\varepsilon^{-1} \nabla \times \boldsymbol{H}) \, d\Omega \\ & - k_0^2 \iiint_{\Omega} \boldsymbol{H}^* \cdot \boldsymbol{H} d\Omega \\ & + \iint_{\Gamma} \boldsymbol{H}^* \cdot \boldsymbol{n} \times (\varepsilon^{-1} \nabla \times \boldsymbol{H}) \, d\Gamma \end{aligned} \tag{3.3}$$

where $\iiint_{\Omega} d\Omega$ is the volume integral in the region Ω , $\iint_{\Gamma} d\Gamma$ is the surface integral over the boundary $\Gamma(= \Gamma_1 + \Gamma_2 + \Gamma_0)$, $\boldsymbol{n}$ is the outward unit normal vector on the boundary Γ , and $*$ indicates complex conjugate.

3.3 Finite-Element Formulation

The region Ω is divided into rectangular parallelepipeds as shown in Fig. 3.2. The magnetic field $H_r(r{=}x, y, z)$ in each element is approximated by edge element [79]. In edge element, each edge of a rectangular parallelepiped has a variable which consists of only one component of magnetic field along the direction of the edge. H_r is expanded in terms of the values of H_r at four nodes in the element as follows:

$$H_r = \{N^r\}^T \{H_r\}_e, \qquad r = x, y, z \tag{3.4}$$

where $\{H_r\}_e$ is the nodal magnetic field vector in each element, T indicates a transpose, and the shape function vector $\{N^r\}$ is expressed as

$$\{N^x\} = \begin{bmatrix} N_1^x \\ N_2^x \\ N_3^x \\ N_4^x \end{bmatrix} = \begin{bmatrix} 1/4[1-(y-y_c)/l_y][1-(z-z_c)/l_z] \\ 1/4[1+(y-y_c)/l_y][1-(z-z_c)/l_z] \\ 1/4[1+(y-y_c)/l_y][1+(z-z_c)/l_z] \\ 1/4[1-(y-y_c)/l_y][1+(z-z_c)/l_z] \end{bmatrix} \tag{3.5}$$

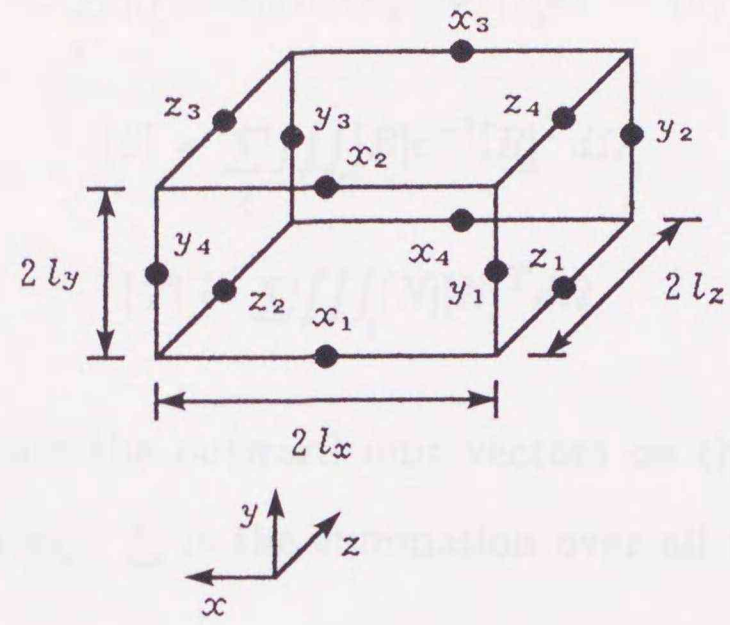

Fig. 3.2. Edge element.

$$\{N^y\} = \begin{bmatrix} N_1^y \\ N_2^y \\ N_3^y \\ N_4^y \end{bmatrix} = \begin{bmatrix} 1/4[1-(z-z_c)/l_z][1-(x-x_c)/l_x] \\ 1/4[1+(z-z_c)/l_z][1-(x-x_c)/l_x] \\ 1/4[1+(z-z_c)/l_z][1+(x-x_c)/l_x] \\ 1/4[1-(z-z_c)/l_z][1+(x-x_c)/l_x] \end{bmatrix} \tag{3.6}$$

$$\{N^z\} = \begin{bmatrix} N_1^z \\ N_2^z \\ N_3^z \\ N_4^z \end{bmatrix} = \begin{bmatrix} 1/4[1-(x-x_c)/l_x][1-(y-y_c)/l_y] \\ 1/4[1+(x-x_c)/l_x][1-(y-y_c)/l_y] \\ 1/4[1+(x-x_c)/l_x][1+(y-y_c)/l_y] \\ 1/4[1-(x-x_c)/l_x][1+(y-y_c)/l_y] \end{bmatrix}. \tag{3.7}$$

Here the coordinate (x_c, y_c, z_c) is the center of gravity of a rectangular parallelepiped shown in Fig. 3.2.

When the finite-element method is applied to (3.3), the following matrix equation is obtained:

$$[S]\{H\} - k_0^2[T]\{H\} + \sum_{e'} \iint_{e'} j\omega\varepsilon_0[N](\boldsymbol{n}_1 \times \boldsymbol{E})|_{\Gamma_1} d\Gamma$$

$$+ \sum_{e'} \iint_{e'} j\omega\varepsilon_0 [N](\boldsymbol{n}_2 \times \boldsymbol{E})|_{\Gamma_2} d\Gamma = \{0\} \tag{3.8}$$

$$[S] = \sum_{e} \iiint_{e} [B]\varepsilon^{-1}[B]^T d\Omega \tag{3.9}$$

$$[T] = \sum_{e} \iiint_{e} [N][N]^T d\Omega. \tag{3.10}$$

Here $\boldsymbol{n}_1$ and $\boldsymbol{n}_2$ are the outward unit vectors on the boundaries Γ_1 and Γ_2 , respectively, $\sum_{e}$ is the summation over all the elements, $\sum_{e'}$ is the summation only over the elements related to the boundaries Γ_1 and Γ_2 ; $\iiint_e d\Omega$ is the volume integral in each edge element, $\iint_e d\Gamma$ is the surface integral on each element in the boundaries Γ_1 and Γ_2 , and $\boldsymbol{E}$ is the electric field vector. The matrices $[B]$ and $[N]$, and the vector $\{H\}$ are given by

$$[B] = \begin{bmatrix} \{0\} & \partial\{N^x\}/\partial z & -\partial\{N^x\}/\partial y \\ -\partial\{N^y\}/\partial z & \{0\} & \partial\{N^y\}/\partial x \\ \partial\{N^z\}/\partial y & -\partial\{N^z\}/\partial x & \{0\} \end{bmatrix} \tag{3.11}$$

$$[N] = \begin{bmatrix} \{N^x\} & \{0\} & \{0\} \\ \{0\} & \{N^y\} & \{0\} \\ \{0\} & \{0\} & \{N^z\} \end{bmatrix} \tag{3.12}$$

$$\{H\} = \begin{bmatrix} \{H_x\} \\ \{H_y\} \\ \{H_z\} \end{bmatrix} \tag{3.13}$$

where $\{H_r\}$ $(r = x, y, z)$ is the vector composed of the value of H_r at all nodes in the whole region Ω and $\{0\}$ is a null vector.

Let $\{H\}_1$ and $\{H\}_2$ be the nodal magnetic field vectors related to the nodes on the boundaries Γ_1 and Γ_2, respectively. Also, let $\{H\}_0$ be the nodal magnetic field vector obtained by removing $\{H\}_1$ and $\{H\}_2$ from $\{H\}$. Then, equation (3.8) is rewritten as

$$\begin{bmatrix} [R]_{11} & [R]_{10} & [R]_{12} \\ [R]_{01} & [R]_{00} & [R]_{02} \\ [R]_{21} & [R]_{20} & [R]_{22} \end{bmatrix} \begin{bmatrix} \{H\}_1 \\ \{H\}_0 \\ \{H\}_2 \end{bmatrix} = \begin{bmatrix} -\sum_{e'} \iint_{e'} j\omega\varepsilon_0 [N](\boldsymbol{n}_1 \times \boldsymbol{E})|_{\Gamma_1} d\Gamma \\ \{0\} \\ -\sum_{e'} \iint_{e'} j\omega\varepsilon_0 [N](\boldsymbol{n}_2 \times \boldsymbol{E})|_{\Gamma_2} d\Gamma \end{bmatrix} \tag{3.14}$$

where $[R]_{11}, \cdots, [R]_{22}$ are the submatrices of the following matrix $[R]$:

$$[R] = [S] - k_0^2 [T]. \tag{3.15}$$

Eliminating $\{H\}_0$ from (3.14), we obtain the following equation:

$$\begin{bmatrix} [P]_{11} & [P]_{12} \\ [P]_{21} & [P]_{22} \end{bmatrix} \begin{bmatrix} \{H\}_1 \\ \{H\}_2 \end{bmatrix} = \begin{bmatrix} -\sum_{e'} \iint_{e'} j\omega\varepsilon_0 [N](\boldsymbol{n}_1 \times \boldsymbol{E})|_{\Gamma_1} d\Gamma \\ -\sum_{e'} \iint_{e'} j\omega\varepsilon_0 [N](\boldsymbol{n}_2 \times \boldsymbol{E})|_{\Gamma_2} d\Gamma \end{bmatrix} \tag{3.16}$$

where

$$[P]_{11} = [R]_{11} - [R]_{10}[R]_{00}^{-1}[R]_{01} \tag{3.17a}$$

$$[P]_{12} = [R]_{12} - [R]_{10}[R]_{00}^{-1}[R]_{02} \tag{3.17b}$$

$$[P]_{21} = [R]_{21} - [R]_{20}[R]_{00}^{-1}[R]_{01} \tag{3.17c}$$

$$[P]_{22} = [R]_{22} - [R]_{20}[R]_{00}^{-1}[R]_{02}. \tag{3.17d}$$

When the division of the region Ω is not sufficient owing to the

restriction of the computer memory, the substructure method is introduced in the finite-element method [63], [64], [70]. This method is as follows: first, the analysis region Ω is divided into some subregions, then the finite-element method is applied to each subregion, and elimination of internal variables is iterated for these subregions, at last the dimension of the matrix equation to be solved can be reduced to the number of the nodes on the input and output boundaries and this dimension is the same as that of (3.16).

3.4 Analytical Formulation

Assuming that the dominant TE_{10} mode is incident from the left of Γ_1 as shown in Fig. 3.1, we may relate the transverse electric field $\boldsymbol{E}_{ti}$ to the transverse magnetic field $\boldsymbol{H}_{ti}$ on the boundary Γ_i $(i = 1, 2)$ as follows [63]:

$$\begin{aligned}\boldsymbol{E}_{ti}(\xi, \eta, \zeta_i) &= \delta_{i1} 2a_{i10} e^{-j\beta_{i10}\zeta_i} \boldsymbol{e}_{110}(\xi, \eta) \\ &- \sum_m \sum_n \frac{1}{j\beta_{imn}} \iint_{\Gamma_i} \boldsymbol{h}^*_{1mn}(\xi', \eta') \cdot j\omega\mu_0 \boldsymbol{H}_{ti}(\xi', \eta')\, d\xi'\, d\eta'\ \boldsymbol{e}_{1mn}(\xi, \eta) \\ &- \sum_m \sum_n \frac{j\beta_{imn}}{-k_0^2} \iint_{\Gamma_i} \boldsymbol{h}^*_{2mn}(\xi', \eta') \cdot j\omega\mu_0 \boldsymbol{H}_{ti}(\xi', \eta')\, d\xi'\, d\eta'\ \boldsymbol{e}_{2mn}(\xi, \eta)\end{aligned} \tag{3.18}$$

where a_{i10} is the amplitude of the incident mode and the propagation constant β_{imn} is given by

$$\beta_{imn} = \sqrt{k_0^2 - (m\pi/a_i)^2 - (n\pi/b_i)^2}. \tag{3.19}$$

The mode functions $\boldsymbol{e}_{lmn}$ and $\boldsymbol{h}_{lmn}$ $(l = 1, 2)$ are given by

(2.23)−(2.27). Equation (3.18) can be discretized as follows:

$$\begin{bmatrix} \{E_\xi\}_i \\ \{E_\eta\}_i \end{bmatrix} = \begin{bmatrix} \{0\} \\ \delta_{i1}\{g\}_i \end{bmatrix} - \begin{bmatrix} [Z_{\xi\xi}]_i & [Z_{\xi\eta}]_i \\ [Z_{\eta\xi}]_i & [Z_{\eta\eta}]_i \end{bmatrix} \begin{bmatrix} j\omega\mu_0\{H_\xi\}_i \\ j\omega\mu_0\{H_\eta\}_i \end{bmatrix} \tag{3.20}$$

where $[Z_{\xi\xi}]$, $\cdots$, $[Z_{\eta\eta}]$ are the matrices obtained by discretization of (3.18), and $\{g\}_i$ is given by (2.32).

Letting $[A]_{11}, [A]_{12}, \cdots, [A]_{44}$ be the submatrices of $[P]_{11}, \cdots, [P]_{22}$ of (3.16), and combining (3.16) with (3.20), the final matrix equation is obtained as follows:

$$\begin{bmatrix} [\overline{A}]_{11} & [\overline{A}]_{12} & [A]_{13} & [A]_{14} \\ [\overline{A}]_{21} & [\overline{A}]_{22} & [A]_{23} & [A]_{24} \\ [A]_{31} & [A]_{32} & [\overline{A}]_{33} & [\overline{A}]_{34} \\ [A]_{41} & [A]_{42} & [\overline{A}]_{43} & [\overline{A}]_{44} \end{bmatrix} \begin{bmatrix} j\omega\mu_0\{H_\xi\}_1 \\ j\omega\mu_0\{H_\eta\}_1 \\ j\omega\mu_0\{H_\xi\}_2 \\ j\omega\mu_0\{H_\eta\}_2 \end{bmatrix} = \begin{bmatrix} [B]_1^\eta\{g\}_1 \\ \{0\} \\ \{0\} \\ \{0\} \end{bmatrix} \tag{3.21}$$

where

$$[\overline{A}]_{11} = [A]_{11} + [B]_1^\eta\,[Z_{\eta\xi}]_1 \tag{3.22a}$$

$$[\overline{A}]_{12} = [A]_{12} + [B]_1^\eta\,[Z_{\eta\eta}]_1 \tag{3.22b}$$

$$[\overline{A}]_{21} = [A]_{21} - [B]_1^\xi\,[Z_{\xi\xi}]_1 \tag{3.22c}$$

$$[\overline{A}]_{22} = [A]_{22} - [B]_1^\xi\,[Z_{\xi\eta}]_1 \tag{3.22d}$$

$$[\overline{A}]_{33} = [A]_{33} + [B]_2^\eta\,[Z_{\eta\xi}]_2 \tag{3.22e}$$

$$[\overline{A}]_{34} = [A]_{34} + [B]_2^\eta\,[Z_{\eta\eta}]_2 \tag{3.22f}$$

$$[\overline{A}]_{43} = [A]_{43} - [B]_2^\xi\,[Z_{\xi\xi}]_2 \tag{3.22g}$$

$$[\overline{A}]_{44} = [A]_{44} - [B]_2^\xi\,[Z_{\xi\eta}]_2 \tag{3.22h}$$

$$[B]_i^\xi = \sum_{e'} \iint_{e'} k_0^2 \{N^\eta\}\{N^\xi\}^T|_{\Gamma_i} d\Gamma \tag{3.23a}$$

$$[B]_i^{\eta} = \sum_{e'} \iint_{e'} k_0^2 \{N^{\xi}\}\{N^{\eta}\}^T|_{\Gamma_i} d\Gamma. \tag{3.23b}$$

Here ξ and η directions on Γ_i $(i = 1, 2)$ correspond to ξ and η shown in Fig. 3.1, respectively. The values of $H_{ti}(\xi, \eta)$ on Γ_i computed from (3.21) allow the determination of the reflection coefficient S_{11} and the transmission coefficient S_{21} of the TE_{10} mode as follows:

$$S_{11} = \frac{\iint_{\Gamma_1} \boldsymbol{h}_{110}^*(\xi, \eta) \cdot j\omega\mu_0 \boldsymbol{H}_{t1}(\xi, \eta)\, d\Gamma - j\beta_{110} a_{110} e^{-j\beta_{110}\zeta_1}}{- j\beta_{110}\, a_{110}\, e^{j\beta_{110}\zeta_1}} \tag{3.24}$$

$$S_{21} = \sqrt{\frac{\beta_{210}}{\beta_{110}}}\, \frac{\iint_{\Gamma_2} \boldsymbol{h}_{110}^*(\xi, \eta) \cdot j\omega\mu_0 \boldsymbol{H}_{t2}(\xi, \eta)\, d\Gamma}{- j\beta_{210}\, a_{110}\, e^{j\beta_{210}\zeta_2}}. \tag{3.25}$$

3.5 Numerical Results

First, a waveguide loaded with dielectric is considered. When the discontinuity problem as shown in Fig. 2.3 is solved by the finite-element method using the functional (3.3), it has been found that spurious solutions appear if the traditional tetrahedral elements are used [63], [64] as shown in Chapter 2.

Figs. 3.3 and 3.4 show the element division with edge elements and the reflection characteristics, respectively. It is found from Fig. 3.4 that spurious solution does not appear. The finite-element method using edge element is more effective for suppression of spurious solutions than the method using the penalty function method, because a new spurious solution dependent on the penalty coefficient is generated when the penalty function method is introduced in the

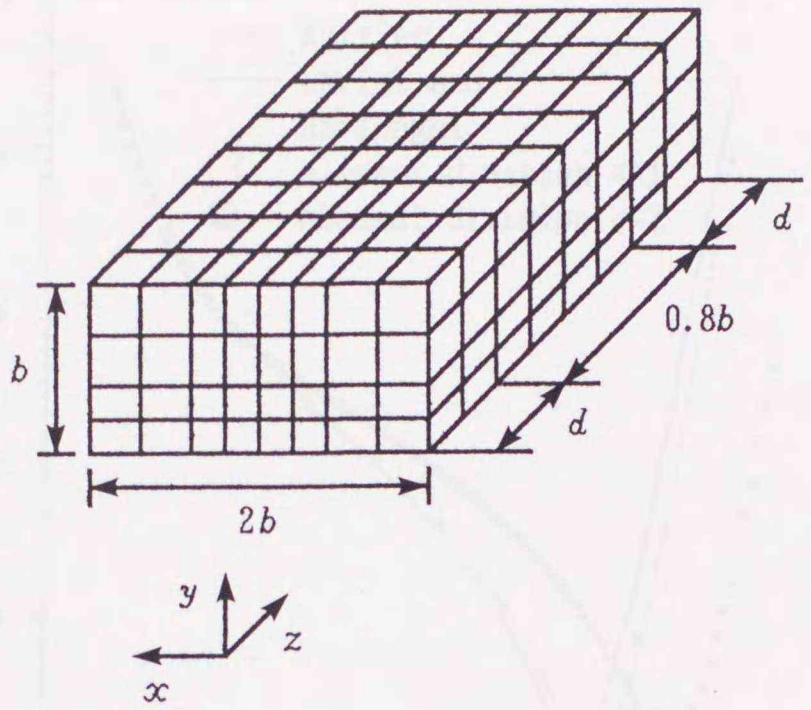

(a)

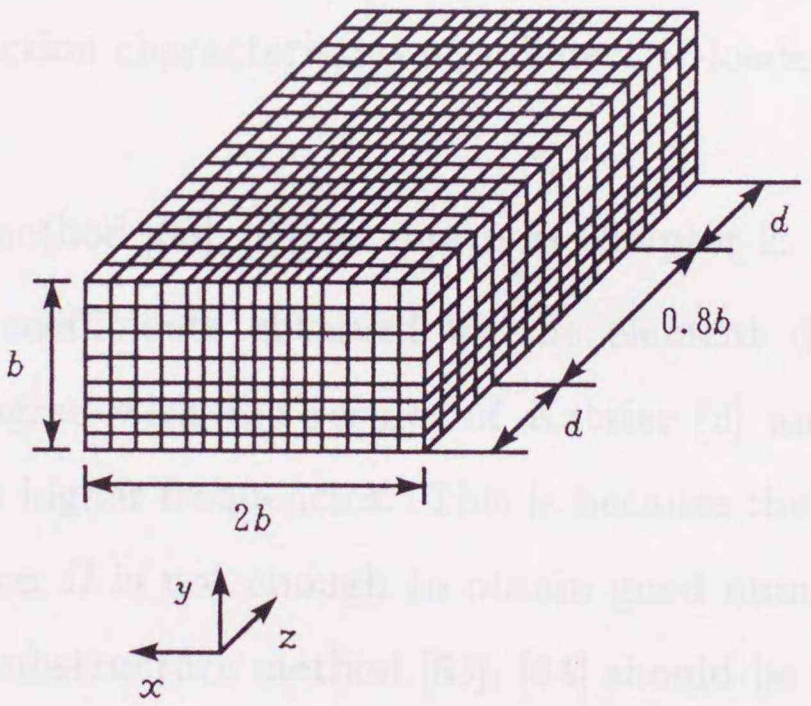

(b)

Fig. 3.3. Element division using edge elements ($d = 0.8b$).
(a) Element division #1. (b) Element division #2.

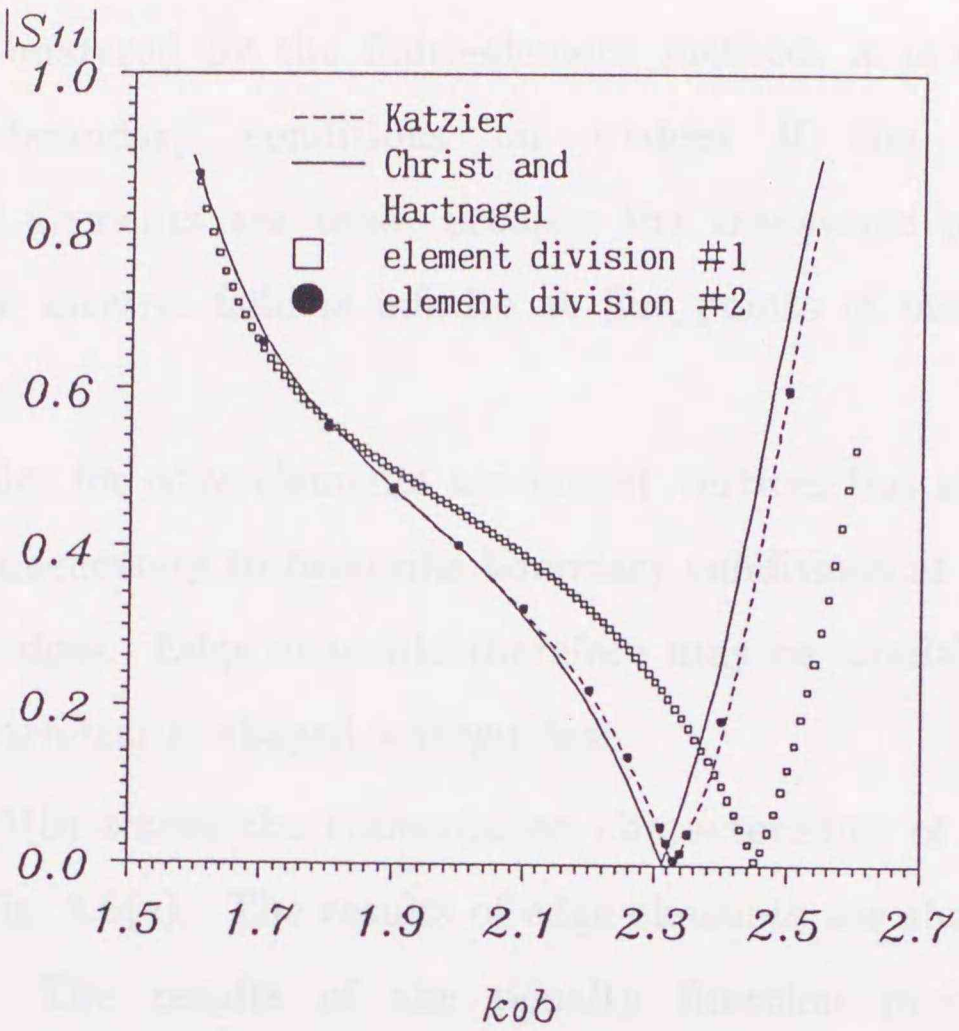

Fig. 3.4. Reflection characteristics of a dielectric-loaded waveguide.

finite-element method [63], [64] as shown in Chapter 2.

Reflection coefficients obtained by the element division #1 in Fig. 3.3(a) disagree with the results of Katzier [3] and Christ and Hartnagel [5] at higher frequencies. This is because the element division of the region Ω is not enough to obtain good numerical convergence. So the substructure method [63], [64] should be introduced to divide the analysis region into much more elements. The results obtained by the element division #2 in Fig. 3.3(b) for which the substructure method is used agree well with other results [3], [5].

Then, arbitrarily shaped waveguides are considered. When the waveguides with metal wedges as shown in Figs. 3.5(a), 3.6(a), and

3.7(a) are analyzed by the finite-element method, it is difficult to prescribe boundary conditions on wedges if the traditional tetrahedral elements are used, because the transverse part of the magnetic or electric field is infinite at fine points of metal wedges [77], [78].

Variables for edge elements are not at vertices but at edges, so that it is unnecessary to prescribe boundary conditions at fine points of metal wedges. Edge elements therefore may be available for the analysis of arbitrarily shaped waveguides.

Fig. 3.5(b) shows the transmission characteristics of waveguide shown in Fig. 3.5(a). The results of edge elements are shown by the solid line. The results of the penalty function method using tetrahedral elements in which the field is left free at fine points of a metal wedge and the normal magnetic field is set zero there are, respectively, represented by dots and squares, where the penalty coefficient s [46]–[53], [63], [64] is 1. The results of the edge elements agree well with those of the two-dimensional finite-element method [35] and boundary-element method [45].

In [34], Picon says that the finite-element method with tetrahedral elements based on three components of electric field succeeds in solving the problems with metal wedges if the condition $\nabla \cdot E = 0$ is imposed on the functional. We also confirm that when the penalty function method is introduced in the finite-element method with tetrahedral elements, stable field distribution is obtained. But it is clearly seen from Fig. 3.5(b) that even if the penalty function method is used, correct solutions are not always

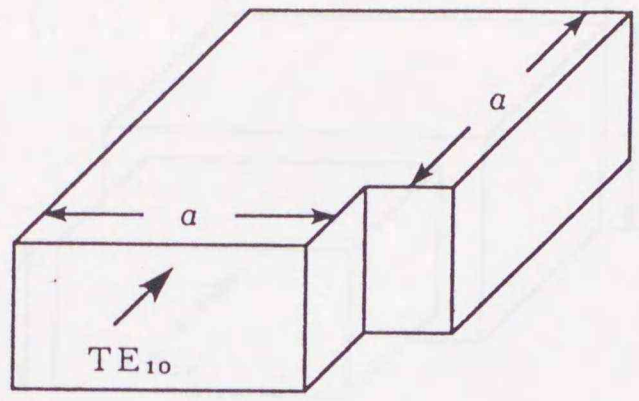

(a)

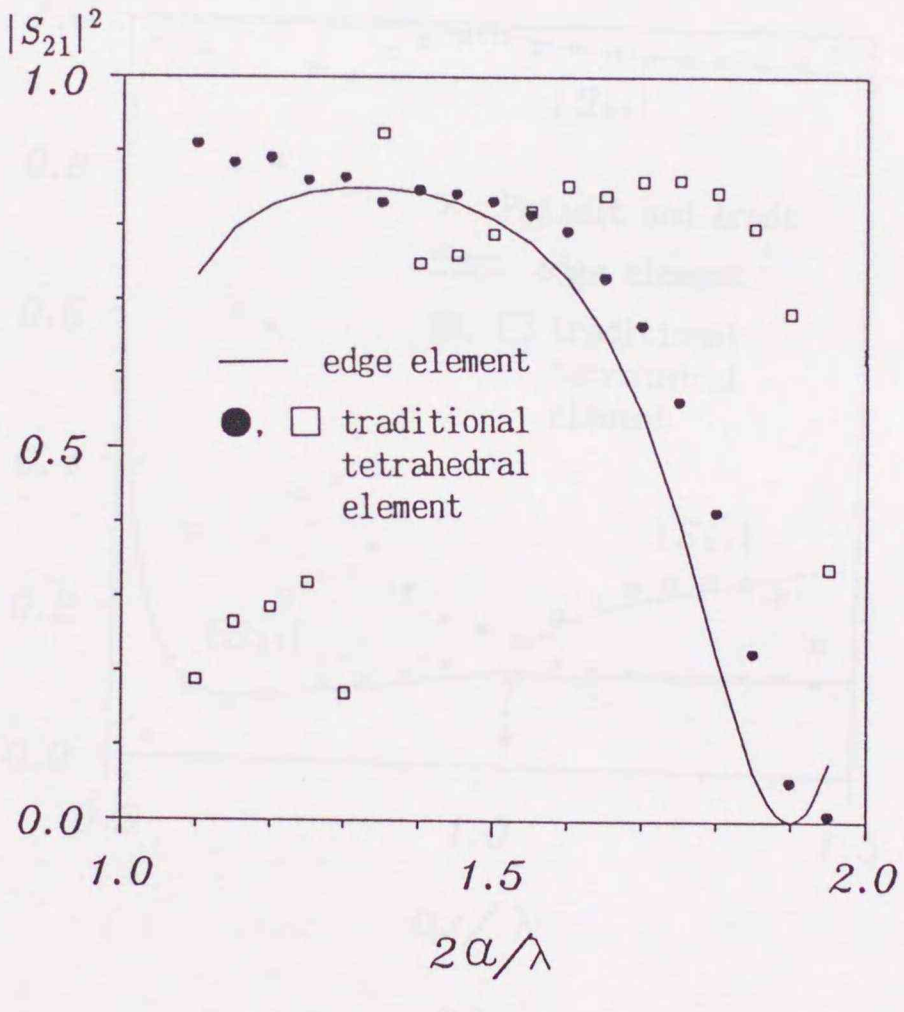

(b)

Fig. 3.5. Right-angle corner bend.
(a) Structure. (b) Power transmission coefficient.

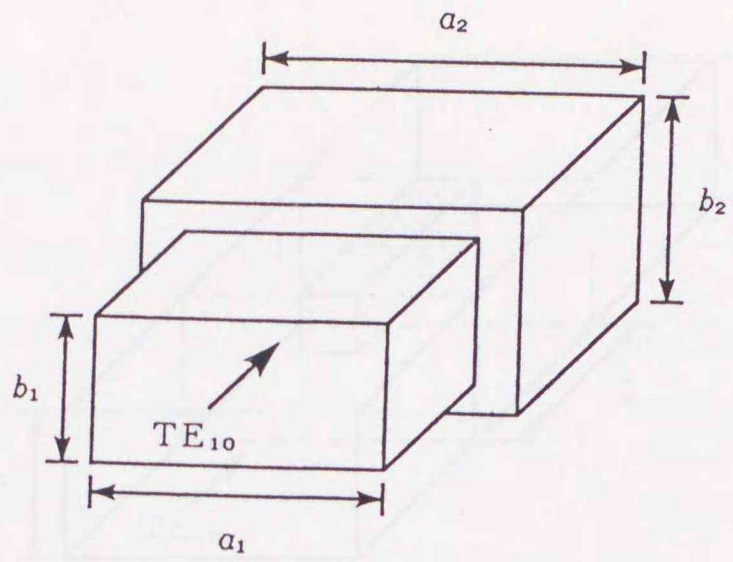

(a)

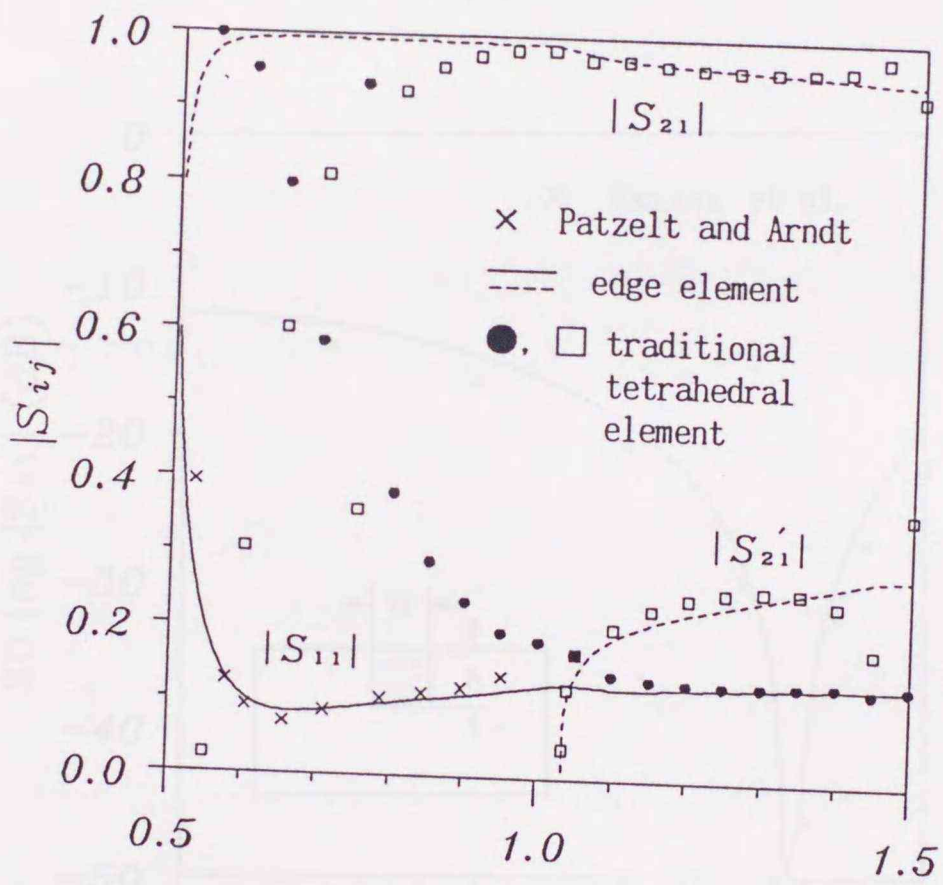

(b)

Fig. 3.6. Concentric step discontinuity.
(a) Structure ($a_1 = 15.8$ mm, $b_1 = 7.9$ mm, $a_2 = 22.9$ mm, $b_2 = 10.2$ mm).
(b) Scattering characteristics ($|S_{21}'|$ is the magnitude of transmission coefficient of TE_{30} mode).

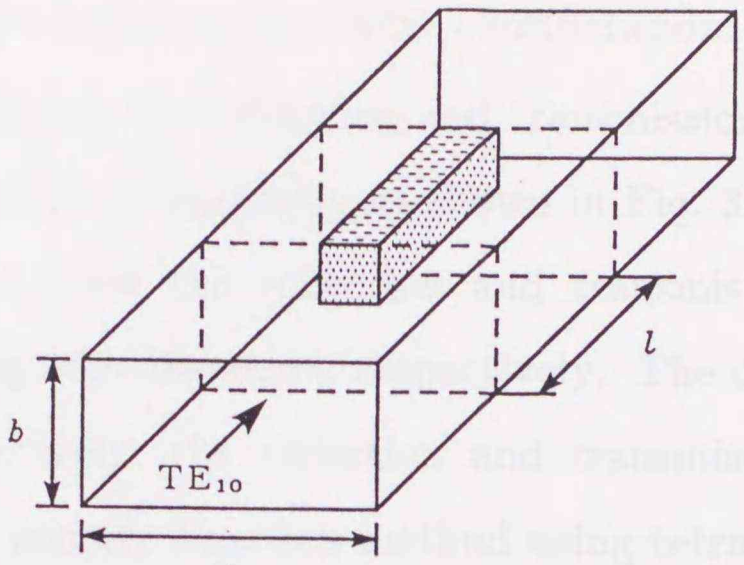

(a)

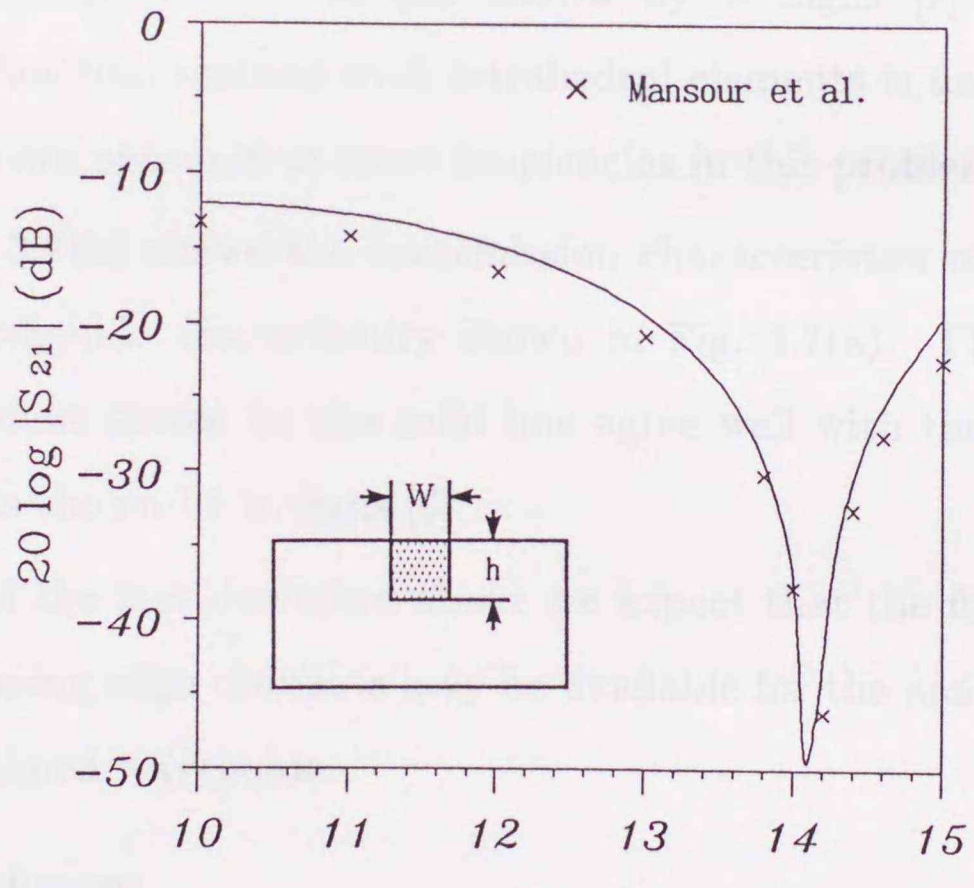

(b)

Fig. 3.7. *E*-plane ridge waveguide discontinuity.
(a) Structure ($a = 19.05$ mm, $b = 9.524$ mm, $l = 5.08$ mm, $W = 1.016$ mm, $h = 7.619$ mm).
(b) Transmission characteristics.

obtained in the frequency range under consideration.

Fig. 3.6(b) shows the reflection and transmission characteristics of a concentric step discontinuity as shown in Fig. 3.6(a). The solid and broken lines show the reflection and transmission coefficients obtained by using edge elements, respectively. The dots and squares represent, respectively, the reflection and transmission coefficients obtained by the penalty function method using tetrahedral elements in which the field is left free at fine points of metal wedges and the penalty coefficient s is 1. The results of edge elements agree well with the experimental results shown by $\times$ signs [2]. When the penalty function method with tetrahedral elements is used, incorrect solutions are obtained at some frequencies in this problem, too.

Fig. 3.7(b) shows the transmission characteristics of an E-plane ridge waveguide discontinuity shown in Fig. 3.7(a). The results of edge element shown by the solid line agree well with the experimental results shown by $\times$ signs [6].

From the fact described above we expect that the finite-element method using edge elements may be available for the analysis of arbitrarily shaped waveguides.

3.6 Conclusions

When the finite-element method using edge elements is applied to the three-dimensional electromagnetic discontinuity problems, spurious solutions do not appear. Moreover, this method is successfully applied to the three-dimensional problems with metal wedges.

CHAPTER 4

A Combination Method of Finite and Boundary Elements

4.1 Introduction

A significant number of studies on scattering by the obstacles in a waveguide have been reported for many years. Marcuvitz's *Waveguide Handbook* [7] describes the equivalent circuit parameters for inductive obstacles and dielectric posts in a rectangular waveguide. Leviatan, Li *et al.* [13], [16], and Auda and Harrington [17] have studied inductive posts and diaphragms in a rectangular waveguide by the moment method. Vahldieck *et al.* [15] have given the design for a metal insert filter by the method of field expansion into eigenmodes.

Nielsen [10] by the modal expansion method, Araneta [18] by adding one more terms in the variational expressions given by Schwinger, and Sahalos and Vafiadis [21] by a method similar to Nielsen's [10] using not a rectangular interaction region but a circular one have dealt with the discontinuity problem of a circular cylindrical dielectric post centered in a rectangular waveguide. Hsu and Auda [22] and Leviatan and Sherfer [23] have by the moment method given analyses of homogeneous dielectric posts of arbitrary shape, size, location, and number, lossy as well as lossless in a rectangular waveguide. Arndt *et al.* [14], [20] have designed dielectric-

slab-filled waveguide phase shifters by the method of field expansion into eigenmodes.

Davies [9] has by the modal expansion method proposed an analysis for a symmetrical waveguide junction circulator with a circular ferrite post. Okamoto [12] has by the method based on integral equations analyzed waveguide junctions with arbitrarily shaped ferrite posts. Uher *et al.* [24] have designed ferrite-slab-loaded waveguide nonreciprocal phase shifters by the method of field expansion into eigenmodes.

Recently, Koshiba *et al.* [35]–[37], Webb and Parihar [38], and Lee and Cendes [39] have analyzed the *H*-plane waveguide junctions by the finite-element method (FEM). The FEM is very useful for arbitrarily shaped discontinuities including inhomogeneous and anisotropic media. However, it requires large computer memory and long computation time to solve the final matrix equation. More recently, Kagami and Fukai [42], and Koshiba and Suzuki [45] have studied the *H*-plane waveguide junctions by the boundary-element method (BEM). The BEM is one of the "boundary" type methods based on the integral equation method. It is therefore possible to reduce the matrix dimension and to use computer memory more economically compared with a "domain" type method, such as the FEM. However, the BEM cannot be effectively applied to a problem involving inhomogeneous and anisotropic media.

This paper presents a numerical method for the solution of scattering of *H*-plane waveguide junctions with arbitrary cross sections where junctions are allowed to be loaded with dielectric or

ferrite of arbitrary shape, size, and location, lossy as well as lossless. This approach is a combination of the finite and boundary element methods (CFBEM). The waveguide junction is divided into two regions. One is the inhomogeneous region with dielectric or ferrite, and the other is the homogeneous region without dielectric or ferrite. The FEM and BEM are applied to the inhomogeneous and homogeneous regions, respectively. The finite-element can be combined with the boundary-element on the common nodal points because these two methods are discretized in the same way. Also, analytical solutions are used for the uniform waveguides connected to the junctions.

Discontinuity problems with a large homogeneous region or with variation of the location of an inhomogeneous region can be effectively treated by the CFBEM. To show the validity and usefulness of this method, a lossy dielectric post and a ferrite slab in a rectangular waveguide are investigated in detail, and the computed results are compared with earlier theoretical and experimental results.

Mei [80] has proposed a unimoment method in which the finite-difference or finite-element method is used together with integral equations or harmonic expansions. However, it seems that this method has not been fully applied to waveguide junctions with inhomogeneous and anisotropic media.

4.2 Basic Equations

The waveguide junction shown in Fig. 4.1 is investigated, where the boundary Γ_i connects the discontinuities to the rectangular

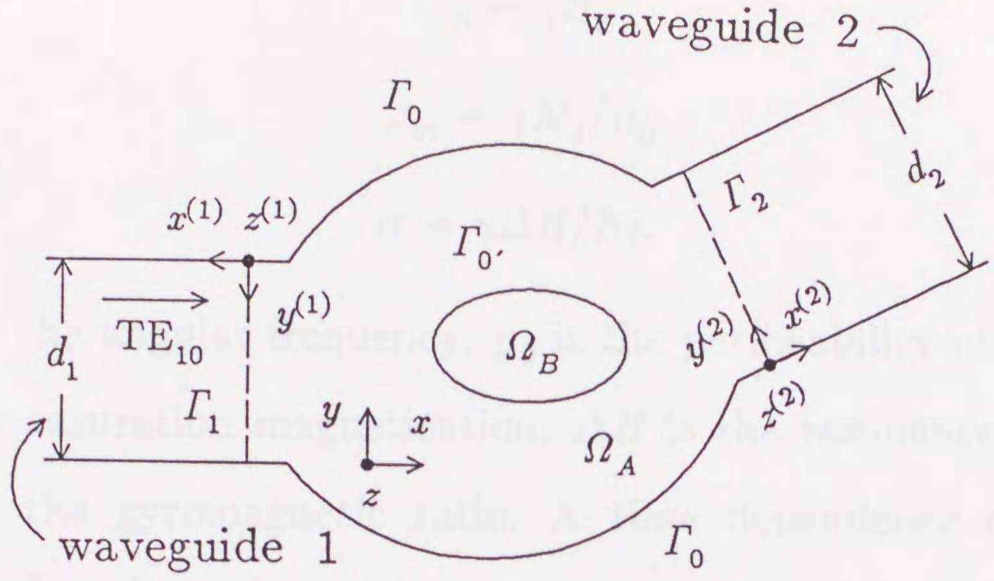

Fig. 4.1. H-plane waveguide junction.

waveguide $i(i=1,2)$, d_i is the width of the waveguide for the H-plane junction, $\Gamma_{0'}$ encloses the region Ω_B containing the dielectric or ferrite, Γ_0 is the short-circuit boundary, the region Ω_A is surrounded by the Γ_1, Γ_2, $\Gamma_{0'}$, and Γ_0, and the boundaries Γ_1, Γ_2, and Γ_0 enclose the waveguide discontinuities completely. Besides, the dielectric or ferrite is assumed to be full height and to be uniform along the z axis.

For a dc magnetic field H_0 in the z direction, the permeability tensor for ferrite takes on the form

$$[\mu] = \mu_0 \begin{bmatrix} \mu & -j\kappa & 0 \\ j\kappa & \mu & 0 \\ 0 & 0 & 1 \end{bmatrix} \tag{4.1}$$

where

$$\mu = 1 + \frac{(\omega_0 + j\omega\alpha)\omega_m}{(\omega_0 + j\omega\alpha)^2 - \omega^2} \tag{4.2}$$

$$\kappa = -\frac{\omega\omega_m}{(\omega_0 + j\omega\alpha)^2 - \omega^2} \tag{4.3}$$

$$\omega_0 = \gamma H_0 \tag{4.4}$$

$$\omega_m = \gamma M_s/\mu_0 \tag{4.5}$$

$$\alpha = \gamma \Delta H/2\omega. \tag{4.6}$$

Here ω is the angular frequency, μ_0 is the permeability of free space, M_s is the saturation magnetization, ΔH is the resonance linewidth, and γ is the gyromagnetic ratio. A time dependence $\exp(j\omega t)$ is assumed. For the region without ferrite $\mu = 1$ and $\kappa = 0$ in (4.1).

Considering the excitation by the dominant TE_{10} mode, we have the following basic equations for the field E_z, H_x, and H_y because the fields do not vary with the z axis [37]:

$$\frac{\partial H_y}{\partial x} - \frac{\partial H_x}{\partial y} = j\omega\varepsilon_0\varepsilon E_z \tag{4.7}$$

$$H_x = \frac{1}{j\omega\mu_0(\mu^2 - \kappa^2)}\left\{ -\mu\frac{\partial E_z}{\partial y} + j\kappa\frac{\partial E_z}{\partial x}\right\} \tag{4.8}$$

$$H_y = \frac{1}{j\omega\mu_0(\mu^2 - \kappa^2)}\left\{ \mu\frac{\partial E_z}{\partial x} + j\kappa\frac{\partial E_z}{\partial y}\right\} \tag{4.9}$$

where

$$\varepsilon = \varepsilon' - j\varepsilon''. \tag{4.10}$$

Here ε_0 is the permittivity of free space and ε is the relative permittivity.

4.3 Boundary-Element Formulation

For $\varepsilon = 1$, $\mu = 1$, and $\kappa = 0$ in the region Ω_A, from (4.7)$-$(4.9) we obtain the following Helmholtz equation:

$$\left[\frac{\partial^2}{\partial x^2}+\frac{\partial^2}{\partial y^2}\right]\phi + k_0^2\phi = 0 \tag{4.11}$$

where ϕ is E_z and $k_0^2 = \omega^2\varepsilon_0\mu_0$.

Applying the boundary-element method with the quadratic line element to the region Ω_A, the following matrix equation is obtained [42], [45], [68], [71]:

$$\begin{bmatrix}[H]_1 & [H]_2 & [H]_{0'} & [H]_0\end{bmatrix}\begin{bmatrix}\{\phi\}_1^A\\ \{\phi\}_2^A\\ \{\phi\}_{0'}^A\\ \{\phi\}_0^A\end{bmatrix}$$

$$= \begin{bmatrix}[G]_1 & [G]_2 & [G]_{0'} & [G]_0\end{bmatrix}\begin{bmatrix}\{\psi\}_1^A\\ \{\psi\}_2^A\\ \{\psi\}_{0'}^A\\ \{\psi\}_0^A\end{bmatrix} \tag{4.12}$$

where ψ is $\partial E_z/\partial n$, i.e., the outward normal derivative of E_z, and the subscripts 1, 2, $0'$, and 0 denote the quantities corresponding to the boundaries Γ_1, Γ_2, $\Gamma_{0'}$, and Γ_0 in Fig. 4.1, respectively.

4.4 Finite-Element Formulation

Dividing the region Ω_B into a number of quadratic triangular elements Ω_e's, using a Galerkin procedure on (4.7) over the element Ω_e, and considering the contribution of all elements, we obtain the following matrix equation [37], [68], [71]:

$$[A]\{\phi\}^B = [B]_{0'}\{\psi\}_{0'}^B \tag{4.13}$$

$$[A] = \sum_e \iint_e \frac{1}{\mu^2 - \kappa^2} \big[\mu\big(\{N_x\}\{N_x\}^T + \{N_y\}\{N_y\}^T\big) + j\kappa\big(\{N_x\}\{N_y\}^T - \{N_y\}\{N_x\}^T\big) - k_0^2\varepsilon\{N\}\{N\}^T\big] dxdy \tag{4.14}$$

$$[B]_{0'} = \sum_{e'} \int_{e'} \{N\}\{N\}^T d\Gamma \tag{4.15}$$

where $\{N\}$ is the shape function vector, $\{N_x\} \equiv \partial\{N\}/\partial x$, $\{N_y\} \equiv \partial\{N\}/\partial y$, T denotes a transpose, $\iint_e dxdy$ is carried over the element Ω_e, $\int_{e'} d\Gamma$ is carried over the element contour $\Gamma_{e'}$ on $\Gamma_{0'}$, and $\sum_e$ and $\sum_{e'}$ extend over all elements Ω_e's and the elements related to $\Gamma_{0'}$, respectively.

Equation (4.13) may be rewritten as follows:

$$\begin{bmatrix} [A]_{1'1'} & [A]_{1'0'} \\ [A]_{0'1'} & [A]_{0'0'} \end{bmatrix} \begin{bmatrix} \{\phi\}^B_{1'} \\ \{\phi\}^B_{0'} \end{bmatrix} = \begin{bmatrix} \{0\} \\ [B]_{0'} \{\psi\}^B_{0'} \end{bmatrix} \tag{4.16}$$

where $[A]_{1'1'}, \cdots, [A]_{0'0'}$ are the submatrices of $[A]$, and $\{0\}$ is a null vector. The components of the $\{\phi\}^B_{0'}$ vector are the values of the electric field E_z at nodal points on the boundary $\Gamma_{0'}$, and the components of the $\{\phi\}^B_{1'}$ vector are the values of E_z at nodal points in the interior region except the boundary $\Gamma_{0'}$ from the region Ω_B.

Eliminating $\{\phi\}^B_{1'}$ from (4.16), we obtain the following equation:

$$[A]_{0'}\{\phi\}^B_{0'} = [B]_{0'}\{\psi\}^B_{0'} \tag{4.17}$$

$$[A]_{0'} = [A]_{0'0'} - [A]_{0'1'}[A]^{-1}_{1'1'}[A]_{1'0'}. \tag{4.18}$$

4.5 Analytical Formulation

Assuming that the dominant TE_{10} mode of unit amplitude is incident from waveguide $j(j=1,2)$ in Fig. 4.1, $\phi(\equiv E_z)$ on $\Gamma_i(i=1,2)$ may be expressed analytically as

$$\phi(x^{(i)}=0,y^{(i)}) = 2\delta_{ij}f_{i1}(y^{(i)}) - \sum_m \frac{1}{j\beta_{im}} \int_0^{d_i} f_{im}(y^{(i)}) f_{im}(y_0^{(i)}) \psi(x^{(i)}=0,y_0^{(i)})\, dy_0^{(i)} \qquad (4.19)$$

where

$$f_{im}(y^{(i)}) = \sqrt{2/d_i} \sin m\pi y^{(i)}/d_i\,, \qquad m = 1,2,3,\cdots \qquad (4.20)$$

$$\beta_{im} = \sqrt{k_0^2 - (m\pi/d_i)^2}\,, \qquad m = 1,2,3,\cdots \qquad (4.21)$$

and δ_{ij} is the Kronecker delta function.

Equation (4.19) can be discretized as follows:

$$\{\phi\}_i^A - [Z]_i\{\psi\}_i^A = \delta_{ij}\{f\}_i \qquad (4.22)$$

where

$$\{f\}_i = 2\{f_1\}_i \qquad (4.23)$$

$$[Z]_i = -\sum_m (1/j\beta_{im})\{f_m\}_i \sum_{e'} \int_{e'} f_{im}(y_0^{(i)}) \cdot \{N(x^{(i)}=0,y_0^{(i)})\}^T dy_0^{(i)}. \qquad (4.24)$$

Here the components of the $\{f_m\}_i$ vector are the values of $f_{im}(y^{(i)})$ at the nodal points on Γ_i, and $\sum_{e'}$ extends over the elements related to Γ_i.

4.6 Combination of Finite and Boundary Elements

On the short-circuit boundary Γ_0, the electric-field component ϕ

taken:

$$\{\phi\}_0^A = \{0\} \qquad \text{on} \quad \Gamma_{0'} \tag{4.25}$$

The continuity conditions of ϕ and its outward normal derivative ψ at the interface $\Gamma_{0'}$ between regions Ω_A and Ω_B are expressed as

$$\{\phi\}_{0'}^A = \{\phi\}_{0'}^B, \qquad \{\psi\}_{0'}^A = -\{\psi\}_{0'}^B \qquad \text{on} \quad \Gamma_{0'} \tag{4.26}$$

where the minus sign of ψ originates from the outward normal direction of the adjacent two regions opposite each other.

Using (4.26), equation (4.17) may be expressed as

$$[A]_{0'}\{\phi\}_{0'}^A + [B]_{0'}\{\psi\}_{0'}^A = \{0\} \; . \tag{4.27}$$

Considering (4.25), we obtain from (4.12):

$$\left[[H]_1 \;\; [H]_2 \;\; [H]_{0'}\right] \begin{bmatrix} \{\phi\}_1^A \\ \{\phi\}_2^A \\ \{\phi\}_{0'}^A \end{bmatrix}$$

$$- \left[[G]_1 \;\; [G]_2 \;\; [G]_{0'} \;\; [G]_0\right] \begin{bmatrix} \{\psi\}_1^A \\ \{\psi\}_2^A \\ \{\psi\}_{0'}^A \\ \{\psi\}_0^A \end{bmatrix} = \{0\}. \tag{4.28}$$

From (4.22), (4.27), and (4.28) we obtain the following final matrix equation:

$$\begin{bmatrix} [1] & [0] & [0] & -[Z]_1 & [0] & [0] & [0] \\ [0] & [1] & [0] & [0] & -[Z]_2 & [0] & [0] \\ [0] & [0] & [A]_{0'} & [0] & [0] & [B]_{0'} & [0] \\ [H]_1 & [H]_2 & [H]_{0'} & -[G]_1 & -[G]_2 & -[G]_{0'} & -[G]_0 \end{bmatrix} \begin{bmatrix} \{\phi\}_1^A \\ \{\phi\}_2^A \\ \{\phi\}_{0'}^A \\ \{\psi\}_1^A \\ \{\psi\}_2^A \\ \{\psi\}_{0'}^A \\ \{\psi\}_0^A \end{bmatrix} = \begin{bmatrix} \delta_{1j}\{f\}_1 \\ \delta_{2j}\{f\}_2 \\ \{0\} \\ \{0\} \end{bmatrix} \tag{4.29}$$

where [1] is a unit matrix and [0] is a null matrix.

The values of ϕ at nodal points on Γ_i, i.e., $\{\phi\}_i$, are computed from (4.29), and then $\phi(x^{(i)}=0, y^{(i)})$ on Γ_i can be calculated. The solutions on Γ_i allow the determination of scattering parameters S_{ij} of the TE_{10} mode as follows:

$$S_{ii} = \int_0^{d_i} \phi(x^{(i)}=0, y^{(i)}) f_{i1}(y^{(i)})\, dy^{(i)} - 1 \tag{4.30}$$

$$S_{ij} = \sqrt{\beta_{i1}/\beta_{j1}} \int_0^{d_i} \phi(x^{(i)}=0, y^{(i)}) f_{i1}(y^{(i)})\, dy^{(i)}, \qquad i \neq j\ . \tag{4.31}$$

4.7 Numerical Results

A lossy dielectric post in a rectangular waveguide as shown in Fig. 4.2 is investigated first, where d is the width of the rectangular waveguide and r is the radius of the cylindrical post.

The equivalent circuit for a post in a rectangular waveguide in which only the dominant TE_{10} mode can propagate unattenuated is the T network shown in Fig. 4.3, where Z_0 is the characteristic impedance of the TE_{10} mode.

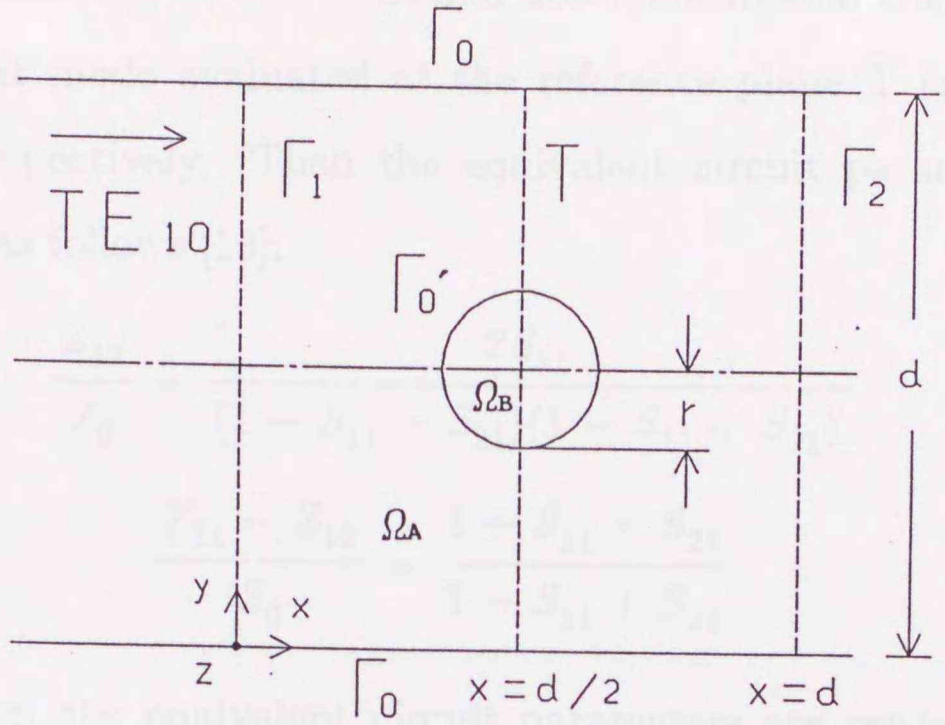

Fig. 4.2. Dielectric post in a rectangular waveguide.

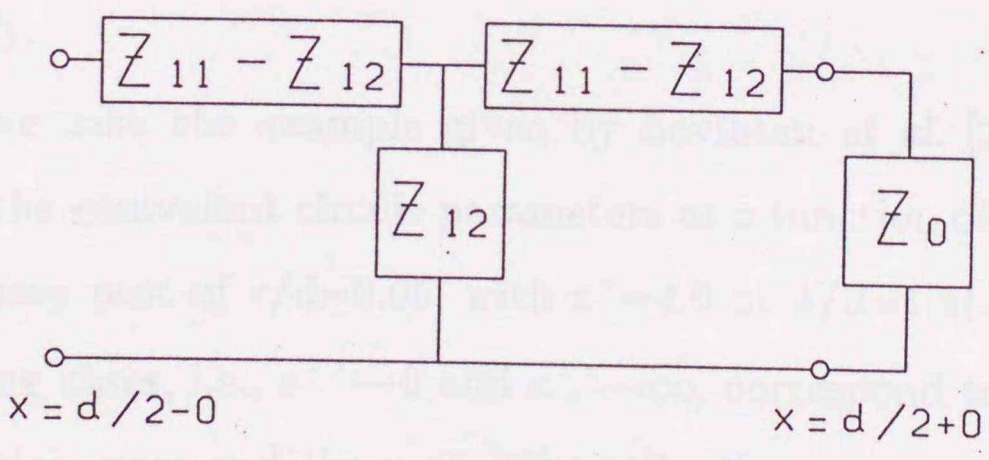

Fig. 4.3. Equivalent circuit for dielectric post in a rectangular waveguide.

Let S_{11} and S_{21} be the reflection and transmission coefficients of the dominant mode evaluated at the reference plane T ($x = d/2$ in Fig. 4.2), respectively. Then the equivalent circuit parameters are determined as follows [13]:

$$\frac{Z_{12}}{Z_0} = \frac{2S_{21}}{(1 - S_{11} - S_{21})(1 - S_{11} + S_{21})}$$

$$\frac{Z_{11} - Z_{12}}{Z_0} = \frac{1 + S_{11} - S_{21}}{1 - S_{11} + S_{21}}.$$

Moreover, the equivalent circuit parameters are represented by the resistances and reactances as follows:

$$Z_{12}/Z_0 = R_a + jX_a$$

$$(Z_{11} - Z_{12})/Z_0 = R_b + jX_b$$

where R_a and R_b are the normalized shunt and series resistances, and X_a and X_b are the normalized shunt and series reactances, respectively.

Now we take the example given by Leviatan *et al.* [23], which computes the equivalent circuit parameters as a function of ε'' for a centered lossy post of r/d=0.05, with ε'=4.0 at λ/d=1.4(λ=$2\pi/k_0$). Two limiting cases, i.e., $\varepsilon'' \to 0$ and $\varepsilon'' \to \infty$, correspond to the ones for the lossless post and the perfectly conducting post, respectively. Here a regular polygon with 24 sides, the area of which is equal to that of the circle, is used instead of the circle.

Figs. 4.4 and 4.5 show the normalized shunt and series resistances versus ε'', respectively. Figs. 4.6 and 4.7 show the normalized shunt and series reactances versus ε'', respectively.

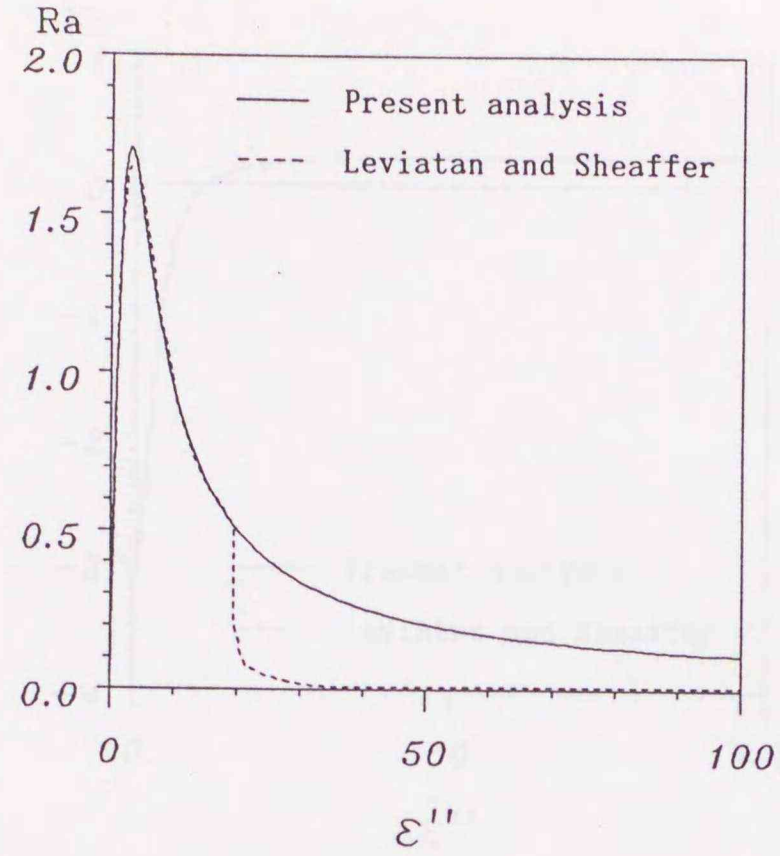

Fig. 4.4. Normalized shunt resistance R_a versus ε''.

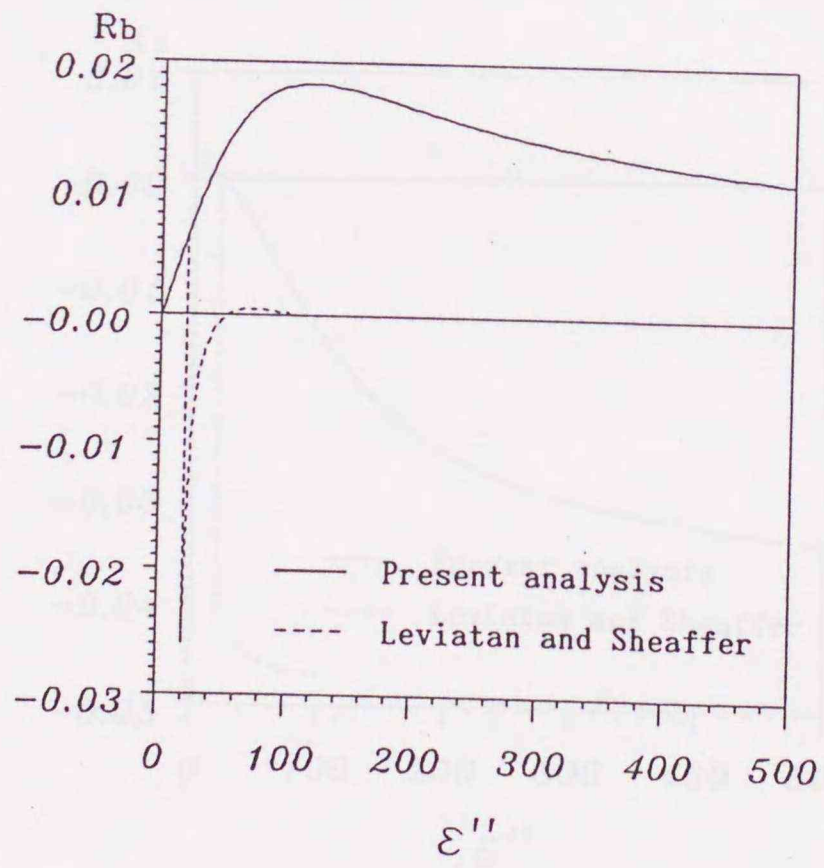

Fig. 4.5. Normalized series resistance R_b versus ε''.

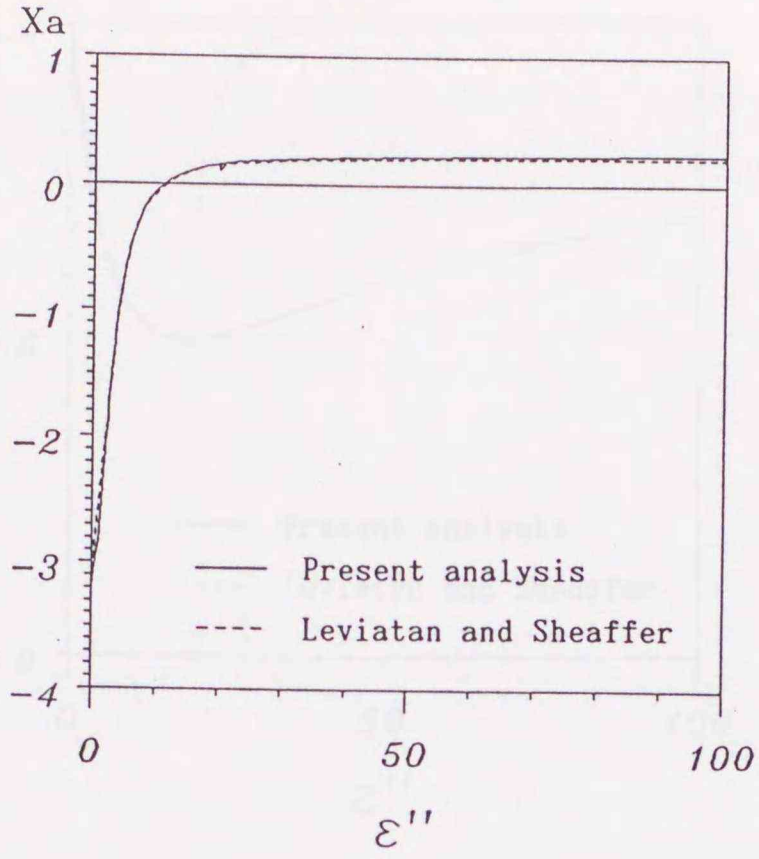

Fig. 4.6. Normalized shunt reactance X_a versus ε''.

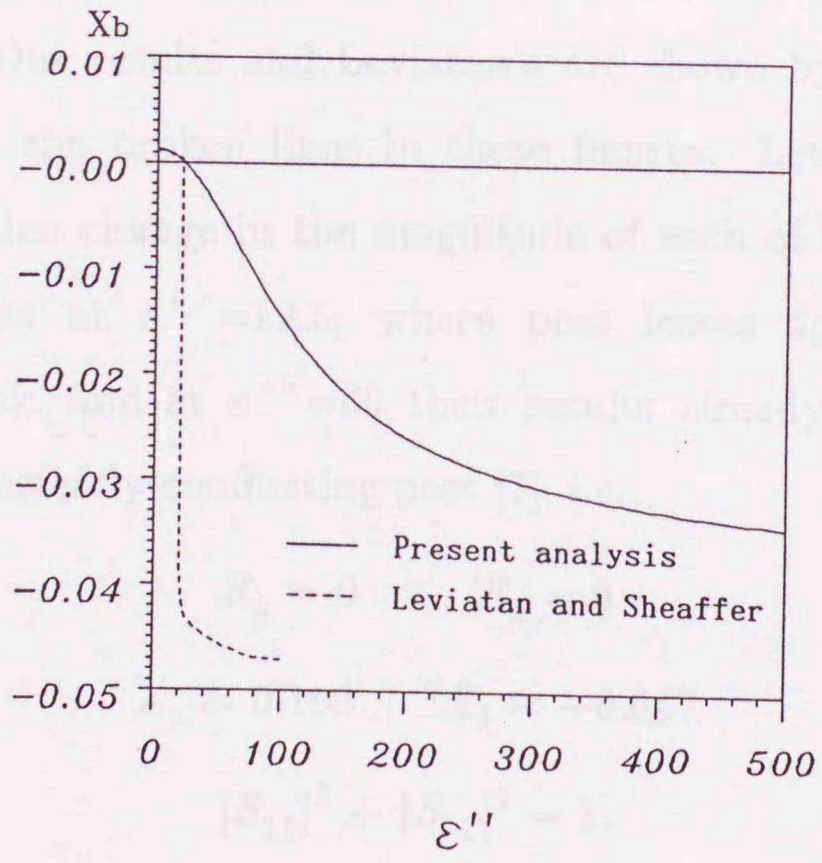

Fig. 4.7. Normalized series reactance X_b versus ε''.

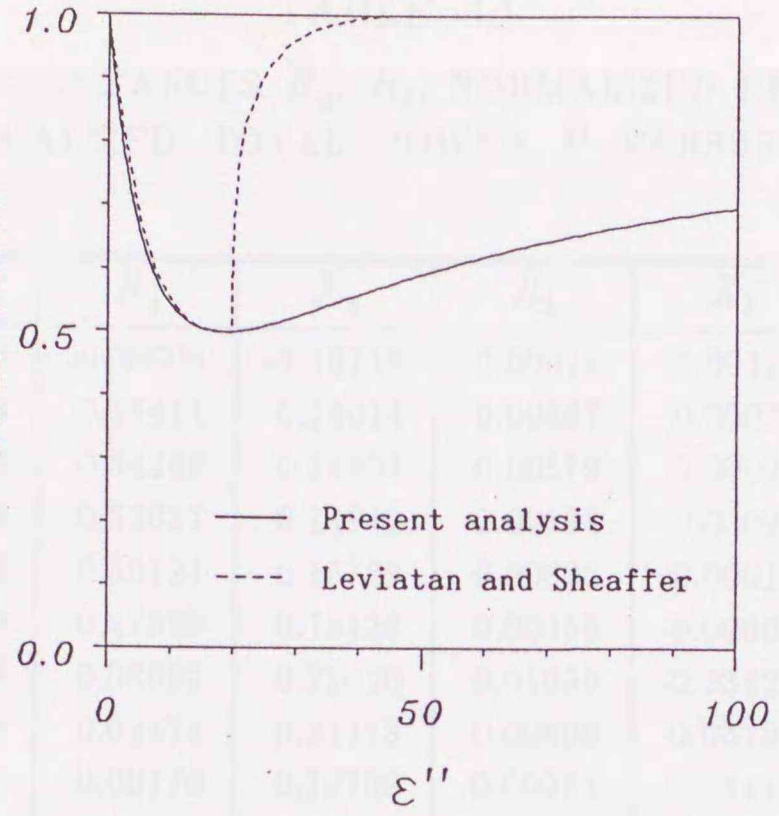

Fig. 4.8. Normalized total power versus ε''.

Fig. 4.8 shows the normalized total power P, i.e., $|S_{11}|^2 + |S_{21}|^2$, versus ε''. Our results and Leviatan's are shown by, respectively, the solid and the broken lines in these figures. Leviatan's results show the sudden change in the magnitude of each of the resistances and reactances at ε''=19.5, where post losses appear to have reached a peak, and at ε''=60 their results already approach the ones for the perfectly conducting post [7], i.e.,

$$R_a = 0 \qquad R_b = 0$$

$$X_a \approx 0.190 \qquad X_b \approx -0.047$$

$$|S_{11}|^2 + |S_{21}|^2 = 1.$$

Moreover, their R_b has negative values at $19.5 \leq \varepsilon'' \leq 50$ although the resistor R_b should never have a negative resistance [26]. On the

TABLE 4.1

NORMALIZED RESISTANCES R_a, R_b, NORMALIZED REACTANCES X_a, X_b, AND NORMALIZED TOTAL POWER P VERSUS ε'' (r/d=0.05, λ/d=1.4, ε'=4.0)

ε''	R_a	X_a	R_b	X_b	P
0	-0.00003	-3.18718	-0.00014	0.00125	1.00029
18.0	0.55411	0.14014	0.00567	0.00031	0.49887
18.4	0.54268	0.14403	0.00579	0.00027	0.49881
19.0	0.52637	0.14942	0.00598	0.00021	0.49892
20.0	0.50121	0.15739	0.00628	0.00010	0.49960
21.0	0.47829	0.16428	0.00658	-0.00002	0.50081
500.0	0.03692	0.22020	0.01099	-0.03423	0.85207
1000.0	0.02474	0.21173	0.00806	-0.03795	0.89332
10000.0	0.00770	0.19709	0.00284	-0.04413	0.96291
100000.0	0.00233	0.19091	0.00082	-0.04669	0.98864
1000000.0	0.00026	0.19027	-0.00003	-0.04697	0.99919
4000000.0	0.00006	0.19026	-0.00011	-0.04697	1.00019
10000000.0	0.00003	0.19026	-0.00013	-0.04697	1.00039
100000000.0	0.00000	0.19026	-0.00014	-0.04697	1.00051

TABLE 4.2

NORMALIZED RESISTANCES R_a, R_b, NORMALIZED REACTANCES X_a, X_b, AND NORMALIZED TOTAL POWER P FOR A PERFECTLY CONDUCTING POST BY THE FEM AND THE BEM (r/d=0.05, λ/d=1.4)

METHOD	R_a	X_a	R_b	X_b	P
FEM	-0.29×10^{-6}	0.19027	0.00002	-0.04738	0.99991
BEM	-0.40×10^{-6}	0.19026	-0.00013	-0.04697	1.00052

other hand, all of our results have no rapid changes. Some negative values for our R_b appear in Table 4.1. This is because the total power obtained by the CFBEM becomes more than unity. Since the energy error is less than 0.06 percent, computation error seems to cause negative values for R_b. Table 4.1 shows that our results reach the ones for the perfectly conducting post at $\varepsilon'' > 10^6$ and that post losses are the greatest at $\varepsilon'' = 18.4$.

Marcuvitz's results [7] for the perfectly conducting post of the same volume and location as the lossy dielectric post are compared with the results obtained by the FEM or the BEM, which are shown in Table 4.2. Our results agree well with Marcuvitz's.

From the fact described above, we may expect that our results are more reasonable than Leviatan's [23].

Second, ferrite-loaded waveguide nonreciprocal phase shifters are investigated. Nonreciprocal phase shift may be realized in a rectangular waveguide by placing a ferrite slab magnetized by a dc magnetic field H_0 as shown in Fig. 4.9. Differential phase shift ($\Delta\phi = \arg S_{21} - \arg S_{12}$) and low $VSWR$ are important to characterize the nonreciprocal phase shifter, so that phases of the forward (S_{21}) and backward (S_{12}) transmission coefficients and the amplitudes of the S parameters are obtained. Figs. 4.10 and 4.11 show, respectively, the differential phase shift and the magnitude of reflection coefficient as a function of frequency, where ferrite is TT1-2800, $H_0 = 1.2\times10^5$ A/m, $d = 15.799$ mm, $\delta = 0.7$ mm, $l = 20$ mm, and the slab is assumed to be loaded parallel to the wall and 0.7 mm distant from the wall in Fig. 4.9.

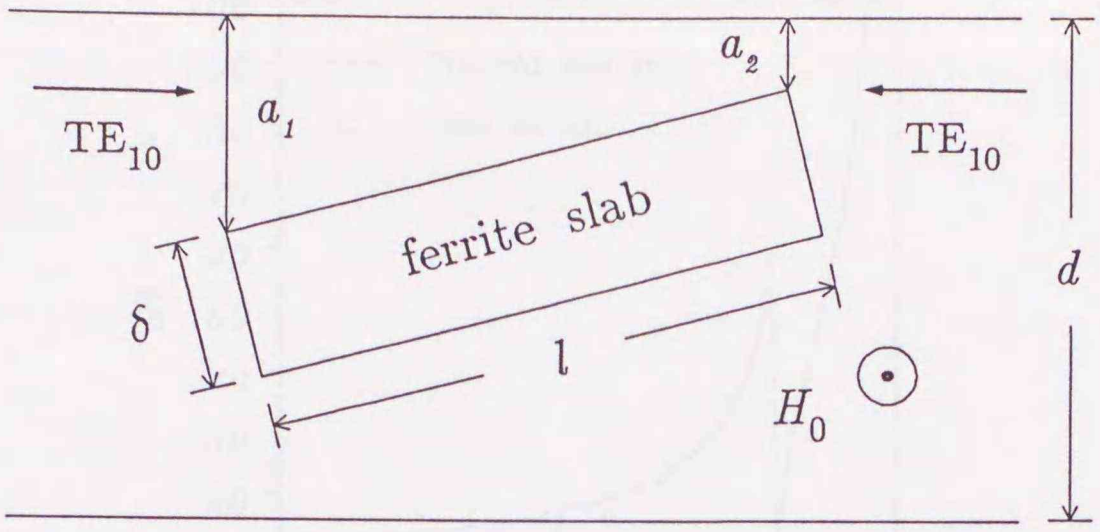

Fig. 4.9. Ferrite slab in a rectangular waveguide.

Our results and the experimental ones of Uher *et al.* [24] are shown by the solid and the × signs in Figs. 4.10 and 4.11, respectively. Both $\Delta\phi$'s agree well at $f > 16$ GHz, as do the $|S_{11}|$'s at $f > 16.5$ GHz, but the frequencies where the $|S_{11}|$'s take minima are different from each other.

The longer ferrite slab is dealt with, the larger the discontinuity region becomes. So that it gets more and more difficult to analyze the discontinuity region by only the FEM, because the FEM needs large memory for computation. On the other hand, the CFBEM does not need so much memory for computation, since here the FEM is applied only to the region with ferrite. For example, the computer memory required to analyze a ferrite slab ($l = 20$ mm) in a rectangular waveguide is about 7.5 Mbyte with the CFBEM, while it is a few hundred Mbyte with the FEM only.

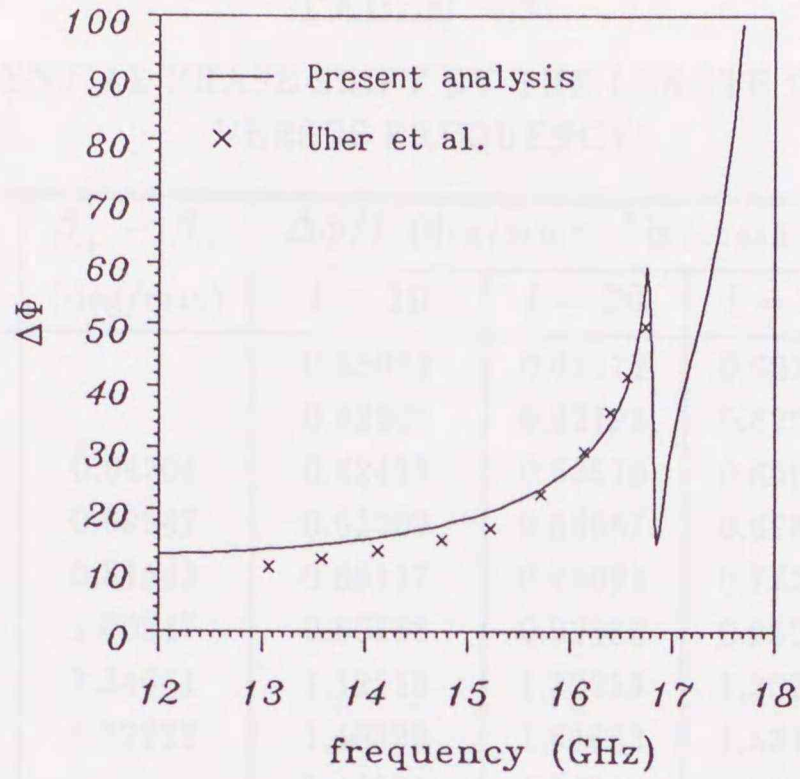

Fig. 4.10. Differential phase shift in degrees versus frequency ($a_1 = a_2 = 0.7$ mm, $\delta = 0.7$ mm, $l = 20$ mm).

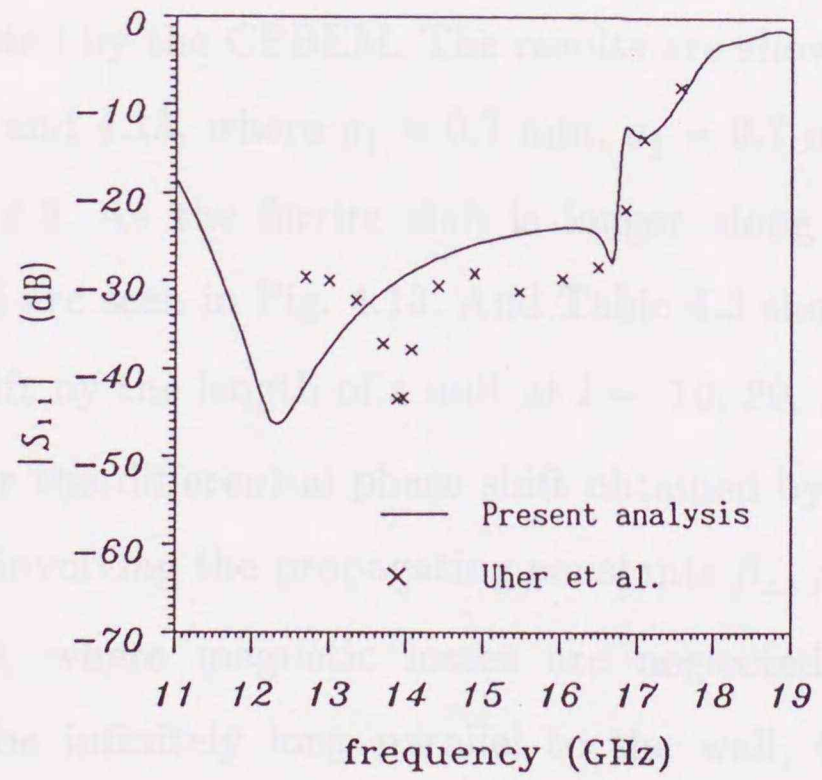

Fig. 4.11. Reflection coefficient in decibels versus frequency ($a_1 = a_2 = 0.7$ mm, $\delta = 0.7$ mm, $l = 20$ mm).

TABLE 4.3

DIFFERENTIAL PHASE SHIFT BY THE LENGTH OF A UNIT VERSUS FREQUENCY

frequency (GHz)	$\beta_+ - \beta_-$ (deg/mm)	$\Delta\phi/l$ (deg/mm): l is length of ferrite slab			
		$l = 10$	$l = 20$	$l = 30$	$l = 40$
11		0.65072	0.61572	0.60390	0.60176
12		0.62567	0.62793	0.62928	0.63350
12.2659	0.64204	0.62435	0.63510	0.63934	0.64507
13	0.69947	0.63302	0.66687	0.67876	0.68869
14	0.81543	0.68117	0.75092	0.77300	0.78911
15	1.00947	0.80168	0.92185	0.95028	0.97296
16	1.34641	1.12516	1.32253	1.30771	1.33855
16.3581	1.52222	1.40329	1.64663	1.53181	1.60977
17		3.46521	1.52196	2.13124	1.57972

So the differential phase shift $\Delta\phi$ and the magnitude of the reflection coefficient $|S_{11}|$ versus variations in the length of ferrite slab can be easily computed by the CFBEM. The results are shown, respectively, in Figs. 4.12 and 4.13, where $a_1 = 0.7$ mm, $a_2 = 0.7$ mm, and $\delta = 0.7$ mm in Fig. 4.9. As the ferrite slab is longer along the wall, more peaks of $|S_{11}|$ are seen in Fig. 4.13. And Table 4.3 shows the differential phase shift by the length of a unit at $l =$ 10, 20, 30, and 40 mm.

Moreover the differential phase shift obtained by a transcendental equation involving the propagating constants β_+, β_- [82] is shown in Table 4.3, where magnetic losses are neglected and ferrite is assumed to be infinitely long parallel to the wall, 0.7 mm distant from the wall and $\delta = 0.7$ mm. Here let $\Delta\phi$ be $(\beta_+ - \beta_-)$. The propagation constants are difficult to obtain at $f < 12.26$ GHz because the transcendental equation has complex as well as real coefficients

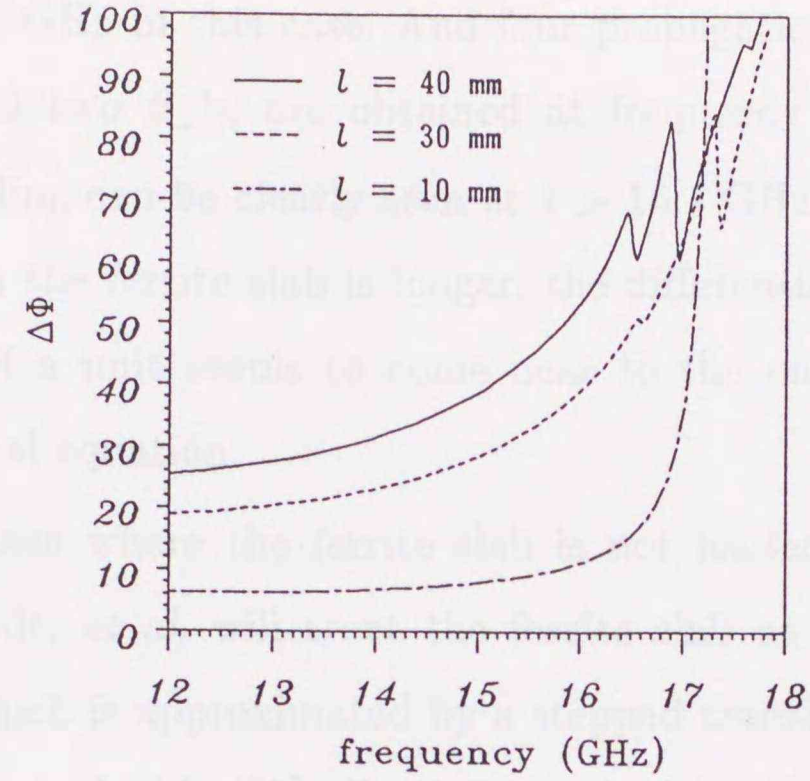

Fig. 4.12. Differential phase shift in degrees versus variation of length of ferrite slab ($a_1 = a_2 = 0.7$ mm, $\delta = 0.7$ mm).

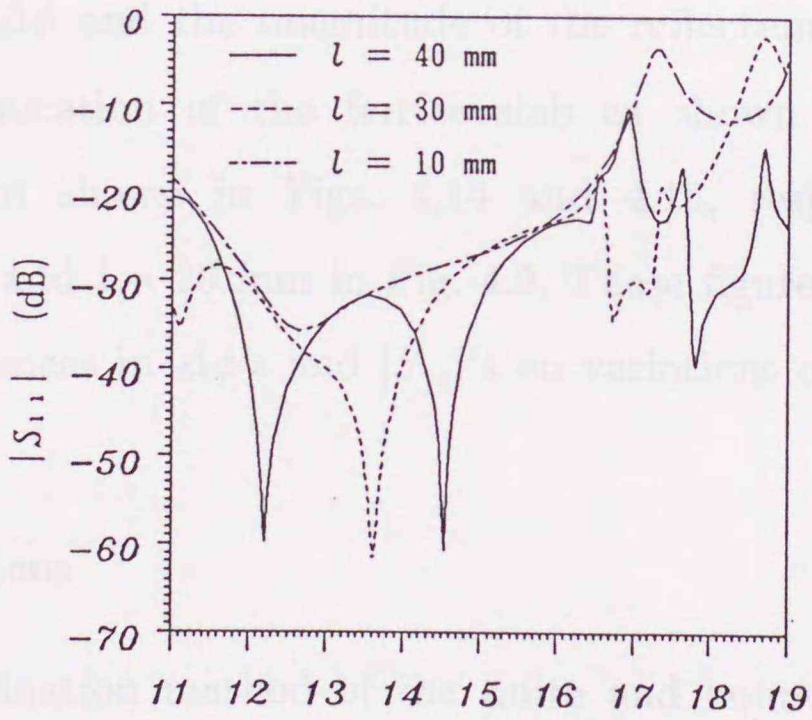

Fig. 4.13. Reflection coefficient in decibels versus variation of length of ferrite slab ($a_1 = a_2 = 0.7$ mm, $\delta = 0.7$ mm).

at $f < 12.26$ GHz in this case. And four propagation constants, i.e., two β_+'s and two β_-'s, are obtained at frequency $f > 16.36$ GHz (modal coupling can be clearly seen at $f > 16.7$ GHz in Fig. 4.10). In Table 4.3, as the ferrite slab is longer, the differential phase shift by the length of a unit seems to come near to the one obtained by a transcendental equation.

In the case where the ferrite slab is not loaded parallel to the wall, F. Arndt, *et al.* will treat the ferrite slab as linearly tapered structure, which is approximated by a stepped transition with a hundred steps at each side [20]. So their method is difficult to apply to problems with variations in the angle of the ferrite slab to the the wall. The CFBEM can be effectively applied even to the problems with variations of the location of the ferrite slab. So the differential phase shift $\Delta\phi$ and the magnitude of the reflection coefficient $|S_{11}|$ versus the location of the ferrite slab as shown in Fig. 4.9 are obtained and shown in Figs. 4.14 and 4.15, respectively, where $\delta = 0.7$ mm and $l = 20$ mm in Fig. 4.9. These figures exhibit considerable differences in $\Delta\phi$'s and $|S_{11}|$'s on variations of the location of ferrite.

4.8 Conclusions

A combination method of the finite and boundary elements is formulated for the analysis of H-plane waveguide junction with arbitrary cross sections where the junction is loaded with dielectric or ferrite of arbitrary shape, size, and location. The waveguide junction is divided into two regions. One is the inhomogeneous region with

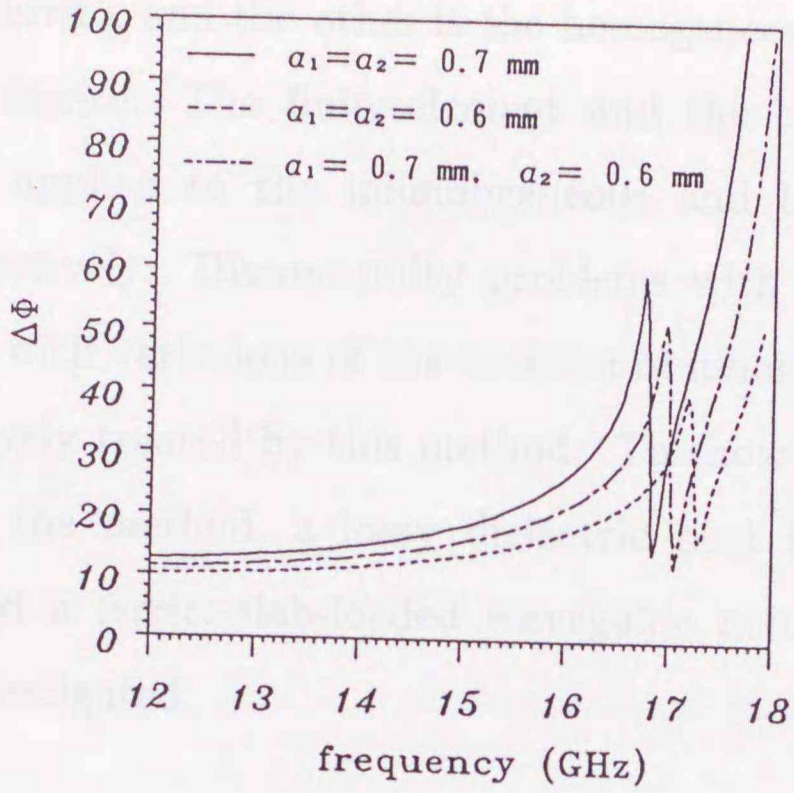

Fig. 4.14. Differential phase shift in degrees versus variation of location of ferrite slab ($\delta = 0.7$ mm, $l = 20$ mm).

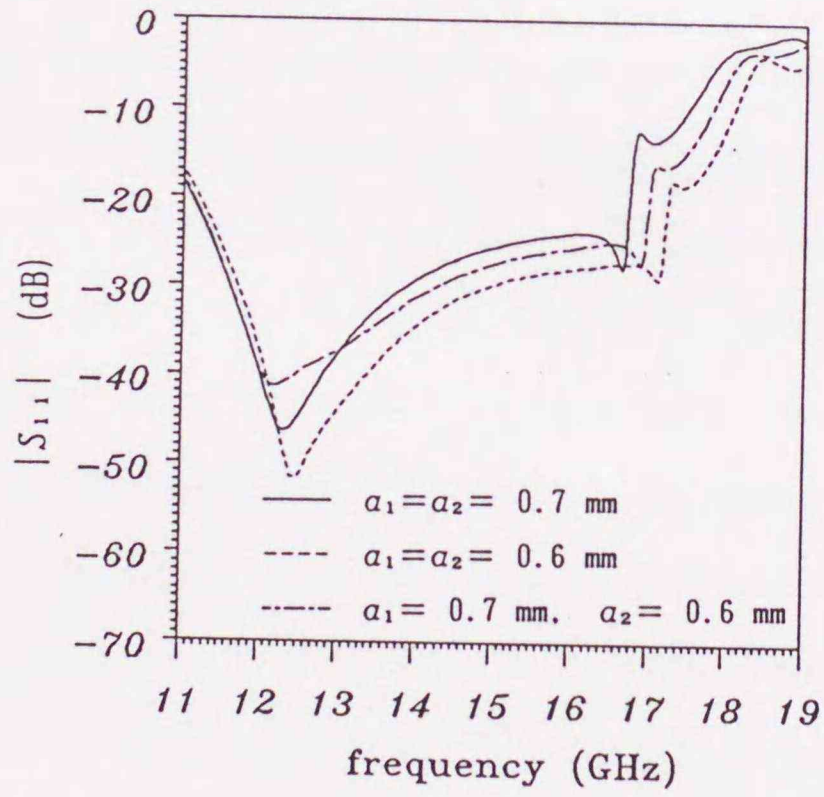

Fig. 4.15. Reflection coefficient in decibels versus variation of location of ferrite slab ($\delta = 0.7$ mm, $l = 20$ mm).

dielectric or ferrite, and the other is the homogeneous region without dielectric or ferrite. The finite-element and the boundary-element methods are applied to the inhomogeneous and the homogeneous regions, respectively. Discontinuity problems with large homogeneous region or with variations of the location of inhomogeneous region can be effectively treated by this method. To show the validity and usefulness of the method, a lossy dielectric post in a rectangular waveguide and a ferrite-slab-loaded waveguide nonreciprocal phase shifter are investigated.

CHAPTER 5

Equivalent Circuit for Dielectric Posts

5.1 Introduction

Discontinuity problems of dielectric posts in a waveguide have been recently studied [7]–[27]. Dielectric resonators are simple in structure; ceramic dielectrics with relative permittivity and temperature stability being used to design microwave filters. Sahalos and Vafiadis [21] have considered the design of bandpass and bandstop filters, and Gesche and Löchel [25] a tunable bandstop filter. The equivalent circuit, which can be used to represent dielectric resonance in a rectangular waveguide, is useful in the design of microwave filters. The T network is commonly used for this purpose. Marcuvitz [7] and Araneta *et al.* [18] have mentioned differing types of resonances, e. g., the antiresonance in series reactance, and that for the shunt reactance of the T network. However, it is found that the shunt reactance of a T network decreases with increasing frequency [22], [26]. Hence it does not obey Foster's theorem. This difficulty is overcome by Hsu and Auda [26], who have physically realized lossy dielectric post resonance with the lumped lattice network.

It is shown that some of the lossless dielectric post resonance in a rectangular waveguide can be physically realized by lumped lattice

networks, and the interaction between two posts can be evaluated by this circuit. There are two types of dielectric post resonances, i. e., the antiresonances of a series reactance and of a cross reactance for a lattice network. The variations of the post location are related to the variations of branch reactances of the network.

These problems are analyzed using a combination of the finite and boundary element methods (CFBEM) [66]–[71]. With the FEM, a substructure method [28] is adopted. When this method is used, the dimension of the matrix equation to be solved can be greatly reduced.

5.2 Basic Equations

Consider a rectangular waveguide containing a dielectric post as shown in Fig. 5.1, where the boundaries Γ_1 and Γ_2 connect the discontinuities to the rectangular waveguide. Γ_P encloses the region Ω_B containing the dielectrics. The region Ω_A is surrounded by Γ_1, Γ_2, Γ_P, and the short-circuit boundary Γ_0. The boundaries Γ_1, Γ_2, and Γ_0 enclose the waveguide discontinuities completely. The dielectric post is assumed to be of full height and uniform along the y axis.

Considering the excitation by the dominant TE_{10} mode, the following basic equation is obtained:

$$\left[\frac{\partial^2}{\partial x^2}+\frac{\partial^2}{\partial z^2}\right]E_y + k^2 E_y = 0 \tag{5.1}$$

$$k^2 = k_0^2 \varepsilon \tag{5.2}$$

$$k_0^2 = \omega^2 \varepsilon_0 \mu_0 \tag{5.3}$$

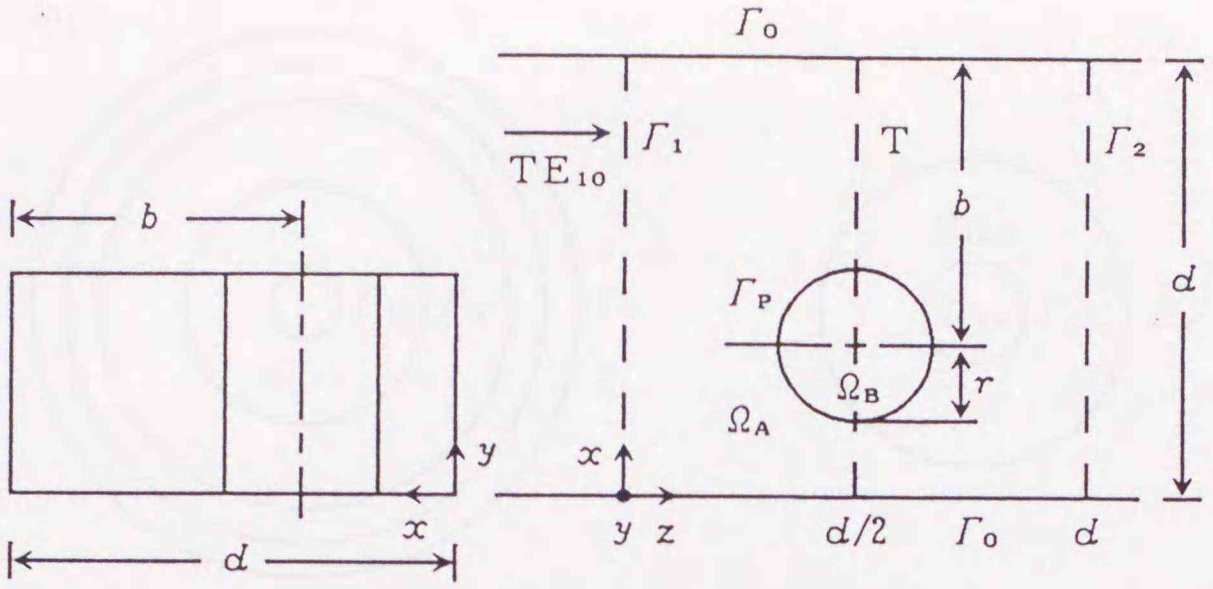

Fig. 5.1. Dielectric post in a rectangular waveguide.

$$\varepsilon = \varepsilon' - j\varepsilon'' \tag{5.4}$$

where E_y is the electric field, ω is the angular frequency, ε_0 and μ_0 are the permittivity and permeability of free space, respectively, and ε is the relative permittivity.

5.3 Outline of Analysis Method

BEM with quadratic line elements and FEM with quadratic triangular elements are applied to the region Ω_A and the region Ω_B, respectively [66]–[71].

A substructure method [28] is also adopted in the FEM. The region containing the dielectric post is divided into substructures surrounded by concentric circles as shown in Fig. 5.2.

Applying FEM to the region Ω_{IN} and Ω_{OUT}, we obtain (5.5) and (5.6), respectively, [35]–[37]:

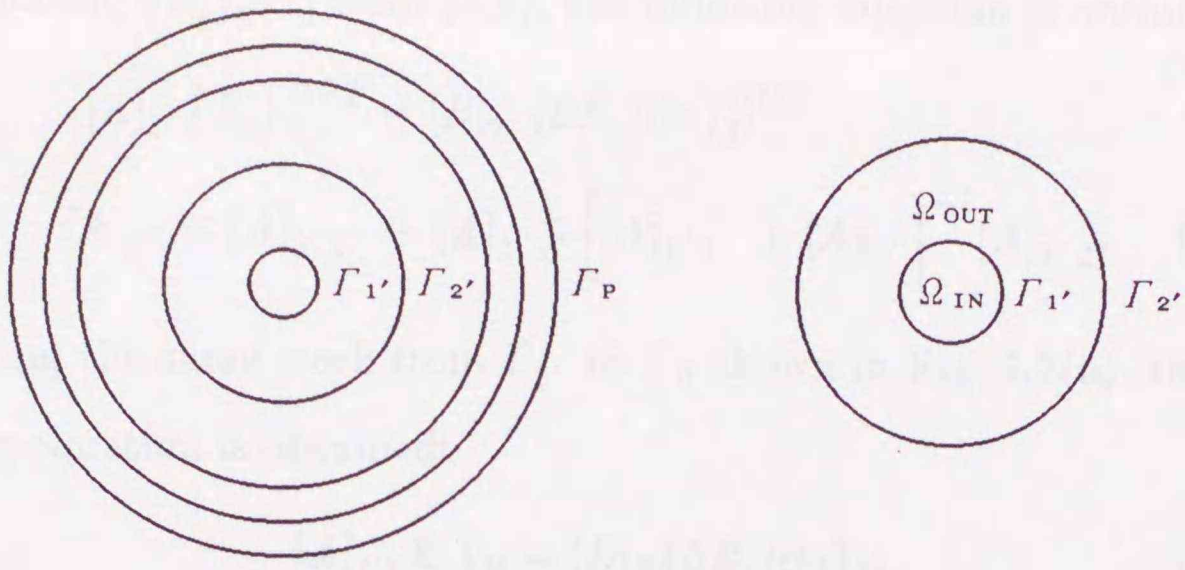

(a) (b)

Fig. 5.2. Dielectric region.
(a) Dielectric region divided into substructures.
(b) Regions surrounded by two concentric circles.

$$\Omega_{IN}:\ [A]_{1'}\,\{E_y\}_{1'}^{IN} = [B]_{1'}\cdot\{\partial E_y/\partial n\}_{1'}^{IN} \tag{5.5}$$

$$\Omega_{OUT}:\ \begin{bmatrix}[A]_{1'1'} & [A]_{1'2'}\\ [A]_{2'1'} & [A]_{2'2'}\end{bmatrix}\begin{bmatrix}\{E_y\}_{1'}^{OUT}\\ \{E_y\}_{2'}^{OUT}\end{bmatrix} = \begin{bmatrix}[B]_{1'}\cdot\{\partial E_y/\partial n\}_{1'}^{OUT}\\ [B]_{2'}\cdot\{\partial E_y/\partial n\}_{2'}^{OUT}\end{bmatrix} \tag{5.6}$$

where $[A]$ and $[B]$ are matrices obtained by the FEM, $\partial E_y/\partial n$ is the outward normal derivative of E_y, the subscript $1'$ and $2'$ indicate the quantities corresponding to the boundaries $\Gamma_{1'}$ and $\Gamma_{2'}$, respectively.

The continuity conditions of E_y and $\partial E_y/\partial n$ at the interface $\Gamma_{1'}$ between the regions Ω_{IN} and Ω_{OUT} are expressed as follows [66]-[71]:

$$\{E_y\}_{1'}^{IN} = \{E_y\}_{1'}^{OUT},\quad \{\partial E_y/\partial n\}_{1'}^{IN} = -\{\partial E_y/\partial n\}_{1'}^{OUT} \quad \text{on} \quad \Gamma_{1'} \tag{5.7}$$

Using (5.7), (5.6) may be expressed as

$$\begin{bmatrix}[A]_{1'1'}+[A]_{1'} & [A]_{1'2'}\\ [A]_{2'1'} & [A]_{2'2'}\end{bmatrix}\begin{bmatrix}\{E_y\}_{1'}^{OUT}\\ \{E_y\}_{2'}^{OUT}\end{bmatrix} = \begin{bmatrix}\{0\}\\ [B]_{2'}\cdot\{\partial E_y/\partial n\}_{2'}^{OUT}\end{bmatrix} \tag{5.8}$$

Eliminating $\{E_y\}_{2'}^{OUT}$ from (5.8), the following equation is obtained:

$$[A]_{2'}\{E_y\}_{2'}^{OUT} = [B]_{2'}\{\partial E_y/\partial n\}_{2'}^{OUT} \tag{5.9}$$

$$[A]_{2'} = [A]_{2'2'} - [A]_{2'1'}\left[[A]_{1'1'} + [A]_{1'}\right]^{-1}[A]_{1'2'} \tag{5.10}$$

Iterating the same work from $\Gamma_{1'}$ to Γ_P shown in Fig. 5.2(a), the following equation is obtained:

$$[A]_P\{E_y\}_P = [B]_P\{\partial E_y/\partial n\}_P \tag{5.11}$$

Equation (5.11) can be combined using the BEM on the boundary Γ_P shown in Fig. 5.1 [66]–[71].

When a substructure method is used, the dimension of the matrix equation to be solved can be reduced. Here the size of the triangular elements in each substructure surrounded by the two concentric circle is different from those of other substructures, but the method used to divide each substructure into triangular elements remains the same. Therefore, only the array for one substructure is necessary and the computer memory required can be reduced.

On the boundaries Γ_1 and Γ_2 shown in Fig. 5.1, the analytical solutions found for the uniform waveguides connected to the junctions are combined with the BEM [66]–[71].

The equivalent circuit for a post in a rectangular waveguide is shown in terms of two-port networks. The T network is most commonly used. In the case where the post structure are symmetric about a plane perpendicular to the axis of the transmission line, the lattice network can be used [26], [83]. It has been shown in Reference [83] that any two-port network is physically realisable in the

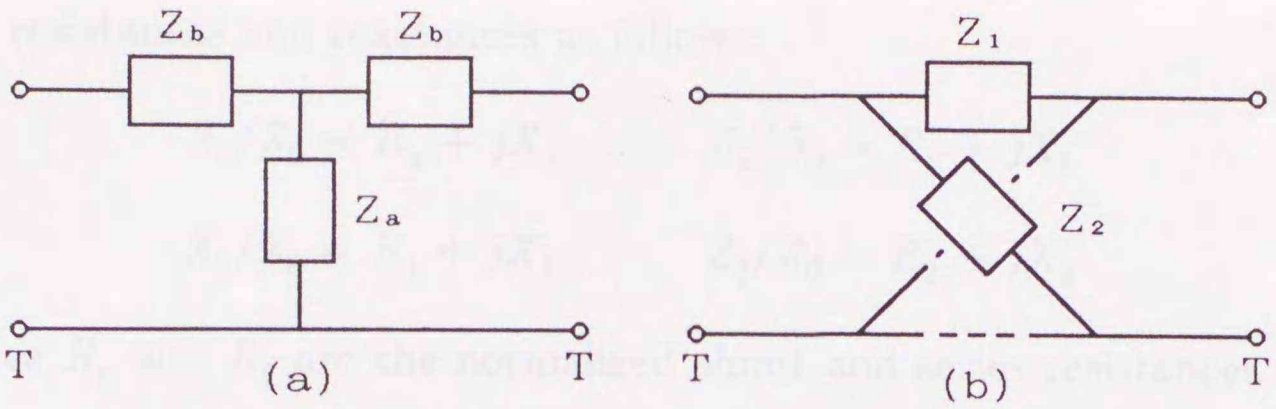

Fig. 5.3. Equivalent networks.
(a) T network. (b) Lattice network.

lattice form, i. e., it is unnecessary to use any negative inductances or capacitances to construct the lattice.

Let S_{11} and S_{21} be the reflection and transmission coefficients at the reference plane T ($z=d/2$ in Fig. 5.1), respectively. The equivalent circuit parameters of the T and lattice networks shown in Fig. 5.3. are determined as follows:

$$\frac{Z_a}{Z_0} = \frac{2S_{21}}{(1 - S_{11} - S_{21})(1 - S_{11} + S_{21})} \tag{5.12a}$$

$$\frac{Z_b}{Z_0} = \frac{1 + S_{11} - S_{21}}{1 - S_{11} + S_{21}} \tag{5.12b}$$

$$\frac{Z_1}{Z_0} = \frac{1 + S_{11} - S_{21}}{1 - S_{11} + S_{21}} \tag{5.13a}$$

$$\frac{Z_2}{Z_0} = \frac{1 + S_{11} + S_{21}}{1 - S_{11} - S_{21}} \tag{5.13b}$$

where Z_0 is the characteristic impedance of the TE_{10} mode.

Moreover the equivalent circuit parameters are represented by the resistances and reactances as follows:

$$Z_a/Z_0 = R_a + jX_a \qquad Z_b/Z_0 = R_b + jX_b$$

$$Z_1/Z_0 = R_1 + jX_1 \qquad Z_2/Z_0 = R_2 + jX_2$$

where R_a and R_b are the normalized shunt and series resistances for the T network, X_a and X_b are the normalized shunt and series reactances for the T network, R_1 and R_2 are the normalized series and cross resistances for the lattice network, and X_1 and X_2 are the normalized series and cross reactances for the lattice network.

5.4 Numerical Results

The example given by Marcuvitz [7], Nielsen [10], Araneta *et al.* [18], Sahalos and Vafiadis [21], Hsu and Auda [22], and Leviatan and Sheaffer [23] is followed. These compute the scattering parameters and equivalent network elements as a function of relative permittivity ε for a centered lossless dielectric post of r/d=0.05 at λ/d=1.4, where d is the width of the rectangular waveguide, r is the radius of the cylindrical post as shown in Fig. 5.1, and λ is the wavelength in free space. Here a regular polygon with 24 sides is used instead of the circle.

Fig. 5.4 shows the variation of magnitude of the reflection coefficient R (by the solid line) and transmission coefficient T (by the broken line) against ε. Our results agree well with those of Leviatan [23] shown by the dots (in Reference [23], only the reflection R is shown up to ε=200). As the permittivity becomes high, considerably

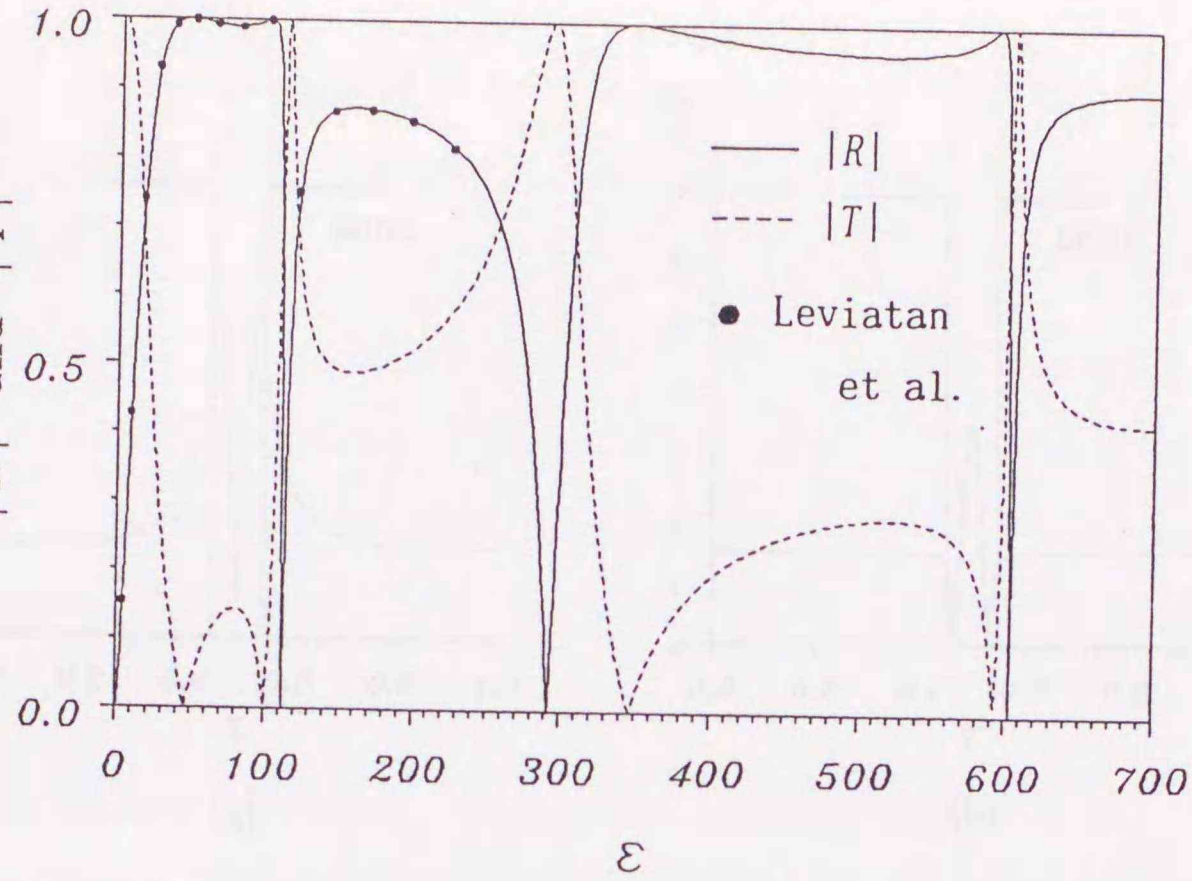

Fig. 5.4. Magnitudes of reflection and transmission coefficients against ε (r/d=0.05, b/d=0.5).

more effort and large computer memory is required to divide the region to which the FEM is applied. However, when a substructure method is used, it is easy to divide this region, and the array is only used for one substructure, so that the required computer memory can be greatly reduced.

These exist three resonance points in the ε range shown in Fig. 5.4. The first resonance occurs at ε=112.5, the second at ε=291.7, and the third at ε=603.1.

The electric field distributions at resonance are shown in Fig. 5.5, where $x=b=d/2$ and Z is z/d ($0\leq z\leq d$) in Fig. 5.1. These figures show that there are two types of dielectric post resonances. At the first and third resonances the fields are trapped on the post surface and their amplitudes decrease toward the center of the post (surface

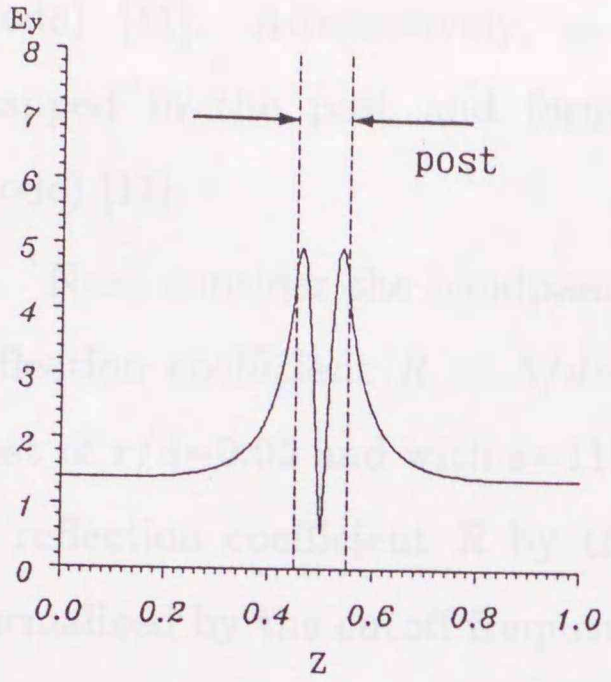

(a)

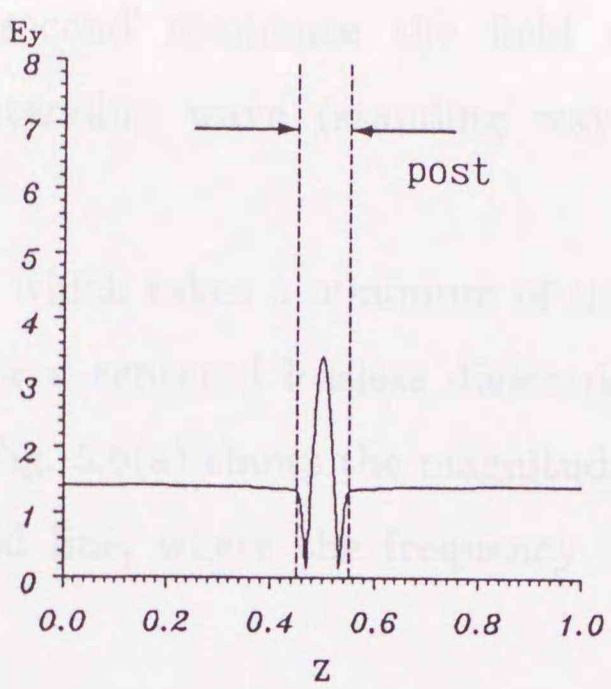

(b)

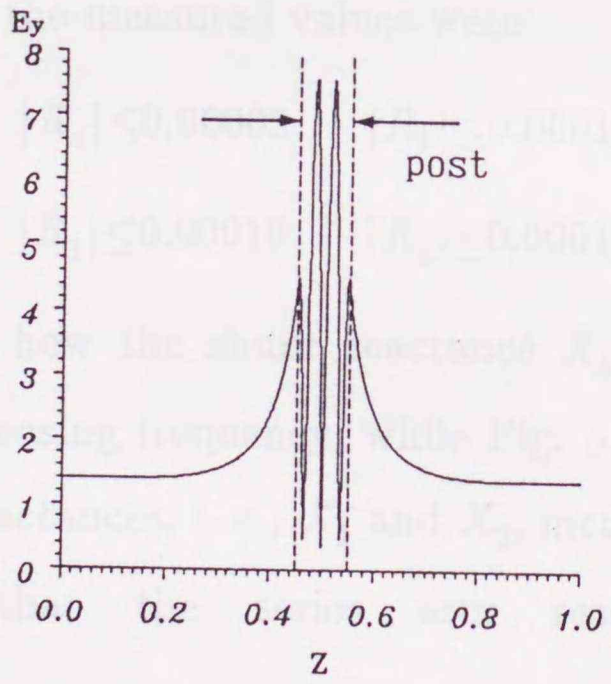

(c)

Fig. 5.5. Field distributions at resonance points.
(a) First resonance. (b) Second resonance. (c) Third resonance.

mode) [11]. Alternatively, at the second resonance the field is trapped in the post and forms a standing wave (standing wave mode) [11].

Next consider the bandpass filter which takes a minimum of the reflection coefficient R at λ/d=1.4 for a centered lossless dielectric post of r/d=0.05 and with ε=112.5. Fig. 5.6(a) shows the magnitude of reflection coefficient R by the solid line, where the frequency is normalized by the cutoff frequency f_c.

Figs. 5.6(b) and (c) show X_a and X_b for the T network, and X_1 and X_2 for the lattice network, respectively. In the case of the lossless dielectric post, normalized resistances R_a, R_b, R_1, and R_2 are theoretically zero, the measured values were

$$|R_a| \leq 0.00002 \qquad |R_b| \leq 0.00019$$

$$|R_1| \leq 0.00019 \qquad |R_2| \leq 0.00016$$

Fig. 5.6(b) shows how the shunt reactance X_a for the T network decrease with increasing frequency, while Fig. 5.6(c) shows that the series and cross reactances, i. e., X_1 and X_2, increase with increasing frequency and that the series arm resonance occurs at f_0/f_c=1.42089.

We next consider the equivalent lattice circuit shown in Fig. 5.6(d), where the series reactance corresponds to a resonant parallel LC network and the cross reactance to an inductor. Using the relationship between the original and equivalent circuit reactances, the normalized lumped lattice circuit is obtained as

$$L_1\omega_c = 0.0233 \quad C_1\omega_c = 21.26 \quad L_2\omega_c = 0.227$$

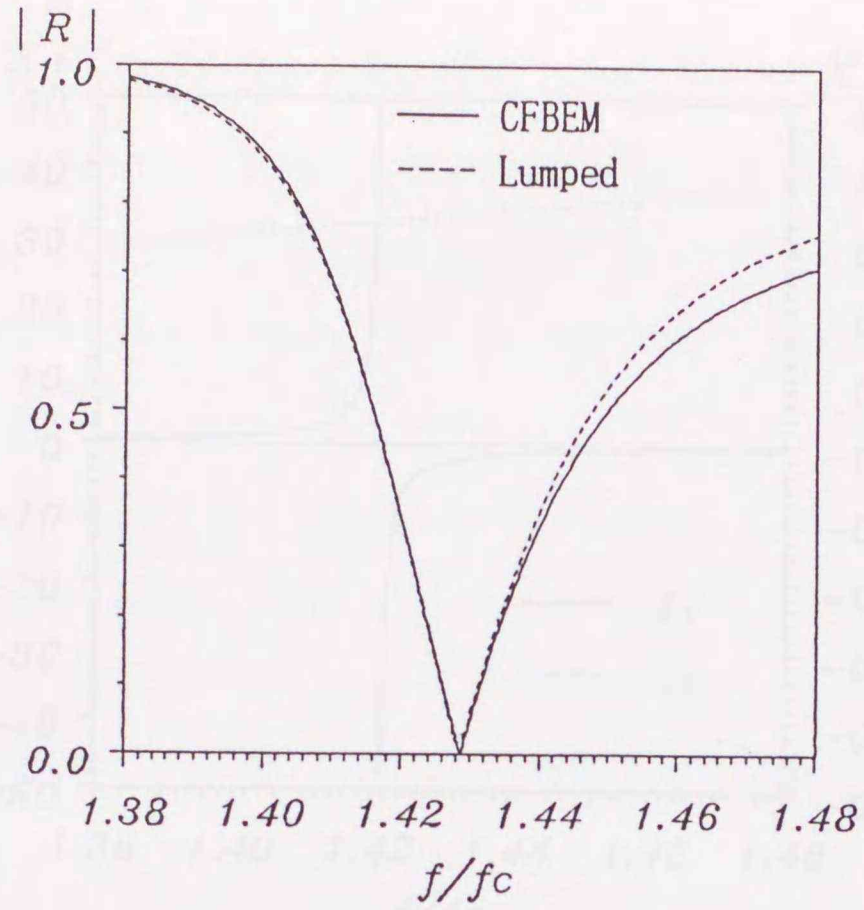

(a)

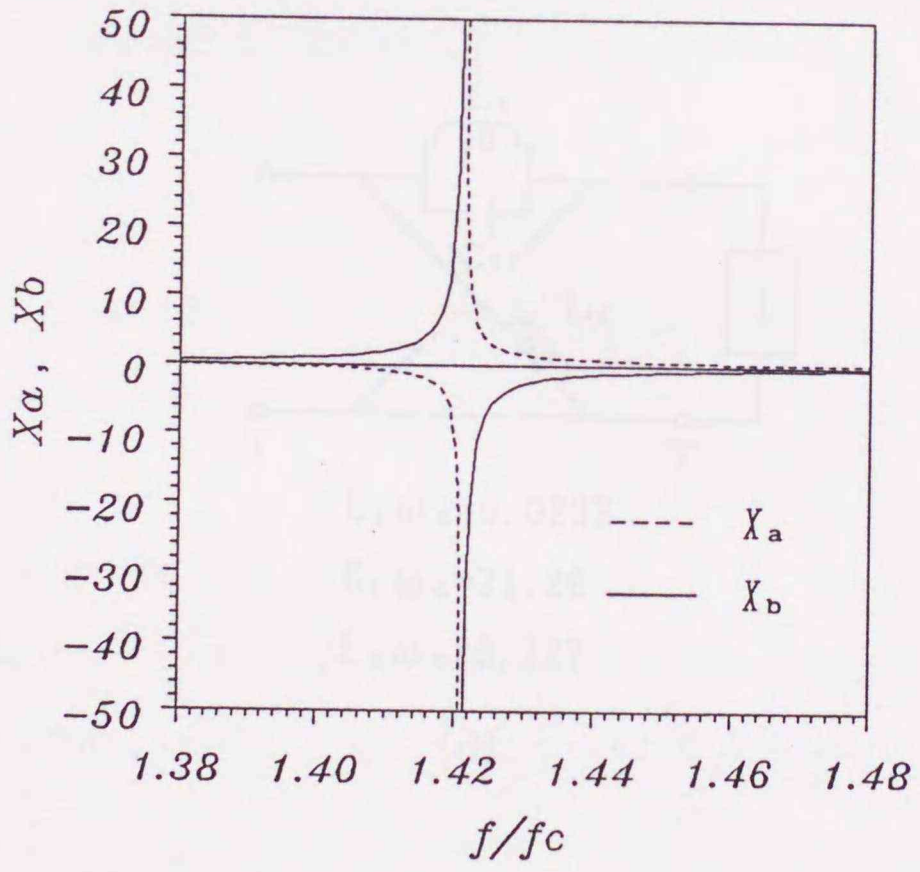

(b)

Fig. 5.6. Centered lossless dielectric post of $r/d = 0.05$ with $\varepsilon = 112.5$.

(a) Magnitude of reflection coefficient versus f/f_c.

(b) Reactances X_a and X_b for T network versus f/f_c.

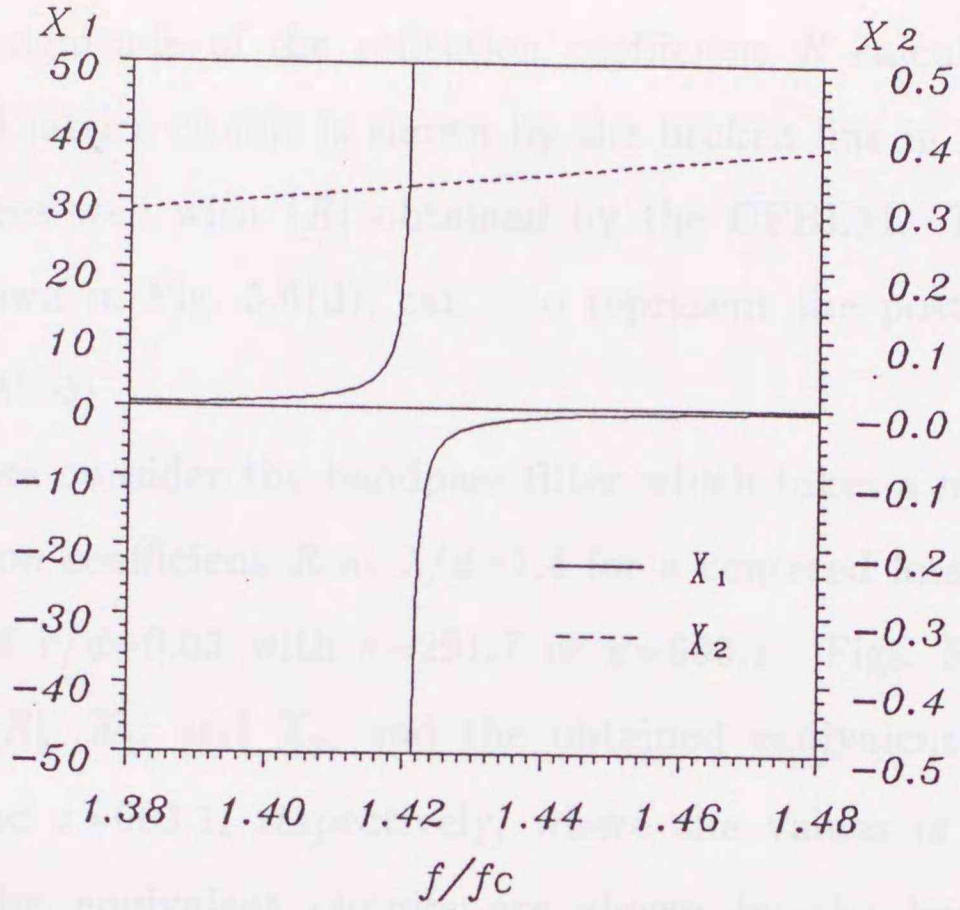

(c)

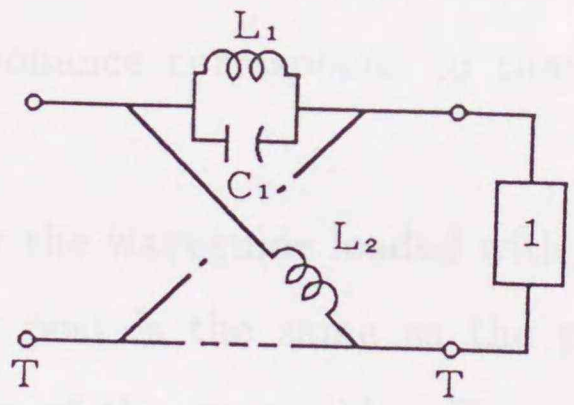

$L_1 \omega_c = 0.0233$

$C_1 \omega_c = 21.26$

$L_2 \omega_c = 0.227$

(d)

Fig. 5.6. Centered lossless dielectric post of $r/d = 0.05$ with $\varepsilon = 112.5$.

(c) Reactances X_1 and X_2 for lattice network versus f/f_c.

(d) Equivalent lattice circuit.

The magnitude of the reflection coefficient R calculated using the lumped lattice circuit is shown by the broken line in Fig. 5.6(a), and it agrees well with $|R|$ obtained by the CFBEM. This simple circuit, shown in Fig. 5.6(d), can also represent the post resonance very accurately.

Then we consider the bandpass filter which takes a minimum of the reflection coefficient R at λ/d=1.4 for a centered lossless dielectric post of r/d=0.05 with ε=291.7 or ε=603.1. Figs. 5.7 and 5.8 show the $|R|$, X_1, and X_2, and the obtained equivalent circuit at ε=291.7 and ε=603.1, respectively, where the values of $|R|$ calculated by the equivalent circuits are shown by the broken lines. These figures show that the first and the third resonances (shown in Fig. 5.5) correspond to the antiresonance of the series reactance X_1, while the second resonance corresponds to that of the cross reactance X_2.

Next we consider the waveguide loaded with two posts shown in Fig. 5.9, where each post is the same as the previous one and is located in the middle of the waveguide. If there is no interaction between the posts, the equivalent circuit of the waveguide may be assumed to be a chain of previous equivalent circuits connected in cascade as shown in Fig. 5.10. C_l is the transmission line of length l.

Figs. 5.11(a) , (b), and (c) show the magnitudes of the reflection coefficient R versus f/f_c with various l/d values, where the solid and broken lines correspond to the results obtained by the CFBEM and by the equivalent circuit cascaded by previous ones, respectively. It can be seen that the two agree well at $l/d \geq 0.5$.

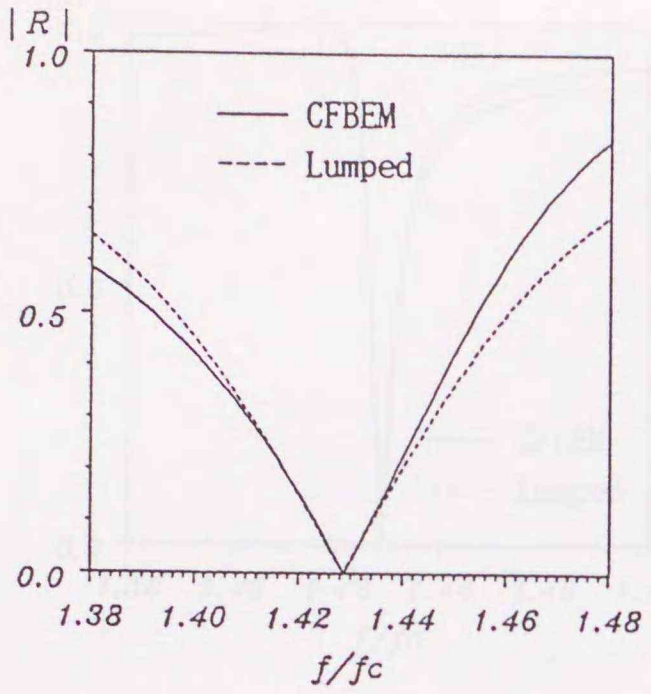

(a)

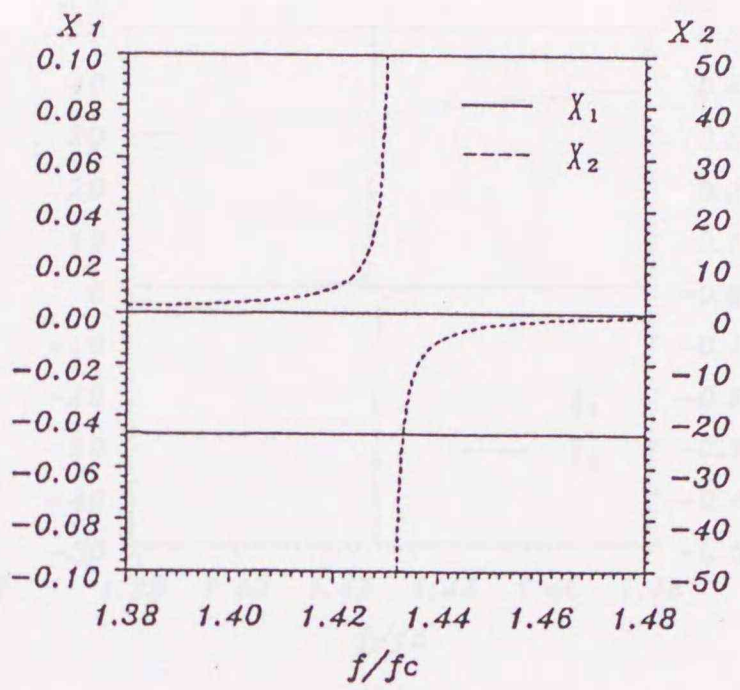

(b)

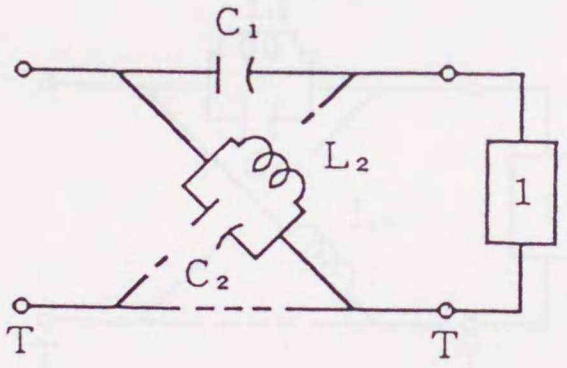

$C_1\omega_c = 14.9$
$L_2\omega_c = 0.05406$
$C_2\omega_c = 9.032$

(c)

Fig. 5.7. Centered lossless dielectric post of $r/d = 0.05$ with $\varepsilon = 291.7$.

(a) Magnitude of reflection coefficient versus f/f_c.

(b) Reactances X_1 and X_2 for lattice network versus f/f_c.

(c) Equivalent lattice circuit.

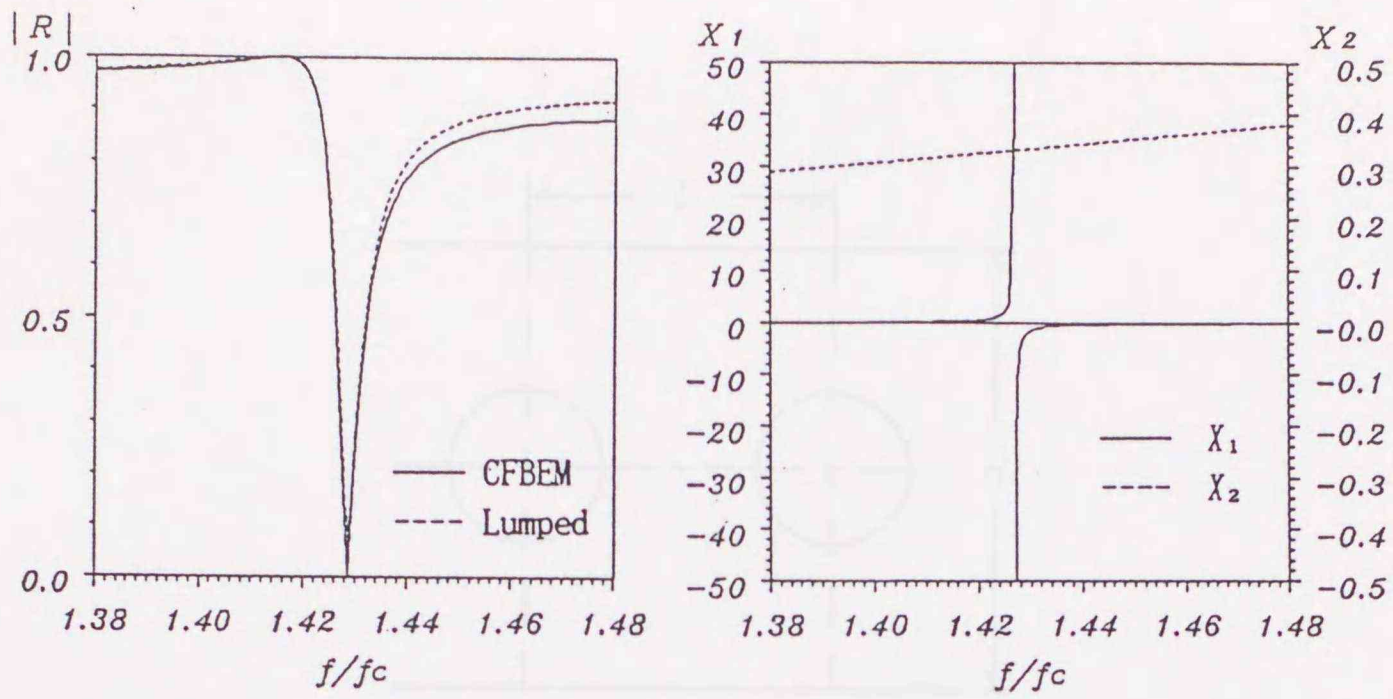

(a) (b)

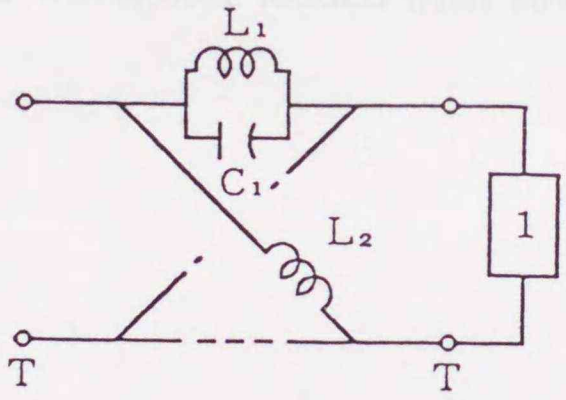

$L_1\omega_c$=0.00410
$C_1\omega_c$=119.7
$L_2\omega_c$=0.233

(c)

Fig. 5.8. Centered lossless dielectric post of $r/d = 0.05$ with $\varepsilon = 603.1$.

(a) Magnitude of reflection coefficient versus f/f_c.

(b) Reactances X_1 and X_2 for lattice network versus f/f_c.

(c) Equivalent lattice circuit.

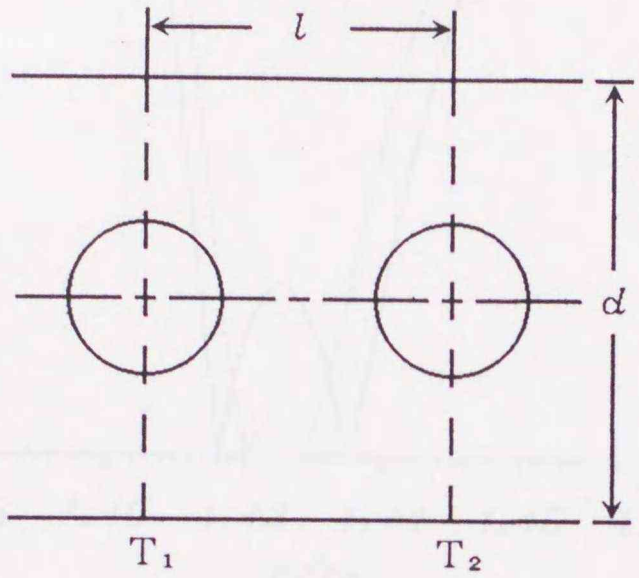

Fig. 5.9. Rectangular waveguide loaded with two centered posts.

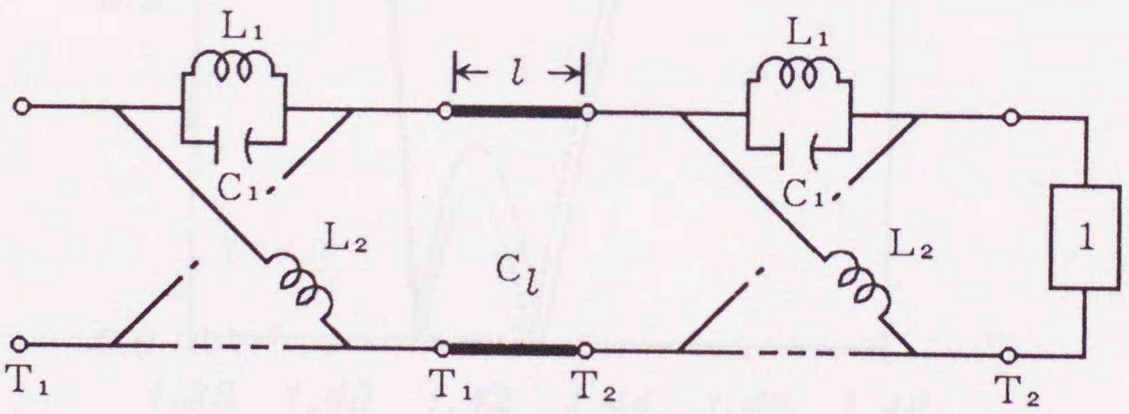

Fig. 5.10. A chain of equivalent circuits connected in cascade.

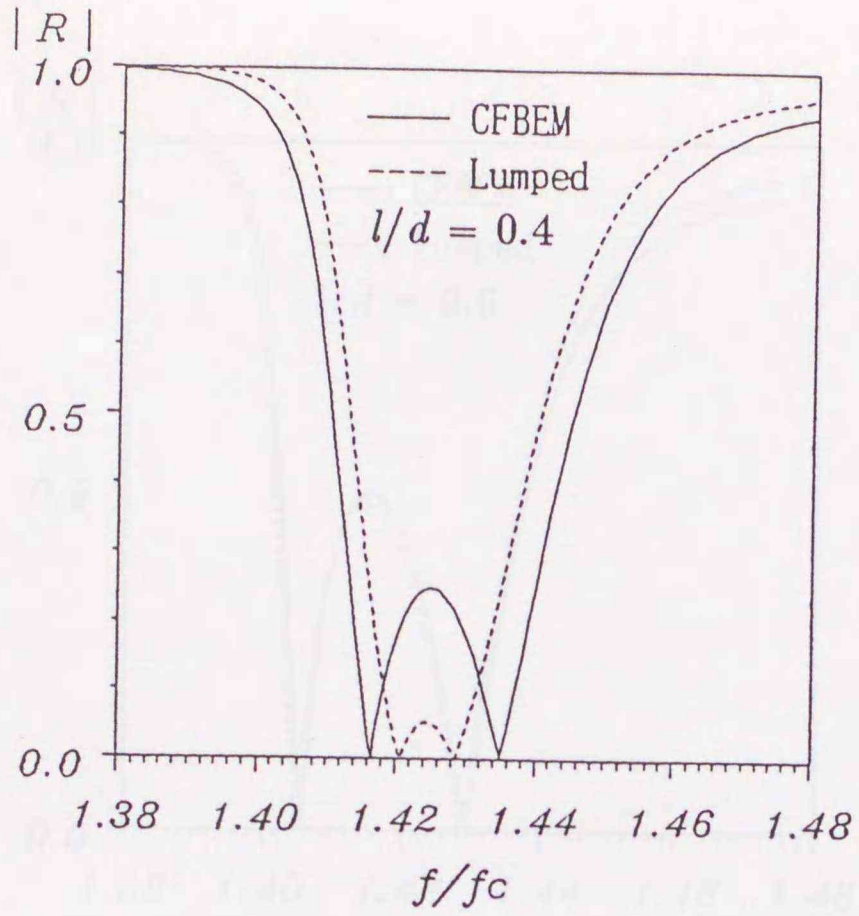

(a)

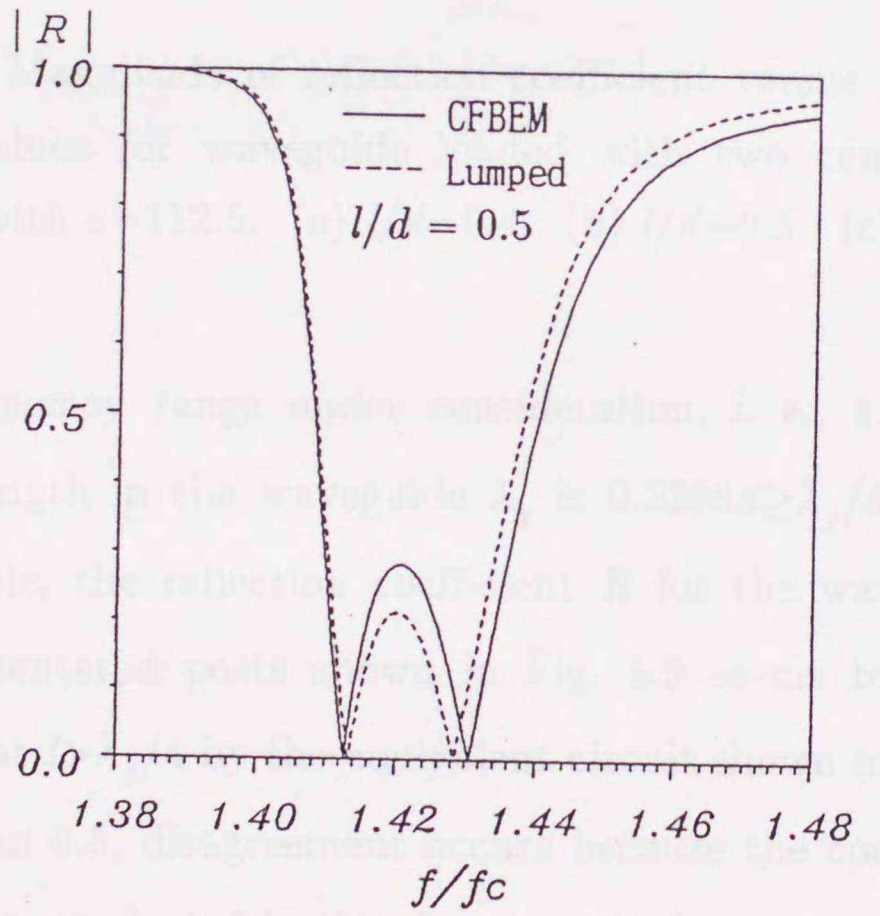

(b)

Fig. 5.11. Magnitude of reflection coefficient versus f/f_c with various l/d values for waveguide loaded with two centered posts of $r/d = 0.05$ with $\varepsilon = 112.5$. (a) $l/d = 0.4$. (b) $l/d = 0.5$. (c) $l/d = 0.6$.

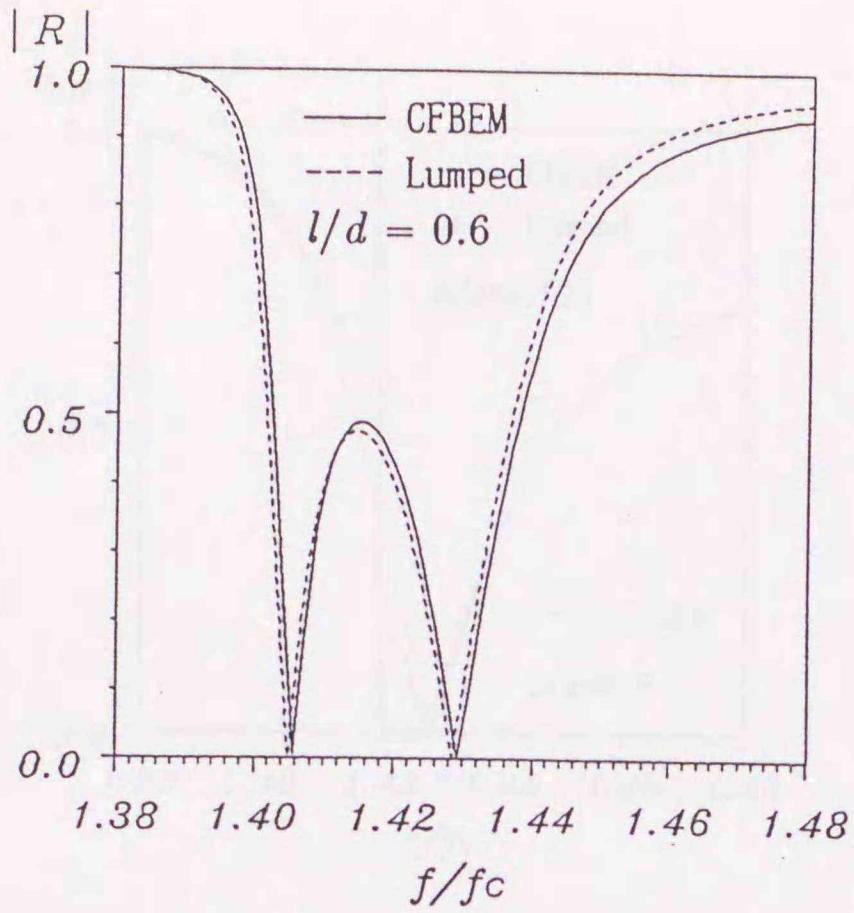

(c)

Fig. 5.11. Magnitude of reflection coefficient versus f/f_c with various l/d values for waveguide loaded with two centered posts of r/d=0.05 with ε=112.5. (a) l/d=0.4. (b) l/d=0.5. (c) l/d=0.6.

In the frequency range under consideration, i. e., $1.38 \leq f/f_c \leq 1.48$, the wavelength in the waveguide λ_g is $0.5258d \geq \lambda_g/4 \geq 0.4583d$. For this example, the reflection coefficient R for the waveguide loaded with two centered posts shown in Fig. 5.9 seems to be evaluated fairly well at $l > \lambda_g/4$ by the equivalent circuit shown in Fig. 5.10. For l/d less than 0.5, disagreement occurs because the coupling between the posts was neglected in the circuit analysis.

The CFBEM can be effectively applied to problems with variations of the post location, so it is possible to move the post from the waveguide center to a side wall, and investigate changes of the reflection coefficient and equivalent circuit parameters. Figs.

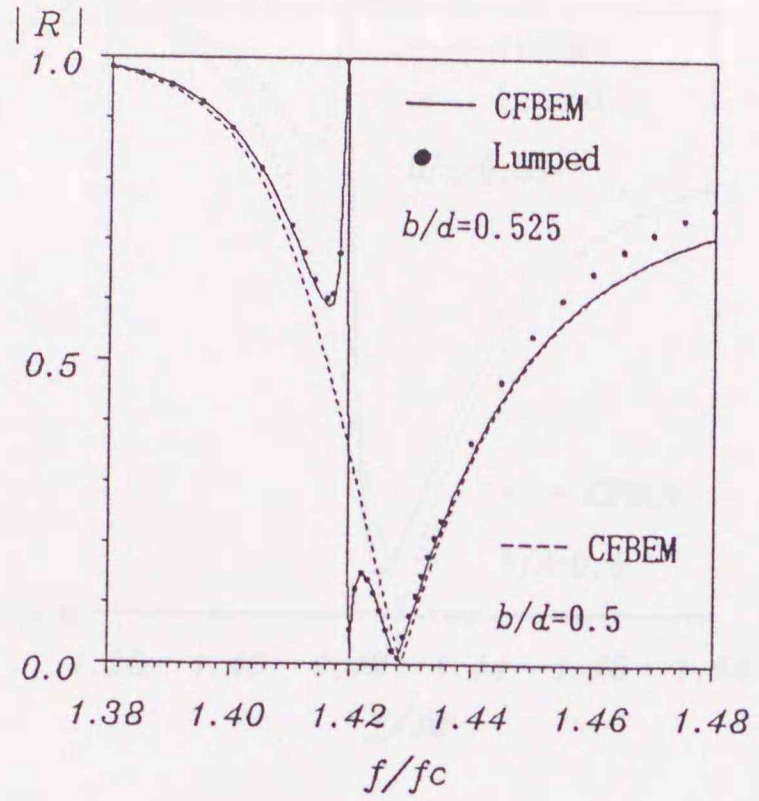

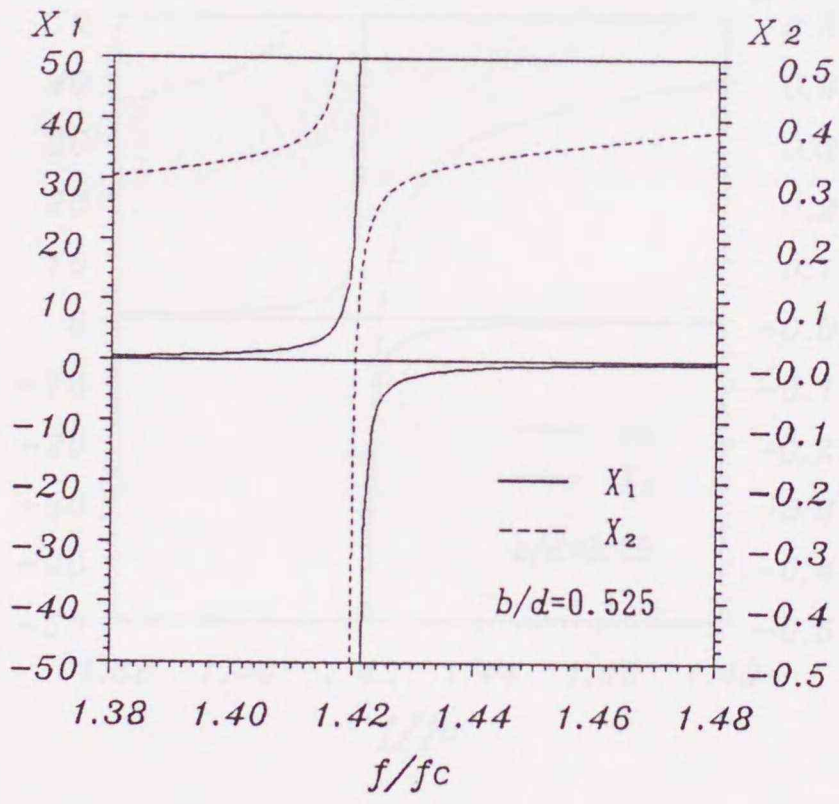

(a)

Fig. 5.12. Reflection coefficient and reactances for lattice network against f/f_c with various b/d ratios ($r/d = 0.05$, $\varepsilon = 112.5$).
(a) $b/d = 0.525$. (b) $b/d = 0.55$. (c) $b/d = 0.60$.

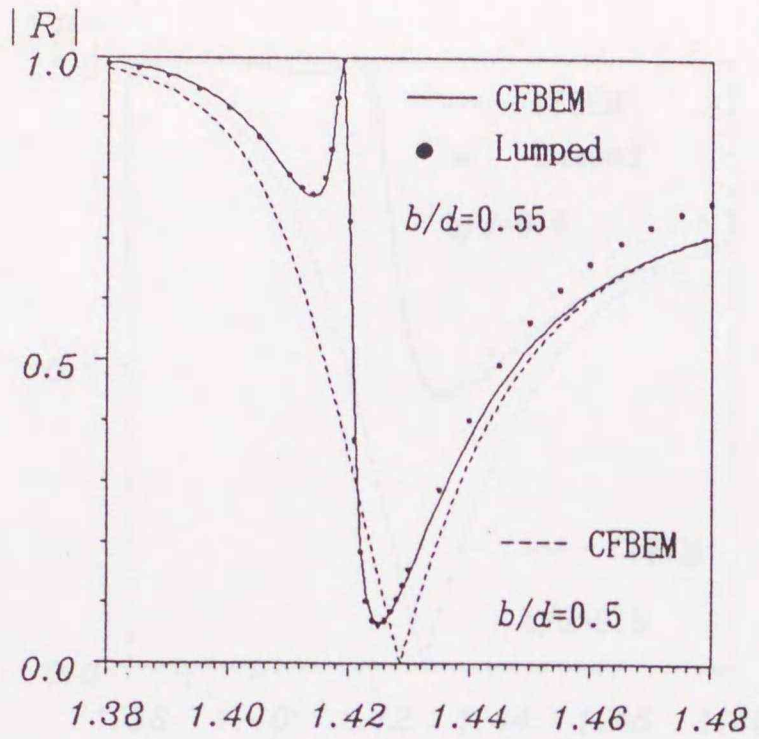

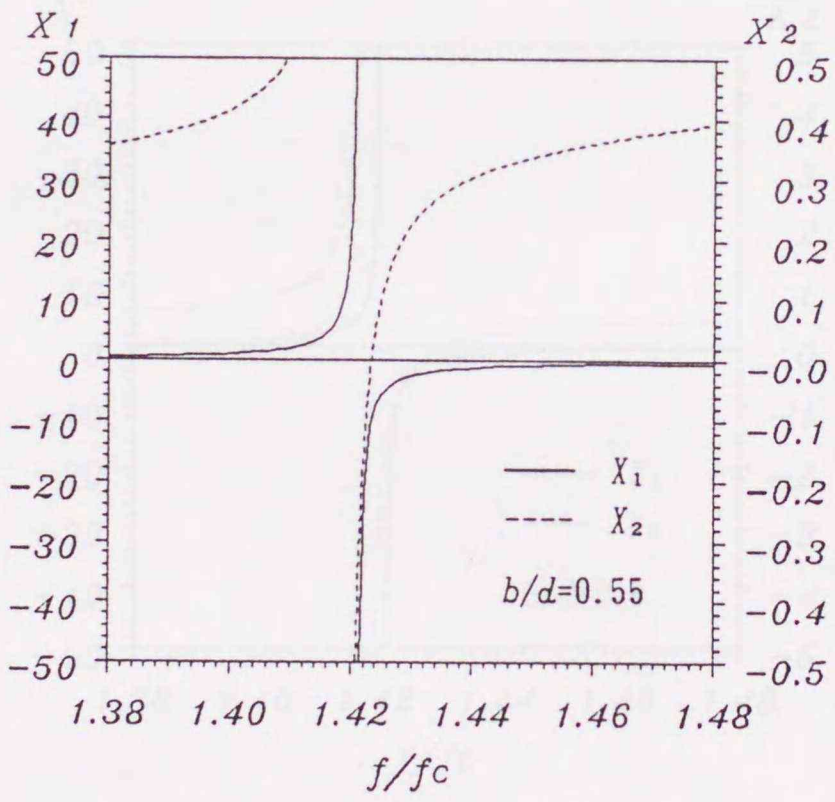

(b)

Fig. 5.12. Reflection coefficient and reactances for lattice network against f/f_c with various b/d ratios ($r/d = 0.05$, $\varepsilon = 112.5$).
(a) $b/d = 0.525$. (b) $b/d = 0.55$. (c) $b/d = 0.60$.

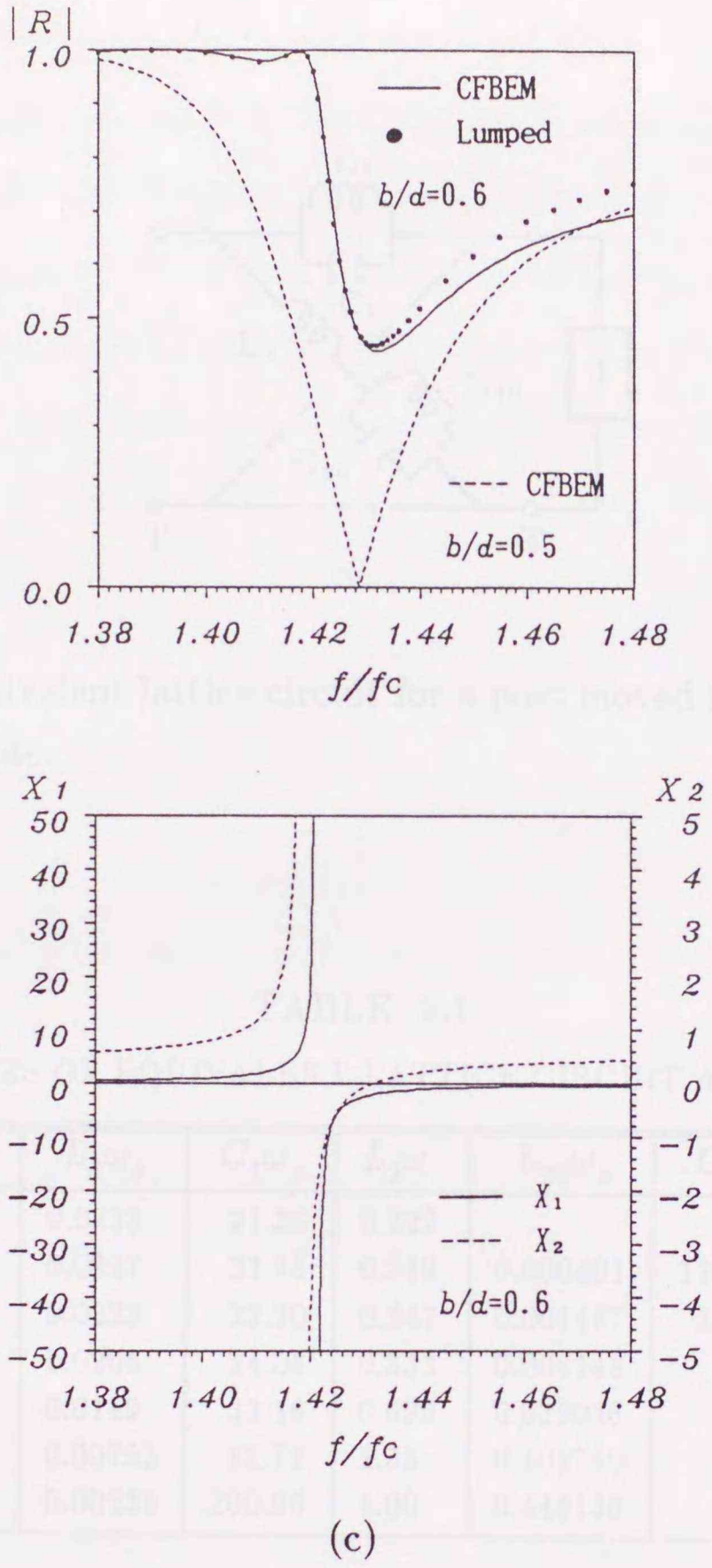

(c)

Fig. 5.12. Reflection coefficient and reactances for lattice network against f/f_c with various b/d ratios ($r/d = 0.05$, $\varepsilon = 112.5$).
(a) $b/d = 0.525$. (b) $b/d = 0.55$. (c) $b/d = 0.60$.

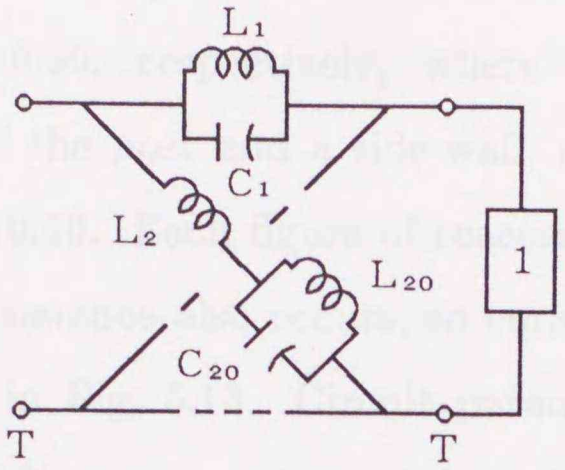

Fig. 5.13. Equivalent lattice circuit for a post moved from the center of the waveguide.

TABLE 5.1

PARAMETERS OF EQUIVALENT LATTICE CIRCUIT AGAINST b/d

b/d	$L_1\omega_c$	$C_1\omega_c$	$L_2\omega_c$	$L_{20}\omega_c$	$C_{20}\omega_c$
0.5	0.0233	21.26	0.227		
0.525	0.0227	21.78	0.239	0.000401	1237.429
0.55	0.0223	22.20	0.247	0.001487	334.035
0.60	0.0205	24.08	0.333	0.006148	80.812
0.70	0.0149	33.16	0.696	0.029046	17.147
0.80	0.00792	61.74	1.55	0.102750	4.877
0.90	0.00233	200.96	4.00	0.446136	1.103

5.12(a), (b), and (c) show the magnitudes of the reflection coefficient R and reactances X_1 and X_2 for the lattice network at b/d=0.525, b/d=0.55, and b/d=0.60, respectively, where b is the distance between the center of the post and a side-wall, and the broken line indicates $|R|$ at b/d=0.50. Each figure of reactance shows explicitly that the cross arm resonance also occurs, so consider the equivalent lattice circuit shown in Fig. 5.13. Circuit parameters obtained are shown in Table 5.1, where parameters at b/d=0.7, 0.8, and 0.9 are also noted. The values of $|R|$ calculated by the equivalent circuit shown in Fig. 5.13 are shown in Fig. 5.12 by the dotted line. As the post is moved further from the center of the waveguide, the reflection coefficient R and the circuit parameters L_1, C_1, and L_2 are increasingly varied from those for a centered post. It is interesting that for b/d greater than 0.6, the post resonance does not occur sharply, but both the cross and series arm resonances of the equivalent lattice circuit occur distinctly. Fig. 5.12(a) shows the possibility of a bandpass filter with high Q being made when the post is moved from the waveguide center.

5.5 Conclusions

A combination of the finite and boundary element methods (CFBEM) has been applied to the analysis of an H-plane waveguide loaded with dielectric posts, and equivalent circuits were derived. Some of the lossless dielectric post resonances in a rectangular waveguide can be physically realized as a lattice circuit, and the interaction between two posts can be evaluated by this circuit.

There are two types of dielectric post resonances, i. e., one corresponding to the antiresonance of the series reactance of the lattice circuit, and the other to the antiresonance of the cross reactance of the lattice circuit.

The variations of the post location are related to the variations of the branch reactances of the lattice circuit.

CHAPTER 6

Conclusions

This paper shows that spurious solutions appear in the three-dimensional discontinuity problems when the functional with three components of magnetic field is directly used. And then, to suppress and eliminate spurious solutions, we try two approaches, that is, the penalty function method [63], [64] and the method using edge elements [65]. Moreover, we introduce a substructure method [63]–[65] to save computer memory and to have a good numerical convergence. This paper also shows that the finite-element method using traditional tetrahedral elements cannot adequately treat the three-dimensional electromagnetic waveguide problems with metal wedges, and that the finite-element method using edge elements succeeds in the analysis of the problems with metal wedges [65]. Then, a combination method of the finite and boundary elements is formulated for the electromagnetic discontinuity problems which can be treated as two-dimensional ones [66]–[71]. This method is effectively applied to the waveguides loaded with ferrite as well as dielectric. Moreover, the way to represent a dielectric resonance in a rectangular waveguide by the equivalent circuit is investigated in detail [69], [70]. Some of the lossless dielectric post resonances can be physically realized by a lattice circuit, and the interaction between two posts can be evaluated by this circuit.

ACKNOWLEDGMENT

I would like to express my appreciation to Professor Masanori Koshiba, the Department of Electronic Engineering, Hokkaido University, for generous provision of continuous guidance and encouragement.

I am also grateful to Professor Kiyohiko Itoh, the Department of Electronic Engineering, Hokkaido University, Professor Ichiro Fukai, the Department of Electric Engineering, Hokkaido University, and Professor Nobuo Nagai, the Research Institute of Applied Electricity, Hokkaido University, for helpful suggestions and observations.

I also wish to acknowledge numerous illuminating discussions of members of the seminar.

List of Author's Publication

[1] K. Ise and M. Koshiba, "Numerical analysis of *H*-plane waveguide junctions with dielectric posts by combination of finite and boundary elements," *Trans. Inst. Electron. Information Commun. Eng. Japan,* vol. J71-C, pp. 250-258, Feb. 1988(in Japanese).

[2] K. Ise and M. Koshiba, "Numerical analysis of ferrite-loaded waveguide nonreciprocal phase shifters by combination of finite and boundary elements," *Trans. Inst. Electron. Information Commun. Eng. Japan,* vol. J71-C, pp. 1217-1220, Oct. 1988(in Japanese).

[3] K. Ise and M. Koshiba, "Numerical analysis of *H*-plane waveguide junctions by combination of finite and boundary elements," *IEEE Trans. Microwave Theory Tech.,* vol. 36, pp. 1343-1351, Sept. 1988.

[4] K. Ise and M. Koshiba, "Equivalent circuits for dielectric posts in a rectangular waveguide," *IEEE Trans. Microwave Theory Tech.,* vol. 37, pp. 1823-1825, Nov. 1989.

[5] K. Ise and M. Koshiba, "Dielectric post resonances in a rectangular waveguide," *Proc. Inst. Elec. Eng.,* pt. H, vol. 137, pp. 61-66, Feb. 1990.

[6] K. Ise, K. Inoue, and M. Koshiba, "Three-dimensional finite-element solution of dielectric scattering obstacles in a rectangular waveguide," *IEEE Trans. Microwave Theory Tech.,* vol. MTT-38, pp. 1352-1359, Sept. 1990.

[7] K. Ise, K. Inoue, and M. Koshiba, "Three-dimensional finite-element solution of scattering from dielectric obstacles in a rectangular waveguide," *the 3rd Asia-Pacific Microwave Conference Proceedings,* pp. 1003-1006, Sept. 1990.

[8] K. Ise and M. Koshiba, "Numerical analysis of *H*-plane waveguide junctions by combination of finite and boundary elements," *Proceedings of the Twelfth International Conference on Boundary Elements in Engineering,* vol. 2, pp. 375-385, Sept. 1990.

REFERENCES

[1] J. J. Wang, "Analysis of a three-dimensional arbitrarily shaped dielectric or biological body inside a rectangular waveguide," *IEEE Trans. Microwave Theory Tech.*, vol. MTT-26, pp. 457-462, July 1978.

[2] H. Patzelt and F. Arndt, "Double-plane steps in rectangular waveguides and their application for transformers, irises, and filters," *IEEE Trans. Microwave Theory Tech.*, vol. MTT-30, pp. 771-776, May 1982.

[3] H. Katzier, "Streuverhalten elektromagnetischer Wellen bei sprunghaften Übergängen geschirmter dielektrischer Leitungen," *Arch. Elek. Übertragung.*, vol. 38, pp. 290-296, 1984.

[4] M. De Pourcq, "Field and power-density calculations in closed microwave systems by three-dimensional finite differences," *Proc. Inst. Elec. Eng.*, pt. H, vol. 132, pp. 360-368, Oct. 1985.

[5] A. Christ and H. Hartnagel, "Three-dimensional finite-difference method for the analysis of microwave-device embedding," *IEEE Trans. Microwave Theory Tech.*, vol. MTT-35, pp. 688-696, Aug. 1987.

[6] R. Mansour, R. S. K. Tong, and R. H. MacPhie, "Simplified description of the field distribution in finlines and ridge waveguides and its application to the analysis of *E*-plane discontinuities," *IEEE Trans. Microwave Theory Tech.*, vol. 36, pp. 1825-1832, Dec. 1988.

[7] N. Marcuvitz, Ed., *Waveguide Handbook.* New York: McGraw-Hill, 1951.

[8] M. Suzuki, "Dielectric elements in a rectangular waveguide," *Journ. Inst. Electric Commun. Eng.*, vol. 38, pp. 22-28, Jan. 1955.

[9] J. B. Davies, "An analysis of the m-port symmetrical *H*-plane waveguide junction with central ferrite post," *IRE Trans. Microwave Theory Tech.*, vol. MTT-10, pp. 596-604, Nov. 1962.

[10] E. D. Nielsen, "Scattering by a cylindrical post of complex permittivity in a waveguide," *IEEE Trans. Microwave Theory Tech.*, vol. MTT-17, pp. 148-153, Mar. 1969.

[11] T. Yoshida, M. Umeno, and S. Miki, "Propagation characteristics of rectangular waveguide containing a cylindrical rod of magnetized ferrite," *IEEE Trans. Microwave Theory Tech.,* vol. MTT-20, pp. 739-743, Nov. 1972.

[12] N. Okamoto, "Computer-aided design of *H*-plane waveguide junctions with full-heigh ferrites of arbitrary shape," *IEEE Trans. Microwave Theory Tech.,* vol. MTT-27, pp. 315-321, Apr. 1979.

[13] Y. Leviatan, P. G. Li, A. T. Adams, and J. Perini, "Single-post inductive obstacle in rectangular waveguide," *IEEE Trans. Microwave Theory Tech.,* vol. MTT-31, pp. 806-811, Oct. 1983.

[14] F. Arndt, J. Bornemann, and R. Vahldieck, "Design of multisection impedance-matched dielectric-slab filled waveguide phase shifters," *IEEE Trans. Microwave Theory Tech.,* vol. MTT-32, pp. 34-38, Jan. 1984.

[15] R. Vahldieck, J. Bornemann, F. Arndt, and D. Grauerholz, "*W*-band low-insertion-loss *E*-plane filter," *IEEE Trans. Microwave Theory Tech.,* vol. MTT-32, pp. 133-135, Jan. 1984.

[16] P. G. Li, A. T. Adams, Y. Leviatan, and J. Perini, "Multiple-post inductive obstacle in rectangular waveguide," *IEEE Trans. Microwave Theory Tech.,* vol. MTT-32, pp. 365-373, Apr. 1984.

[17] H. Auda and R. F. Harrington, "Inductive posts and diaphragms of arbitrary shape and number in a rectangular waveguide," *IEEE Trans. Microwave Theory Tech.,* vol. MTT-32, pp. 606-613, June 1984.

[18] J. C. Araneta, M. E. Brodwin, and G. A. Kriegsmann," High-temperature microwave characterization of dielectric rods," *IEEE Trans. Microwave Theory Tech.,* vol. MTT-32, pp. 1328-1335, Oct. 1984.

[19] Y. Leviatan, D. Shau, and A. T. Adams, "Numerical study of the current distribution on a post in a rectangular waveguide," *IEEE Trans. Microwave Theory Tech.,* vol. MTT-32, pp. 1411-1415, Oct. 1984.

[20] F. Arndt, A. Frye, M. Wellnitz, and R. Wirsing, "Double dielectric-slab-filled waveguide phase shifter," *IEEE Trans. Microwave Theory Tech.,* vol. MTT-33, pp. 373-381, May 1985.

[21] J. N. Sahalos and E. Vafiadis, "On the narrow-band microwave filter design using a dielectric rod," *IEEE Trans. Microwave Theory Tech.,* vol. MTT-33, pp. 1165-1171, Nov. 1985.

[22] C. G. Hsu and H. A. Auda, "Multiple dielectric posts in a rectangular waveguide," *IEEE Trans. Microwave Theory Tech.,* vol. MTT-34, pp. 883-891, Aug. 1986.

[23] Y. Leviatan and G. S. Sheaffer, "Analysis of inductive dielectric posts in rectangular waveguide," *IEEE Trans. Microwave Theory Tech.,* vol. MTT-35, pp. 48-59, Jan. 1987.

[24] J. Uher, F. Arndt, and J. Bornemann, "Field theory design of ferrite-loaded waveguide nonreciprocal phase shifters with multisection ferrite or dielectric slab impedance transformers," *IEEE Trans. Microwave Theory Tech.,* vol. MTT-35, pp. 552-559, June 1987.

[25] R. Gesche and N. Löchel, "Scattering by a lossy dielectric cylinder in a rectangular waveguide," *IEEE Trans. Microwave Theory Tech.,* vol. MTT-36, pp. 137-144, Jan. 1988.

[26] C. G. Hsu and H. A. Auda, "On the realizability of the impedance matrix for lossy dielectric posts in a rectangular waveguide," *IEEE Trans. Microwave Theory Tech.,* vol. MTT-36, pp. 763-765, Apr. 1988.

[27] G. S. Sheaffer and Y. Leviatan, "Composite inductive posts in waveguide — A multifilament analysis," *IEEE Trans. Microwave Theory Tech.,* vol. MTT-36, pp. 779-783, Apr. 1988.

[28] O. C. Zienkiewicz, *The Finite Element Method,* 3rd ed., London, McGraw-Hill, 1977.

[29] K. Kagawa, M. Koshiba, M. Ikeuchi, and S. Kagami, *Finite/Boundary Element Methods for Electrical and Electronic Engineers — Application to Wave Problems,* Tokyo, Ohm Pub. Co., 1984.

[30] J. P. Webb, G. L. Maile, and R. L. Ferrari, "Finite-element solution of three-dimensional electromagnetic problems," *Proc. Inst. Elec. Eng.,* pt. H, vol. 130, pp. 153-159, Mar. 1983.

[31] M. De Pourcq, "Field and power-density calculations by three-dimensional finite elements," *Proc. Inst. Elec. Eng.,* pt. H, vol. 130, pp. 377-384, Oct. 1983.

[32] M. De Pourcq, "New power-density calculation method by three-dimensional finite elements," *Proc. Inst. Elec. Eng.,* pt. H, vol. 131, pp. 411-419, Dec. 1984.

[33] O. Picon, V. F. Hanna, and J. Citerne, "Three dimensional finite-element formulation for finline," in *IEEE-S Int. Microwave Symp. Dig.,* June, pp. 789-792.

[34] O. Picon, "Three-dimensional finite-element formulation for deterministic waveguide problems," *Microwave Opt. Technol. Lett.,* vol. 1, pp. 170-172, July 1988.

[35] M. Koshiba, M. Sato, and M. Suzuki, "Finite-element analysis of arbitrarily shaped *H*-plane waveguide discontinuities," *Trans. Inst. Electron. Commun. Eng. Japan,* vol. E66, pp. 82-87, Feb. 1983.

[36] M. Koshiba, M. Sato, and M. Suzuki, "Application of finite-element method to *E*-plane waveguide discontinuities," *Trans. Inst. Electron. Commun. Eng. Japan,* vol. E66, pp. 457-458, July 1983.

[37] M. Koshiba and M. Suzuki, "Finite-element analysis of *H*-plane waveguide junction with arbitrarily shaped ferrite post," *IEEE Trans. Microwave Theory Tech.,* vol. MTT-34, pp. 103-109, Jan. 1986.

[38] J. P. Webb and S. Parihar, "Finite element analysis of *H*-plane rectangular waveguide problems," *Proc. Inst. Elec. Eng.,* pt. H, vol. 133, pp. 91-94, Apr. 1986.

[39] J. Lee and Z. J. Cendes, "An adaptive spectral response modeling procedure for multipost microwave circuits," *IEEE Trans. Microwave Theory Tech.,* vol. MTT-35, pp. 1240-1247, Dec. 1987.

[40] C. A. Brebbia, *The Boundary Element Method for Engineering,* London, Pentech Press, 1978.

[41] C. A. Brebbia and S. Walker, *Boundary Element Techniques in Engineering,* London, Newnes-Butterworths, 1980.

[42] S. Kagami and I. Fukai, "Application of boundary-element method to electromagnetic field problems," *IEEE Trans. Microwave Theory Tech.,* vol. MTT-32, pp. 455-461, Apr. 1984.

[43] K. Kanao and S. Kurasono, "Waveguide-Type dielectric filter," *Trans. Inst. Electron. Commun. Eng. Japan,* vol. J67-B, pp. 1177-1178, Oct. 1984(in Japanese).

[44] H. Sano and S. Kurasono, "An analysis of Michelson interferometer-type hybrid by boundary element method," *Trans. Inst. Electron. Commun. Eng. Japan,* vol. J67-B, pp 1392-1398, Dec. 1984(in Japanese).

[45] M. Koshiba and M. Suzuki, "Application of the boundary-element method to waveguide discontinuities," *IEEE Trans. Microwave Theory Tech.,* vol. MTT-34, pp. 301-307, Feb. 1986.

[46] K. Inoue, K. Hayata, and M. Koshiba, "Finite-element solution of three-dimensional periodic waveguide problems," *Trans. Inst. Electron. Information Commun. Eng. Japan,* vol. J71-C, pp. 1404-1411, Oct. 1988(in Japanese).

[47] K. Inoue and M. Koshiba, "Finite-element solution of periodic waveguides with circular symmetry," *Trans. Inst. Electron. Information Commun. Eng. Japan,* vol. J73-C-I, pp. 517-523, July 1990(in Japanese).

[48] M. Koshiba, K. Hayata, and M. Suzuki, "Vectorial finite-element formulation without spurious modes for dielectric waveguides," *Trans. Inst. Electron. Commun. Eng. Japan,* vol. E67, pp. 191-196, Apr. 1984.

[49] B. M. A. Rahman and J. B. Davies, "Penalty function improvement of waveguide solution by finite elements," *IEEE Trans. Microwave Theory Tech.,* vol. MTT-32, pp. 922-928, Aug. 1984.

[50] B. M. A. Rahman and J. B. Davies, "Finite element solution of integrated optical waveguides," *J. Lightwave Technol.,* vol. LT-2, pp. 682-688, Oct. 1984.

[51] M. Koshiba, K. Hayata, and M. Suzuki, "Study of spurious solutions of finite-element methods in the three-component magnetic field formulation for dielectric waveguide problems," *Trans. Inst. Electron. Commun. Eng. Japan,* vol. J67-B, pp. 1333-1338, Dec. 1984(in Japanese).

[52] M. Koshiba, K. Hayata, and M. Suzuki, "Improved finite-element formulation in terms of the magnetic field vector for dielectric waveguide," *IEEE Trans. Microwave Theory Tech.,* vol. MTT-33, pp. 227-233, Mar. 1985.

[53] M. Koshiba, K. Hayata, and M. Suzuki, "Finite-element method analysis of microwave and optical waveguide—Trends in countermeasures to spurious solutions—," *Trans. Inst. Electron. Commun. Eng. Japan,* vol. J69-C, pp. 1477-1486, Dec. 1986(in Japanese).

[54] K. Hayata, M. Koshiba, M. Eguchi, and M. Suzuki, "Vectorial finite-element method without any spurious solutions for dielectric waveguiding problem using transverse magnetic-field component," *IEEE Trans. Microwave Theory Tech.*, vol. MTT-34, pp. 1120-1124, Nov. 1986.

[55] K. Hayata, M. Eguchi, and M. Koshiba, "Finite element formulation for guided-wave problems using transverse electric field component," *IEEE Trans. Microwave Theory Tech.*, 37, pp. 256-258, Jan. 1989.

[56] K. Hayata, K. Miura, and M. Koshiba, "Full vectorial finite element formulation for lossy anisotropic waveguides," *IEEE Trans. Microwave Theory Tech.*, 37, pp. 875-883, May 1989.

[57] M. Hara, T. Wada, T. Fukasawa, and F. Kikuchi, "A three dimensional analysis of RF electromagnetic fields by the finite element method," *IEEE Trans. Magn.*, vol. MAG-19, pp. 2417-2420, Nov. 1983.

[58] M. Koshiba, T. Katano, and M. Suzuki, "Finite-element solution of three-dimensional electromagnetic eigenvalue problems," *Trans. Inst. Electron. Commun. Eng. Japan,* vol. J68-A, pp. 533-540, June 1985(in Japanese).

[59] J. P. Webb, "The finite-element method for finding modes of dielectric-loaded cavities," *IEEE Trans. Microwave Theory Tech.*, vol. MTT-33, pp. 635-639, July 1985.

[60] A. Konrad, "A direct three-dimensional finite element method for the solution of electromagnetic fields in cavities," *IEEE Trans. Magn.*, vol. MAG-21, pp. 2276-2279, Nov. 1985.

[61] A. Konrad, "On the reduction of the number of spurious modes in the vectorial finite-element solution of three-dimensional cavities and waveguides," *IEEE Trans. Microwave Theory Tech.*, vol. MTT-34, pp. 224-227, Feb. 1986.

[62] J. P. Webb, "Efficient generation of divergence-free fields for the finite element analysis of 3D cavity resonances," *IEEE Trans. Magn.*, vol. MAG-24, pp. 162-165, Jan. 1988.

[63] K. Ise, K. Inoue, and M. Koshiba, "Three-dimensional finite-element solution of dielectric scattering obstacles in a rectangular waveguide," *IEEE Trans. Microwave Theory Tech.*, vol. MTT-38, pp. 1352-1359, Sept. 1990.

[64] K. Ise, K. Inoue, and M. Koshiba, "Three-dimensional finite-element solution of scattering from dielectric obstacles in a rectangular waveguide," *the 3rd Asia-Pacific Microwave Conference Proceedings,* pp. 1003-1006, Sept. 1990.

[65] K. Ise, K. Inoue, and M. Koshiba, "Three-dimensional finite-element method with edge elements for electromagnetic waveguide discontinuities," *IEEE Trans. Microwave Theory Tech.,* submitted for publication.

[66] K. Ise and M. Koshiba, "Numerical analysis of *H*-plane waveguide junctions with dielectric posts by combination of finite and boundary elements," *Trans. Inst. Electron. Information Commun. Eng. Japan,* vol. J71-C, pp. 250-258, Feb. 1988(in Japanese).

[67] K. Ise and M. Koshiba, "Numerical analysis of ferrite-loaded waveguide nonreciprocal phase shifters by combination of finite and boundary elements," *Trans. Inst. Electron. Information Commun. Eng. Japan,* vol. J71-C, pp. 1217-1220, Oct. 1988(in Japanese).

[68] K. Ise and M. Koshiba, "Numerical analysis of *H*-plane waveguide junctions by combination of finite and boundary elements," *IEEE Trans. Microwave Theory Tech.,* vol. 36, pp. 1343-1351, Sept. 1988.

[69] K. Ise and M. Koshiba, "Equivalent circuits for dielectric posts in a rectangular waveguide," *IEEE Trans. Microwave Theory Tech.,* vol. 37, pp. 1823-1825, Nov. 1989.

[70] K. Ise and M. Koshiba, "Dielectric post resonances in a rectangular waveguide," *Proc. Inst. Elec. Eng.,* pt. H, vol. 137, pp. 61-66, Feb. 1990.

[71] K. Ise and M. Koshiba, "Numerical analysis of *H*-plane waveguide junctions by combination of finite and boundary elements," *Proceedings of the Twelfth International Conference on Boundary Elements in Engineering,* vol. 2, pp. 375-385, Sept. 1990.

[72] T. Weiland, "Three dimensional resonator mode computation by finite difference method," *IEEE Trans. Magn.,* vol. MAG-21, pp. 2340-2343, Nov. 1985.

[73] W.Geyi and W. Hongshi, "Solution of the resonant frequencies of a microwave dielectric resonator using boundary element method," *Proc. Inst. Elec. Eng.,* pt. H, vol. 135, pp. 333-338, Oct. 1988.

[74] W. Geyi and W. Hongshi, "Solution of the resonant frequencies of a cavity resonator by boundary element method (BEM)," *Proc. Inst. Elec. Eng.*, pt. H, vol. 135, pp. 361-365, Dec. 1988.

[75] A. D. Berk, "Variational principles for electromagnetic resonators and waveguides," *IRE Trans. Antennas Propagat.*, vol. AP-4, pp. 104-111, Apr. 1956.

[76] A. Konrad, "Vector variational formulation of electromagnetic fields in anisotropic media," *IEEE Trans. Microwave Theory Tech.*, vol. MTT-24, pp. 553-559, Sept. 1976.

[77] R. E. Collin, *Field Theory of Guided Waves,* New York, McGraw-Hill, 1960.

[78] J. P. Webb, "Finite element analysis of dispersion in waveguides with sharp metal edges," *IEEE Trans. Microwave Theory Tech.*, vol. 36, pp. 1819-1824, Dec. 1988.

[79] A. Kameari, "Calculation of transient 3D eddy current using edge-elements," *IEEE Trans. Magn.*, vol. 26, pp. 466-469, Mar. 1990.

[80] K. K. Mei, "Unimoment method of solving antenna and scattering problems," *IEEE Trans. Antennas Propagt.*, vol. AP-22, pp. 760-766, Nov. 1974.

[81] D. Polder, "On the theory of ferromagnetic resonance," *Phil. Mag.*, vol. 40, pp. 100-115, 1949.

[82] B. J. K. Lax, K. Button, and L. M. Roth, "Ferrite phase shifters in rectangular wave guide," *J. Appl. Phys.*, vol. 25, pp. 1413-1421, 1954.

[83] C. G. Montgomery, R. H. Dicke, and E. M. Purcell, Eds., *Principles of Microwave Circuits,* New York, McGraw-Hill, 1950.

inches 1 2 3 4 5 6 7 8

cm 1 2 3 4 5 6 7 8 9 10 11 12 13 14 15 16 17 18 19

Kodak Color Control Patches

Blue Cyan Green Yellow Red Magenta White 3/Color Black

Kodak Gray Scale

C Y M

A 1 2 3 4 5 6 **M** 8 9 10 11 12 13 14 15 **B** 17 18 19